Trafficking and pH-dependent fusion of enveloped viruses in the endocytic system

Maya E. Cabot
North Garden, Virginia

BA, Haverford College, 2010

MS, University of Virginia, 2018

A Dissertation presented to the Graduate Faculty of the
University of Virginia in Candidacy for the
Degree of Doctor of Philosophy

Degree-Conferring Interdisciplinary Program in
Biophysics
Department of Molecular Physiology and Biological
Physics
University of Virginia
May 2022

Abstract

Most enveloped viruses infect cells by binding receptors at the cell surface and undergo trafficking through the endocytic pathway to a compartment with the requisite conditions to trigger fusion with a host endosomal membrane. Both binding at the cell surface and the eventual fusion of virus and host membranes is mediated by the viral entry and fusion protein(s), proteins on the virus surface that are sometimes simply referred to as glycoproteins. Under conducive conditions the fusion protein(s) undergo conformational changes and induce the merging of the host membrane and viral membrane, allowing viral contents to enter the host cell cytoplasm initiating infection. Factors that induce conformational change to trigger viral fusion with the host membrane can be low pH, receptors in the endosomal membrane, proteases, a high concentration of a specific cation such as calcium in the endosomal lumen, a specific lipid, or some combination of these factors. These features of virus entry are reviewed in Chapter 1.

Broad categories of compartments in the endocytic pathway include early and late endosomes, which can be further categorized into subpopulations with differing rates of maturation and motility characteristics. In Chapter 2, viral particles pseudotyped with the vesicular stomatitis virus glycoprotein on their surface and equipped with a novel pH sensor and a fluorescent content marker were used to measure pH, motion, and fusion at the single particle level in live cells. We found that the VSV-G particles fuse predominantly from more acidic

and more motile endosomes, and that a significant fraction of particles is trafficked to more static and less acidic endosomes that do not support their fusion. Moreover, the fusion-supporting endosomes undergo directed motion.

In Chapter 3, a correlative assay to ascertain the pH of fusion mediated by Ebola virus glycoprotein is described. Ebola virus has a complex entry mechanism and while assays reconstituting fusion have shown that pH plays a critical role, the pH at which Ebola virus fuses in intact cells has not previously been determined. A novel pH sensor, mNectarine-Lamp1 was used to specifically assess late endosomal pH in cells treated with bafilomycin to alkalinize endosomes. The inhibition of viral entry was assessed upon treatment with the same concentration range of bafilomycin. The change in late endosomal pH was then correlated with inhibition of entry. With this approach, we determined that the majority of EBOV particles fuse in U2OS cells below pH 5.7. The methodology presented could be used to determine the pH dependence of fusion in live cells for other enveloped viruses that enter cells through an endosomal pathway.

Acknowledgements

This dissertation is dedicated to my kind, brilliant husband, who has encouraged me, cooked food for me, and put up with our two sweet but tough toddlers on his own many times in the last year when I've needed extra time to work or to decompress from all the work. Binit, you inspire me with your own work ethic, curiosity about the world and humor in the face of adversity.

Thank you to my parents, who have always been so confident in my abilities. Mom, thanks for cooking for us and playing with your grandchildren so often. Dad, thank you for reminding me to try hard but that it's ok to take a deep breath let go of things that just aren't working.

Thank you to the Tamm Lab and former members of the lab of Judy White. Advice and help from all of you made this work both better and more meaningful.

Thank you to my three scientific mentors. Lukas, thank you for being supportive of my career aspirations and for instilling in me a sense of meticulousness and pride in my work that will continue to shape my career and life for the better. Judy, I am so grateful you were willing to continue as a mentor even when Emerita. Volker, I am very grateful that you find LabView programming to be a soothing bedtime activity and that you've always provided such helpful advice in response to my many science-related ramblings and problems.

To my committee members, your open email inboxes and office doors have meant a lot over the last 5+ years. The advice both on microscopy and surviving graduate school has been invaluable.

Non doctior, sed meliore doctrina imbutus.

Table of Contents

Chapter 1: Introduction

1.1 An Abstract of Viral trafficking and the Endocytic Pathway

Viruses must exploit host cell machinery to replicate. To gain access to this machinery, the viral contents must enter the cytoplasm, after which the cell is said to be infected. Enveloped viruses are a special category of virus that bear a host-derived lipid membrane on their exterior. For most enveloped viruses to infect cells they must bind receptors at the cell surface and then be internalized into a vesicle, a small membrane bound compartment within the cell. Enveloped viruses can then undergo trafficking through the endocytic system, a collection of enclosed compartments within the cell that support cargo sorting, recycling and degradation. Both binding at the cell surface and the eventual fusion of virus and host membranes is mediated by the viral entry and fusion protein(s) (sometimes called viral envelope glycoproteins), which are proteins on the virus surface. Under conducive conditions the fusion protein(s) can undergo conformational changes and induce the merging of the host membrane and viral membrane. Factors that induce conformational change to trigger viral fusion with the host membrane can be low pH, receptors in the endosomal membrane, a high concentration of a specific cation such as calcium in the endosomal lumen, a protease, a specific lipid, or some combination of these factors. To achieve fusion, viruses must be trafficked to a compartment with these conducive conditions.

Cargo enters the cell from the plasma membrane for a variety of purposes: some proteins carry cargo into the cell or transmit signals and then are sent back to the plasma membrane, while others are taken up to be degraded with constituent parts reused. Once cargo progresses sufficiently in the endocytic pathway and enters late endosomes, it cannot be recycled directly to the plasma membrane and is typically destined for degradation. To avoid misdirection of cargo for recycling or degradation, there are several tightly regulated steps at which cargo can be retrieved or redirected. The sorting of cargo begins at the cell surface, where specific cargo is concentrated in discrete areas of the plasma membrane. Through a variety of mechanisms, the plasma membrane can form ruffles or invaginations, which become enclosed vesicles within the cytoplasm, a process called endocytosis. Broad categories of compartments in the endocytic pathway include early and late endosomes. Vesicles containing incoming cargo from the plasma membrane typically first fuse with early endosomes, though this may vary based on the pathway by which the endosome is formed. Early endosomes mature to late endosomes in a process that is characterized by the exchange of membrane associated proteins on the cytosolic face of the compartment. Maturation is generally understood to be an irreversible process and is marked by changes in ion concentrations within the endosomal lumen, generation of vesicles internal to the endosome and changes in the membrane composition of the endosome that accompany the transition from early to late endosome. Early endosomes have a pH closer to neutral, while late endosomes

are more acidic. The low pH in late endosomes works in concert with proteases to break down proteins no longer needed by the cell.

In addition to the broad categories of early and late endosome, cargo may be sorted to special subpopulations of early endosomes that can more rapidly mature. While not a physiological cargo, viruses bind to and exploit host lipids or proteins to make their way through the endocytic pathway to a compartment where they can undergo fusion. The sorting of viruses may or may not follow the physiological sorting of their receptors (examples will be discussed in Chapter 2). Important information about the compartment in which the virus fuses and its fusion requirements may also be derived from understanding the pH threshold for viral fusion (examples will be discussed in Chapter 3).

1.2 Endocytosis and Characteristics of the Endocytic System

The plasma membrane is necessary to protect the cytosol from the outside world, contain and concentrate the thousands of different chemical reactions that take place inside the cell and modulate, and amplify signals to and from the cell. To maintain the integrity of the plasma membrane, modulate the levels of proteins involved in signaling and take in bulk nutrients, the cell must be able to internalize material from medium surrounding the cell without breaching the continuity of the plasma membrane. This is achieved by inward budding and vesiculation of small areas of the plasma membrane. These inward buds become vesicles by controlled fission from the plasma membrane.

The process of cells internalizing matter from their environment was first observed in the 1880s and was termed phagocytosis (Schmid et al., 2014) from the ancient Greek for “to eat” (φαγεῖν) and “skin/empty vessel” (κῦτος). Phagocytosis was easily observed with early technology in microscopy because of large scale changes in the cell but it took many years for the process of endocytosis and the endocytic system to be understood in greater detail as microscopy technology evolved (Hansen et al., 1991; Novikoff et al., 1956; Schmid et al., 1989; Yamada, 1955). While phagocytosis is a particular form of endocytosis primarily targeting large particles and is especially important as a cell defense mechanism, endocytosis is more generally the internalization of material of all sizes, often selectively, from outside the cell to the interior. To accomplish this, cells form vesicles that are small compartments made up of lipid bilayer from the plasma membrane (de Bruyn et al., 1983; Dickson et al., 1983; Herman & Albertini, 1983; Kartenbeck et al., 1981). These vesicles may also contain proteins and materials either integral to or attached to the bilayer (Brown & Goldstein, 1979; Jean-Alphonse & Hanyaloglu, 2011). By binding materials that will be internalized, such as lipids or membrane proteins, many viruses hitch a ride inside the cell along with physiological cargo. Vesicles formed from the plasma membrane can go through several possible pathways, but the two primary end fates of the vesicles and their cargo are degradation or recycling.

In the degradative pathway, cargo encounters compartments that are progressively more acidic and hydrolytic enzymes can break down cargo (Kolter

& Sandhoff, 2010; Yadati et al., 2020). The low pH of later endocytic compartments can trigger viral fusion (J. M. White et al., 2016) and is also important for the dissociation of important cargo, such as iron or low-density lipoproteins (LDL), from their transmembrane receptors (transferrin and LDL-receptor respectively. Dissociation precedes recycling of receptors to the cell surface (Alberts et al., 2002; Brown & Goldstein, 1979; Diaz et al., 1988; Goldstein et al., 1982; Harding et al., 1983; Schneider & Williams, 1985; Vasile et al., 1983). The first compartments that cargo typically encounters in the endocytic pathway are early endosomes (EE) which are mildly acidic (pH ~7.0-6.0) and act as an important sorting station from which cargo to be recycled can be recovered (as reviewed in Huotari & Helenius, 2011). These compartments are generally more peripheral (eg closer to the plasma membrane than the nucleus) but the relationship between compartment localization and acidity is a cell type dependent phenomenon (D. E. Johnson et al., 2016). The next set of compartments, which are typically closer to the nucleus, deeper inside the cell, are late endosomes (LE), which have pH ~6.0-4.5 (D. E. Johnson et al., 2016; R. J. Lee et al., 1996; Ohkuma & Poole, 1978; Tycko et al., 1983), and contain enzymes that can break down cargo. Entrance into late endosomes is a key decision point as these compartments cannot typically recycle fluids or membrane components directly to the plasma membrane. Lysosomes are compartments containing a high concentration of hydrolytic enzymes that may fuse with late endosomes. Endolysosome is a designation for the organelle that

results from the fusion of late endosomes and lysosomes; this is where much of the degradative cargo is broken down (as reviewed in Luzio et al., 2014). The lipid composition and overall ionic composition of compartments in the endocytic pathway are unique and heavily regulated such that molecular machinery can only operate within the lumen of or on the membrane of the physiologically appropriate compartment (Huotari & Helenius, 2011). An overview of the endocytic pathway is shown in Figure 1.1 and will be described in greater detail through the next few sections of the introduction.

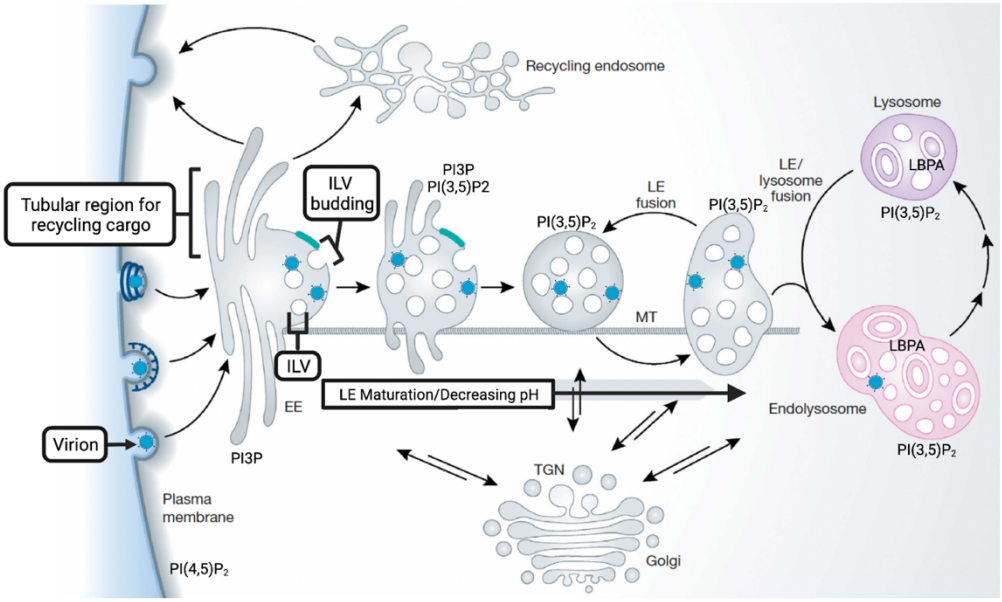

Figure 1.1. An overview of the compartments of the endocytic pathway and the flow of cargo. The endocytic pathway consists of a series of increasingly acidic compartments with differing membrane composition. Incoming cargo from the plasma membrane, including viruses, is contained in vesicles that fuse with early endosomes (EE). Cargo destined for recycling is sorted to tubules, which are then undergo scission. Cargo contained in these tubule-derived vesicles is trafficked to recycling endosomes or back to the plasma membrane. Early endosomes are relatively rich in PI(3)P, which recruits effectors that promote endosome maturation and the formation of intraluminal vesicles (ILV) containing degradative cargo. Late endosomes (LE) are more acidic than EE. Lysosomes

can fuse with LE, delivering hydrolytic enzymes to form endolysosomes, which have very low pH, are rich in ILVs and can conduct degradation of cargo. Endolysosomes and lysosomes are rich in the lipid LBPA. Endosomes at all stages may fuse with endosomes of their own type in homotypic fusion events or form vesicles to fuse with the trans-Golgi network (TGN). However, only EE and recycling endosomes typically generate vesicles that can fuse directly with the plasma membrane. Adapted from Huotari and Helenius 2011.

1.3 The Formation of Vesicles at the Plasma Membrane

Mechanistically, endocytosis occurs through clathrin-coated pits or modes of clathrin-independent endocytosis. The clathrin-independent endocytosis includes a variety of forms including caveolae and macropinocytosis. Clathrin-mediated endocytosis is a tightly regulated process for selective cargo uptake and will be discussed in greater detail below (Kaksonen & Roux, 2018; Mercer & Helenius, 2009; Schmid et al., 2014). Caveolae are fairly stable structures thought to be derived from lipid rafts (Parton & Simons, 2007). They can sequester selected membrane components within the plasma membrane but also occasionally undergo scission to form vesicles within the cell. Macropinocytosis is the process of membrane ruffling driven by actin, generating vesicles called macropinosomes. Generation of macropinosomes drives the bulk uptake of extracellular fluids and the plasma membrane. The fate of macropinosomes may vary based on how the macropinocytosis was induced and the type of cell. In some cells, macropinosomes can acquire markers of early and late endosomes, following a canonical endocytic pathway. In other cells, they can be recycled to the cell surface (as reviewed in Johannes et al., 2015; Mercer &

Helenius, 2009). Some viruses, including Ebola virus, vaccinia mature virion virus and herpes simplex virus 1, exploit macropinocytosis for internalization (Mercer & Helenius, 2009).

Clathrin-mediated endocytosis is a highly selective mode of endocytosis in which cargo selection and the stabilization of the pit are driven by coat proteins. The coordination of the stabilization, scission and uncoating of the pit is conducted in part by phospholipids, as will be discussed in greater detail in the next section. Inner coat proteins bind to lipids in the plasma membrane as well as particular sequences or motifs in receptors to be endocytosed. The inner coat proteins then concentrate proteins to be endocytosed in a discrete area of the cytoplasm. The adapter proteins may also play a role in generating curvature in the lipid bilayer via amphipathic helices, which create local membrane defects and can multiply curvature when numerous defects are in close proximity. An outer layer consisting of self-assembling clathrin subunits interacts with the inner layer to form a cage that coats the vesicle (Figure 1.2). The mechanistic role of the clathrin subunits is either to stabilize or generate vesicle curvature around the cargo. Actin polymerization plays a critical role in membrane deformation for pit enlargement and curvature generation (as reviewed in Kaksonen & Roux, 2018). Actin may play an especially important role when large cargo undergoes clathrin-mediated endocytosis (Cureton et al., 2010). The role of clathrin in the generation or stabilization of membrane curvature is highly debated in the field (Z. Chen & Schmid, 2020). The release of the clathrin cage encircling the vesicle is

coordinated via dephosphorylation of a lipid present in mature pits (phosphatidylinositol-4,5-biphosphate) and the action of the auxilin–HSC70 (heat shock cognate 71 kDa protein) complex. The vesicle may then fuse with early endosomes (Figure 1.2) (Cocucci et al., 2014; Kaksonen & Roux, 2018).

Some cellular receptors present in the plasma membrane and internalized by clathrin mediated endocytosis serve as viral receptors, allowing viruses to concentrate at sites of cargo internalization. One example of a viral receptor that undergoes clathrin mediated endocytosis is low-density lipoprotein (LDL) receptor, which acts as the receptor for vesicular stomatitis virus (VSV) (Finkelshtein et al., 2013; Fischer et al., 1993; X. Sun et al., 2005). VSV as well as other viruses and their receptors will be discussed at greater length in later sub-section of this chapter (see Enveloped Viruses and their Fusion Triggers).

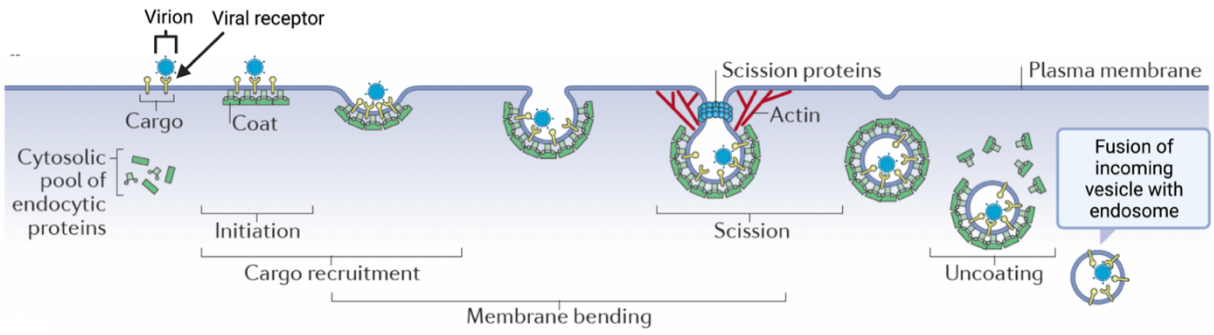

Figure 1.2. Clathrin-mediated endocytosis generates vesicles for the internalization of cargos, including viruses, from the plasma membrane of the cell. Clathrin-mediated endocytosis is a carefully regulated process allowing the concentration and endocytosis of cargo within coated vesicles. Viruses can bind to physiological cargo and exploit this pathway to internalization. The cytoplasmic domains of cargos can interact with coat proteins, both enabling the formation of the coat (initiation) and further concentration of receptors (cargo recruitment). The coat either mediates or stabilizes membrane bending (membrane bending). Dynamin at the neck of the vesicle (blue bead-like

structure) and pulling forces from the actin cytoskeleton help mediate scission. For large cargo, pulling forces from actin are especially important and large actin patches can form on vesicles. Following scission, the vesicle uncoats, permitting fusion with early endosomes and ongoing trafficking. Adapted from Kaksonen & Roux 2018.

1.4 Lipid Composition Provides Spatiotemporal Regulation

The maturation of endosomes within the endocytic pathway is largely regulated by the association of cytosolic proteins with the vesicles within the pathway; this process is coordinated by the presence of specific lipids within the membrane. Thus, lipids function indirectly as the major regulators of several processes key to endocytic maturation. The processes of fission and fusion of compartments in the endocytic pathway (Gautreau et al., 2014), the recruitment of machinery that creates vesicles within endosomes (Bissig & Gruenberg, 2013) and aspects of cargo sorting to degradative or recycling pathways (Diaz-Rohrer et al., 2014; Mayor et al., 1993; Mukherjee et al., 1999) are all lipid dependent processes. In addition, the activity of some endosomal ion channels is regulated by lipids (Q. Chen et al., 2017; Hirschi et al., 2017; Schmiege et al., 2017; She et al., 2018; X. Wang et al., 2012) and so lipids contribute to changes in ionic environment within the endocytic pathway with consequences for endosome function (Freeman et al., 2020).

Phosphatidylinositol (PI) is a relatively low-abundance lipid in cellular membranes comprising less than 1% of cellular lipids (as reviewed in Shewan et al., 2011) but is critical for regulating the assembly of protein complexes on cellular membranes (Gautreau 2014, Cullen and Steinberg 2018, Henne 2013)

as well as being responsible for activating ion channels (Q. Chen et al., 2017; Hirschi et al., 2017; Schmiege et al., 2017; She et al., 2018; X. Wang et al., 2012). The phosphorylation of the inositol head group of phosphatidylinositol results in several different isoforms each of which has a specific localization within cellular membranes. Phosphatidylinositol 4,5-biphosphate ($PI(4,5)P_2$) is primarily found at the plasma membrane. The numbers (4,5) designate the site of the phosphorylation on the lipid head group. Phosphatidylinositol 3-phosphate (PI(3)P) primarily resides in the early endosome membrane and in the membrane of ILVs (Gillooly et al., 2000), while Phosphatidylinositol 3,5-biphosphate ($PI(3,5)P_2$) is found on late endosomal membranes (Bissig & Gruenberg, 2013). Both PI(3)P and $PI(3,5)P_2$ are vitally important because they recruit Rab proteins (discussed in greater detail in a later section), which scaffold and regulate other proteins that allow endosomes to perform vital functions such as fuse with one another or associate with the cellular cytoskeleton. $PI(3,5)P_2$ is synthesized by the phosphorylation of PI(3)P by the kinase PIKfyve. PIKfyve binds PI(3)P and thus can associate with early endosomes (Huotari & Helenius, 2011). The exact mechanism or combination of mechanism by which PI(3,5)P production is coordinated with the overall maturation of endosomes is still under investigation, but scaffolding proteins, the autophosphorylation of PIKfyve and the dephosphorylation of PIKfyve by the protein/lipid phosphatase Fig4 all play roles in regulating PIKfyve lipid kinase activity (Lees et al., 2020; Sbrissa et al., 2007). The lipid turnover from PI(3)P to $PI(3,5)P_2$ may have such complex regulation

because key proteins in the endosome maturation process recognize these phosphoinositides, and thus phosphoinositides play a role in regulating the localization and timing of maturation events (Bissig & Gruenberg, 2013; Huotari & Helenius, 2011).

In addition to phosphoinositides, the lipids cholesterol and lysobisphosphatidic acid (LBPA) play important functional roles in endosome function and maturation. While LBPA makes up only a small portion of cellular lipids, it is highly abundant in the late endosome where it can make up to 15-20 mole percent of all phospholipid content. LBPA may aid the generation of internal vesicles within the endosomal lumen with consequences for sorting (see *Cargo Sorting*) and also mark a specific subpopulation of these vesicles generated later in the endocytic pathway (Gruenberg, 2020). Late endosomes are an important location in the cell for cholesterol storage. Among other functions, late endosomal cholesterol stores are critical for regulating endosome motility (Huotari & Helenius, 2011). Interestingly, LBPA is critical for the regulation of late endosomal cholesterol stores and thus indirectly for cellular cholesterol homeostasis (Chevallier et al., 2008). In sum, the lipid composition of various compartments within the endocytic pathway is vital to the maturation and function of these compartments.

1.5 Cargo Sorting

While some cargo entering the cell is destined to be digested to its constituent parts and reused for metabolism, other cargo is eventually recycled

back to the plasma membrane. From the perspective of a virus that requires certain cues in the endocytic pathway to complete the entry process and undergo fusion with the host cell, recycling is an undesirable fate. There are many levels of control to ensure that proteins destined for degradation continue along the endocytic pathway to the endolysosome, while those that will be reused are recycled to the plasma membrane. This sorting process may begin at the plasma membrane, where specific adaptor proteins may concentrate specific cargo (Cao et al., 1998; F. Huang et al., 2004; Lakadamyali et al., 2006; Traub & Bonifacino, 2013). The concentration of cargo in areas of the plasma membrane can have downstream consequences for cargo sorting to specific subpopulations of early endosomes (Lakadamyali et al., 2006).

Early endosomes are heterogenous in membrane composition and cargo content. Some subpopulations of early endosomes mature faster than others. Subpopulations of endosomes that quickly advance to having the late endosomal marker Rab7 often contain cargo that is destined for degradation (Lakadamyali et al., 2006). Special subpopulations of endosomes may also play a role in cellular signaling (Kalaidzidis et al., 2015; Mao et al., 2006; Miaczynska et al., 2004). For example, APPL1 is a molecule that marks a specific population of early endosomes that is essential to modulating glucose uptake in response to signaling by the important metabolic hormone adiponectin (Mao et al., 2006). Differing populations of endosomes may help sort lipids incoming from the plasma membrane and receive specific kinds of lipid cargo preferentially (C. S.

Chen et al., 1997). Thus, very early sorting events whereby specific cargos are enriched first in discrete areas of the plasma membrane and then in specialized early endosomal subpopulations, act to both maintain important signaling pathways and ensure efficient cargo sorting.

Once incoming vesicles fuse with an existing early endosome (Kamentseva et al., 2020), cargo destined for recycling is sorted into a tubular region that extends from the spheroid central compartment of the endosome (Franke et al., 2019; Geuze et al., 1983, 1987). Molecules called sorting nexins recognize proteins to be recycled (Lucas et al., 2016; McNally et al., 2017). Sorting nexins recruit other molecules and complexes that eventually help promote scission of the tubular region to form a carrier. Retromer and Retriever are two key complexes that mediate the sorting of cargo to the trans-Golgi network and recycling endosomes respectively (McNally et al., 2017; Wassmer et al., 2009). Carriers containing protein for recycling may undergo fusion with the trans-Golgi network (TGN) or a recycling endosome act prior to eventual transit back to the cell surface (Cullen & Steinberg, 2018). The recycling of viruses back to the cell surface has been described in the literature (Owczarek et al., 2019; Poston et al., 2021; L.-J. Zhang et al., 2020), but it is not clear how common this phenomenon is or if the recycling process is related to the identity of the viral receptor.

Another level of control in the sorting process involves sequestering degradative cargo in vesicles internal to the endosome. Cargo that is destined for

degradation is sometimes marked with ubiquitin, which, alongside the lipid PI(3)P, is recognized by Endosomal Sorting Complex Required for Transport-0 (ESCRT-0). ESCRT-0 sequesters the degradative cargo such that it cannot diffuse into the tubular recycling region (Cullen & Steinberg, 2018). The dual binding of a ubiquitylated sequence and lipid by ESCRT-0 ensures that its activity is restricted to early endosomes. ESCRT-0 is one member of a complex, consisting also of ESCRT-1, 2 and 3, that generates membrane buds containing the cargo recruited by ESCRT-0. The topology of the process is the opposite of that depicted for clathrin mediated endocytosis in Figure 1.2; instead of pointing into the cytoplasm, these buds point away from the cytoplasm into the lumen of the endosome (Henne et al., 2013). The accumulation of ESCRT-3 at the neck of the bud and the consequent increase in the curve at the bud neck likely mediate vesicle scission with the assistance of VPS4. The role of VPS4 in mediating disassembly of ESCRT-3 for further use is well described but the mechanism by which it can help mediate vesicle scission has not been definitively demonstrated (Liese et al., 2020; Remec Pavlin & Hurley, 2020; Wollert et al., 2009; Wollert & Hurley, 2010). The vesicles generated within the endosomal lumen are called intraluminal vesicles (ILVs, as discussed above). While the majority of degradative cargo is contained in ILVs, away from any possibility of erroneous recycling, a minor fraction may not be captured and will remain in the limiting (and eventually lysosomal) membrane (Ukkonen et al., 1986).

Membrane microdomains, areas of lipids that are more or less fluid than surrounding areas, may also play an important role in cargo sorting, though the mechanisms and details of the process is under investigation. Cholesterol, sphingomyelin and phosphatidylserine are all enriched in recycling endosomes. Further, cholesterol and sphingomyelin strongly colocalize with cargo undergoing recycling (Gagescu et al., 2000). Both cholesterol and sphingomyelin are primary constituents of nanodomains or microdomains in lipid bilayers that are said to be ordered. These ordered domains have special biophysical properties and both saturated lipids and certain proteins tend to congregate within them (Sezgin et al., 2017). The mechanism of partitioning proteins into ordered domains may rely on the length, surface area, and palmitoylation (a lipid modification) of the transmembrane domain (TMD) of the protein (Lorent et al., 2017). Association with rafts has been shown to mediate the recycling of some proteins, which have longer TMDs, to the plasma membrane (Diaz-Rohrer et al., 2014). Thus, in addition to recycling mediated by sorting nexins, a lipid dependent pathway exists to recycle membrane proteins.

1.6 Endosome Fission and Fusion

The fission and fusion of endosomes is essential to maturation as well as the generation of vesicles carrying cargo to be returned to the cell surface or other organelles such as the TGN. Non-degradative sub-pathways within the endosomal system, such as recycling or transport to the TGN, must be protected from erroneously directing cargo toward degradation. Multiple levels of control

prevent degradative vesicles and the plasma membrane or early endosomes from fusing with one another. Both protein-protein and protein-lipid interactions determine which vesicles or organelles within the endocytic pathway may fuse. The multiple levels of recognition of the lipid and protein composition of the membranes of any two prospective fusion partners serves as “fusion proof-reading”. The recognition may be conducted by tethering factors that hold vesicles close enough together to fuse and may also be conducted by proteins recruiting the fusion machinery. While some aspects of what the minimal requirements are to mediate fusion between vesicles are debated (Gautreau et al., 2014), SNARE proteins are known to play a critical role in the final merger of the highly selected membranes (Jahn & Scheller, 2006).

Members of the Rab family of proteins are commonly used as markers for specific stages of endosomal maturation and can recruit proteins that modify the membrane in which they reside. Rabs can recruit the machinery that allows endosomal membrane fusion, making them a key regulator of endosomal maturation (Gautreau et al., 2014). Among the 66 Rab proteins known to be encoded within the human genome (Klöpper et al., 2012), the Rabs that have garnered the most attention in the endosomal system are Rab5 (associated with early endosomes), Rab7 (associated with late endosomes) and Rab11 (associated with recycling endosomes). This discussion will focus primarily on Rab5 and Rab7 because of their role in advancing the endosomal maturation program and the degradative pathway. Rab GTPases are soluble in their inactive

form when they are bound to Guanosine-5'-diphosphate (GDP) and membrane associated when in their active form bound to Guanosine-5'-triphosphate (GTP). A Guanine nucleotide-exchange factor (GEF) catalyzes the exchange of GDP (inactive) for GTP (active) while a GTPase-activating protein (GAP) can speed the hydrolysis of GTP and conversion back to an inactive state. The mechanism by which individual Rabs associate with specific membranes is still under investigation (Wandinger-Ness & Zerial, 2014). The membrane association of Rabs may be regulated in part by the localization of GEFs and GAPs that operate on individual Rabs, activating Rabs that are needed at a given compartment membrane and inactivating those that are not (Rivera-Molina & Novick, 2009).

The preparation of an endosome to undergo fusion can begin with Rab activity and the recognition of a Rab by proteins conducting endosomal membrane fusion. Once Rab5-GTP has associated with early endosomes, it can mediate interactions with PI(3)-kinase, allowing the production of PI(3)P, a defining lipid for early endosomes (Gautreau et al., 2014). The fusion-promoting protein Early Endosome Antigen-1 (EEA1) recognizes both PI(3)P and Rab5-GTP. Experiments using endosomes and cytosol to reconstitute fusion in vitro have shown EEA1 is capable of mediating endosome fusion on its own, but other cytosolic factors may regulate or promote fusion (Christoforidis et al., 1999). A tethering complex, Class C core vacuole/ endosome tethering (CORVET), may be required for fusion specifically when one member of the fusion pair is an

APPL1+ endosome (see *Cargo Sorting*) by bringing the endosomes into close proximity (docking). CORVET can then bind to SNARE proteins, a family of coiled-coil proteins that conduct essential membrane fusion events in the cell, which then directly mediate fusion between participating endosomes (Balderhaar et al., 2013; Perini et al., 2014). CORVET may play a different role in the case of EEA1+ early endosomes, acting as a complimentary tethering factor for EEA1 to enhance endosome-endosome docking rather than being strictly necessary for docking and fusion (Perini et al., 2014). CORVET possesses two binding sites for Rab5, which select for homotypic fusion (Peplowska 2007, Balderhaar 2013), further illustrating another level at which specific vesicles may be recognized for fusion. Homotypic fusion events may be an important step in the endosomal maturation program as the enlargement of Rab5+ compartments, presumably by fusion events, has been shown as the early endosomes accumulate increasing amounts of Rab5 prior to their maturation to late endosomes (Rink et al., 2005).

The switch from Rab5 to Rab7 is a critical step in the maturation of endosomes as Rab7 has a different set of effectors that advance the endosomal maturation program, including increasing motion and acidification. The inactivation of Rab5 requires activity of a GAP while activation of Rab7 requires a GEF (Gautreau et al., 2014). One hypothesized mechanism of Rab5/Rab7 exchange in mammalian cells is that a single complex, Sand-1/Mon1 and Ccz1, mediates the inactivation of Rab5 and recruitment of Rab7-GTP. Upon a critical concentration of PI(3)P, Sand-1/Mon1 may bind to the endosomal membrane

displacing the Rab5 GEF, Rabex-5, ensuring that when Rab5 hydrolyzes GTP to GDP, Rab5 will remain soluble. Further, Sand-1/Mon1 in complex with Ccz1 can act as a Rab7 GEF to promote Rab7-GTP binding (Borchers et al., 2021). Thus, Rab5-GDP dissociates and becomes soluble in a coordinated fashion with the association of Rab7-GTP with the endosomal membrane

Rab7 recruits a variety of proteins and complexes to the late endosomal membrane that further promote the endosomal maturation program. One such complex is homotypic fusion and protein sorting (HOPS), which has two Rab7 binding domains and serves to tether late endosomes and/or lysosomes together (Gautreau et al., 2014; Lürick et al., 2017). In addition to HOPS, homotypic fusion events require SNARE proteins (Mima et al., 2008; Stroupe et al., 2006, 2009). By mediating the assembly of heterotypic fusion machinery, Rab7-GTP may allow late endosomes to fuse with lysosomes, which are dense in hydrolytic enzymes, to form endolysosomes in which cargo degradation can take place. Rab7-GTP also interacts with Rab-interacting lysosomal protein (RILP), which indirectly mediates interaction with dynein, a plus-end directed motor protein that moves along microtubules and can facilitate translocation of endosomes to the perinuclear region (Gautreau et al., 2014), where in some cell types mature endosomes and endolysosomes primarily reside (D. E. Johnson et al., 2016). RILP also stabilizes the protein complex, vacuolar ATPase (V-ATPase), which acidifies endosomes, and thus Rab7 may also indirectly play a role in generating the endosomal pH gradient (De Luca et al., 2014).

Recycling events and the exit of cargo from the degradative pathway occur primarily by fission, in contrast to the fusion events that accompany the maturation of endosomes and progress of degradative cargo in the endocytic pathway. In early endosomes, recycling cargo is sorted into a tubular region, which then undergoes scission to form a vesicle holding cargo to be recycled. The scission event consists of two parts: constriction of the neck of the tubule and a pulling force on the tubule away from the main body of the endosome. The cytoskeleton is critical for these fission events as it provides pulling forces for the scission of the tubule into a vesicle (Gautreau et al., 2014). A protein complex, Wiskott Aldrich Syndrome protein and scar homologue complex (WASH), that promotes actin polymerization also restricts diffusion of proteins into and out of the tubular region of the endosome. In addition, WASH may be involved in recruiting dynamin, which provides constriction at the neck of the tubule. After or in concert with the constriction of the neck of the tubule, WASH activates actin-related proteins-2/3 (ARP2/3), which polymerizes actin on the tubule surface exerting a pushing force on the endosome surface (Derivery et al., 2009). Complexes involved in cargo sorting, including Retromer, which was discussed in a previous section, can then recruit motor proteins to the surface of the recycling tubule. These motor proteins exert opposing forces, pulling the tubule and endosome in opposite directions (Soppina et al., 2009; Wassmer et al., 2009), which along with constriction and a pushing force from actin may generate fission. Recently, ER-endosome membrane contact sites have been proposed to

mediate endosome fission at a step downstream of cargo sorting and sequestration, perhaps by binding of an ER-associated protein to an ESCRT complex interactor IST1 (increased sodium tolerance 1) and subsequent perturbations of the cytoskeleton at the fission site generating pulling or pushing (Allison et al., 2013; Hoyer et al., 2018).

1.7. The pH Gradient Within the Endocytic Pathway

The pH gradient within the endocytic pathway regulates key physiological processes including the degradation of cargo, the dissociation of recycling cargo from transmembrane receptors (Huotari & Helenius, 2011) and the generation of intraluminal vesicles (Perrin et al., 2021). While early endosomes start at a relatively modest pH of approximately 6-7, the concentration of protons in the late endosomes can be more than ten times higher at a pH of approximately 4.5-6, as pH is a log scale (Huotari & Helenius, 2011). The translocation of late endosomes to the perinuclear region is correlated with this drop in pH (D. E. Johnson et al., 2016).

Two main factors contribute to the pH in the late endosome: how quickly protons are pumped in and how quickly they leak out. The protein complex responsible for pumping protons into the lumen of the endosome is V-ATPase, which consists of two subcomplexes that are each themselves multiprotein complexes; V1 conducts ATP hydrolysis while V0 acts as the transmembrane proton pore. Several processes and factors regulate the activity of the V-ATPase. The V0 and V1 subunits must be assembled together for function. The rate at

which the two subunits associate, and can thus function, may be higher in the late endosome than in the early endosome (Lafourcade et al., 2008). Further, the overall ionic content of the lumen influences transporter efficiency since protons are positively charged and thus V-ATPase activity is electrogenic (Harikumar & Reeves, 1983). Positive charge must leave the endosomal lumen in the form of cations or anions must be internalized to permit the V-ATPase to continue functioning in driving acidification (Fuchs et al., 1989; Steinberg et al., 2010).

Even as the V-ATPase pumps protons into the lumen, though, some protons may leave the lumen via ion channels or transporters in a process termed “proton leak.” Solute carrier proteins (SLCs) are an important group facilitating proton leak as are cation-proton antiporters, which use the proton gradient to drive cations, especially sodium and potassium into the endosomal lumen (Chadwick et al., 2021). Late endosomes close to the plasma membrane are less acidic than endosomes found near the nucleus in some cell types. Endosomes in both locations were found to have similar levels of V-ATPase activity, but late endosomes near the plasma membrane had greater proton leak. Thus proton leak, not V-ATPase activity may be the primary determining factor in the pH of individual late endosomes (D. E. Johnson et al., 2016). Possible reasons for the “leakiness” difference between peripheral and perinuclear endosomes include differences in lipid composition leading to differential regulation of cation channels and antiporters as well as association with motor proteins and their effectors.

1.8. Tools to Study pH Within the Endocytic Pathway

As endosomes mature, pH decreases, thus pH can be an indirect way of measuring endosomal maturation. By attaching a pH sensor to cargo that is endocytosed, the kinetics of cargo uptake, passage through early endosome and localization in late endosomes can be crudely assessed. In addition to indicating the maturity of an endosome, the pH within compartments in the endocytic pathway can provide an overall readout as to the "health" of the endocytic pathway and state of the cell. For example, cancer cells can have different distributions of lysosomal pH as compared to healthy cells of the same kind (Webb et al., 2021) and endosomal acidification can play a role in neurologic disease (Bonam et al., 2019).

Most commonly used pH sensors exploit fluorescence to provide information about endocytic compartment pH. A sensor or sensors within the cell can be excited with one or more specific wavelength(s) of light. The intensity and/or wavelength of the light re-emitted from the sensor upon excitation then provides a readout for pH. Factors other than pH, including the concentration of the sensor and whether the sensor is slightly out of focus in fluorescence microscopy, can affect emission intensity. Ideally, a sensor provides two emissions, one that is insensitive to pH and one that is sensitive, allowing correction for non-pH variables that affect emission intensity (Canton & Grinstein, 2015). Sensors also come in two different modalities: exogenously introduced

(Canton & Grinstein, 2015) and genetically encoded (Benčina, 2013; H. Kim et al., 2021; Martynov et al., 2018).

Introduced sensors are dissolved in the medium in which cells under investigation are grown. Some of the sensor is endocytosed and ultimately localizes to endosomes. If the sensor is transiently introduced and then replaced with medium that does not contain the sensor, this pulse-chase experiment can be used to examine compartments sequentially as the sensor is allowed to traffic for varying amounts of time. With a sufficiently long chase period, the sensor localizes to the late endosome as confirmed by colocalization with a late endosomal antibody or fluorescent marker protein. Examples of sensors that are internalized via endocytosis include dextran fluorescent conjugates and fluorescent conjugates of physiological endocytic cargo such transferrin. A pH insensitive dye such as Texas Red or rhodamine can be conjugated to some molecules to be endocytosed and a pH sensitive dye such as Oregon Green or fluorescein isothiocyanate to others (Canton & Grinstein, 2015; Ma et al., 2017; Steinberg et al., 2010). This ensures that a ratio of the pH-sensitive and pH-insensitive probes can be taken to control for factors such as variation in the uptake of the probe(s). In addition to dye-conjugates, fluorescent weak bases are also commonly used to identify endosomes and, in some cases, can be used to provide a qualitative readout of acidification. Common examples of such reagents are LysoTracker© probes (Canton & Grinstein, 2015) and Acridine orange. These weakly basic dyes can cross cellular membranes but become

trapped in acidic organelles by protonation (De Duve et al., 1974). Because they can have toxic effects on the cell, can accumulate in non-endosome acidic organelles, and cannot be calibrated, these dyes are typically not used in applications where the quantitation of endosomal pH is desirable (Canton & Grinstein, 2015).

Genetically encoded pH sensors are advantageous because they can be specifically targeted to organelles and a wide variety of pH sensitivities is achievable based on the constituent member proteins in the sensor. Targeting is achieved by the expression of a fluorescent protein or proteins as a chimera with a protein resident in the target compartment (Benčina, 2013). A single protein can be used (D. E. Johnson et al., 2009) or a pair of proteins with differential pH sensitivities to provide a ratiometric readout (Tanida et al., 2014). In some cases, a single protein can provide a ratiometric readout due to a spectral shift in emission intensity depending on pH (Mahon, 2011; Miesenböck et al., 1998). A key consideration in the use of genetically encoded pH sensors is the potential for heterogenous expression levels between cells, meaning not all cells provide a uniformly interpretable readout. Potential mis-localization of the probe is also a caveat if the probe is highly overexpressed. Overall though, the modular design of genetically encoded pH sensors, with tunability of both localization and pH sensitivity, provides a powerful tool for measuring pH in both the endocytic pathway and other organelles.

Both endocytosed and genetically encoded sensors can be used for quantitative evaluation of endocytic pH. To determine a pH value, sensors are calibrated by selective introduction of a buffer of a known pH (Canton & Grinstein, 2015; Ma et al., 2017). To allow the lysosomal pH to equilibrate with the buffer of known pH, cellular membranes can be selectively permeabilized to certain ions using molecules known as ionophores such that the intralysosomal pH is intentionally adjusted. Nigericin, a potassium/proton exchanger (Graven et al., 1966) is a commonly used ionophore that permits equilibration of potassium and protons across the lysosomal membrane (Canton & Grinstein, 2015; Steinberg et al., 2010). It is sometimes used in combination with monensin, a sodium selective ionophore (Cussler et al., 1971; D. E. Johnson et al., 2016). Once the lysosomal pH has equilibrated with the buffer of a known pH, individual cells can be imaged and the fluorescence from the pH probe correlated to a given pH for a number of pH conditions, generating a calibration curve. The pH of an individual cell or set of cells in the experimental condition can then be calculated from the calibration curve and the experimental fluorescence data (Canton & Grinstein, 2015).

Fluorescence from pH sensor(s) can be read over many cells using a plate reader device that measures collections of cells in a single well (Ma et al., 2017), for many individual cells using flow cytometry (Nilsson et al., 2004), or in specific regions or compartments of a single cell using fluorescence microscopy (Canton & Grinstein, 2015). While plate reader measurements are relatively easy

to conduct from a technical perspective and provide the advantage of averaging over many cells in the measurement itself, it is not possible to exclude from measurement cells that are either dead or provide other erroneous signals (Ma et al., 2017). Flow cytometry offers a high-throughput method and the opportunity to exclude dead cells, but not to measure endosomes individually (Nilsson et al., 2004). Theoretically, a recent technology that combines flow cytometry and microcopy (ImageStream, Amnis) could allow the measurement of individual compartments; though in the technology's current state of development, achieving the resolution in three dimensions needed to examine selected endosomes within a non-adherent cell would be challenging or impossible. Fluorescence microscopy can be relatively low throughput compared to a plate reader or cytometer, but offers the ability to differentiate individual endosomes (D. E. Johnson et al., 2016) and exclude cells that are dead or may otherwise provide erroneous data (Canton & Grinstein, 2015).

1.9 An overview of viral entry, replication and budding

Viruses are essentially tiny parasites. They cannot replicate on their own and they consist simply of proteins and nucleic acid sequences and, for some, lipids. Viruses exploit host cell proteins and energy derived from the host cell to make copies of themselves. To a virus, every cell that it is capable of invading is a potential copy machine. While it is not advantageous for the virus to kill its host, viruses pathogenic to humans constitute a grave public health burden. A single virus, Respiratory Syncitial Virus (RSV) killed an estimated 118,000 children

globally in 2015 alone (Srikantiah et al., 2021). Viruses do not just affect human health; they also can infect plants, animals and bacteria as well. These tiny machines (typically ranging from 20-100nm in size) are mighty for their size (Louten, 2016).

For animal cells the plasma membrane acts as a barrier, dividing the genetic material, proteins and chemical reactions in the cytoplasm from the wide world of the extracellular space. The plasma membrane, like any other biological membrane, consists of a lipid bilayer containing proteins. The lipids and proteins act as both curators and messengers (Dias & Nylandsted, 2021). Channels allow ions to enter and exit the cell (Brini & Carafoli, 2011). Receptors on the plasma membrane communicate signals from outside the cell to the cytoplasm, initiating necessary physiological changes for processes such as cell proliferation (Hilger et al., 2018). To infect cells, viruses must breach this division between outside the cell and inside to seed their functional components into the cytoplasm. While some viruses are able to enter the cell directly at the plasma membrane other viruses must enter through intracellular compartments with particular characteristics (Dimitrov, 2004; Hernandez-Gonzalez et al., 2021; J. M. White et al., 2016). Once the virus has entered the cell cytoplasm, it can replicate using host resources to copy its own viral genome and produce viral proteins. Assembly of genetic material and viral proteins occurs at a host membrane. Finally, viral particles exit the cell by budding from the plasma membrane or

exocytosis. Enveloped viruses are defined by the host membrane they acquire upon budding (Figure 1.3) (Hernandez-Gonzalez et al., 2021).

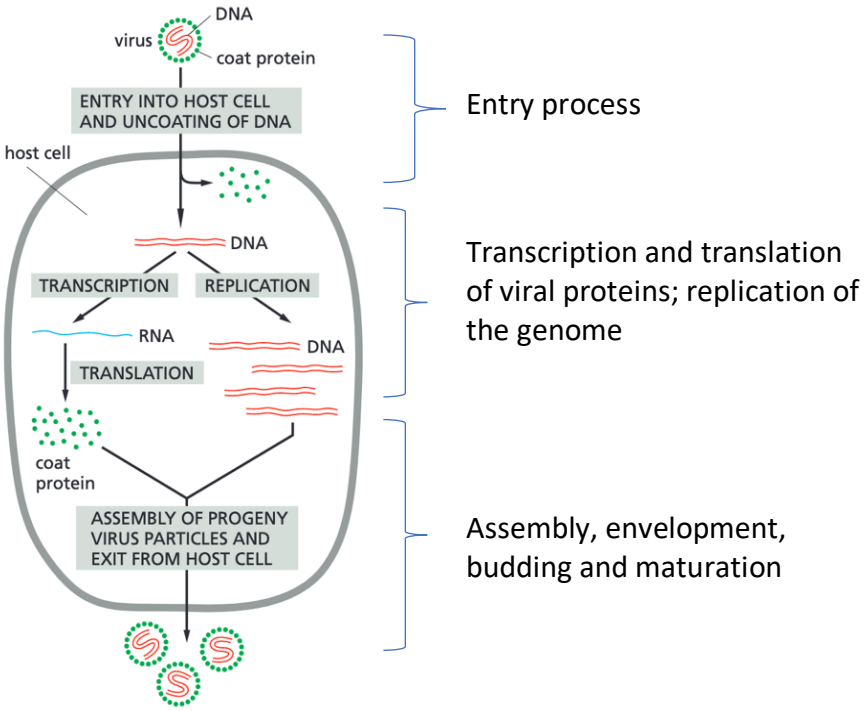

Figure 1.3. The viral entry and replication cycle. Viruses require host proteins to replicate. To access the host machinery mediating transcription and translation, the viral contents must enter the cell. In the illustrated example, the viral genome consists of DNA. A similar process occurs if the viral genome consists of RNA but one or more additional steps are required. For viruses with RNA genomes, an RNA-dependent RNA polymerase or reverse transcriptase is necessary to produce mRNA for translation or circular DNA. In either case, the mRNA encoding viral proteins is used as a template for host ribosomes to produce viral proteins. These viral proteins then assemble and bud to produce a new virion. Prior to or after exit from the cell, these virions may undergo processing events that enable them to infect additional cells. Adapted from Alberts *et al.*, *The Molecular Biology of the Cell*.

Viral Entry

To understand the necessity for some viruses to reach a special compartment to breach the lipid bilayer that protects the cell, we must first

examine the component parts of the virus and their functions. On the surface of the virus are the viral entry and fusion protein(s), which interact(s) with the host cell. Viral entry proteins are also sometimes known as glycoproteins because of the numerous glycosylations (or sugar molecules) that they bear. The interaction of the viral entry protein with host proteins or lipids at the cell surface allows the virus to bind to the cell. Conformational changes of the entry and fusion protein generate the energy required to bring together the viral envelope and the host lipid bilayer that separates the cytosol from the outside world (Dimitrov, 2004). These conformational changes require both the priming and triggering of the fusion protein. During priming, which may occur in the Golgi during particle production (Roby et al., 2015), in the extracellular space (Hoffmann et al., 2020) or in an endocytic compartment (Schornberg et al., 2006), the fusion protein is converted into a fusion competent state. For some viruses, priming may require multiple steps that occur in multiple stages during the maturation of viral particles before they exit the host cell and after viral particles have been internalized. Once primed, the viral fusion protein can be triggered via a cue that allows the viral fusion protein to insert in the host membrane; in some cases this cue is low pH within a compartment in the endocytic pathway (Figure 1.4)(J. M. White et al., 2016). Details of the endocytic pathway and how the pH gradient, host factors and ionic milieu act as triggering cures will be discuss in a later section of this introduction.

To trigger fusion between viral and host membrane, the viral fusion protein must first insert into the host membrane. The insertion requires an extended conformation of the fusion protein (J. M. White et al., 2016). A sequence of 20-30 amino acids known as the viral fusion peptide directly mediates interaction of the viral fusion protein with the host membrane. The structure of these peptides and their interaction with membranes are well studied for a number of viruses (Freitas et al., 2011; Ghosh et al., 2000; Gregory et al., 2011; Han et al., 2001; Harter et al., 1989; Y. Li & Tamm, 2007; Melo et al., 2009; Mendes et al., 2012; Smith et al., 2012). In at least two cases, structural evidence directly shows that low pH induces the exposure of the fusion peptide and insertion of the fusion peptide into the host lipid bilayer (Gregory et al., 2011; Han et al., 2001; Lorieau et al., 2012). After insertion into the target membrane, the fusion protein folds back to bring the host and viral membrane into close apposition with the two membranes merging once they are forced close enough (Figure 1.4) (Chernomordik et al., 1998; Kozlovsky et al., 2002; Tatulian et al., 1995). The formation of an individual fusion pore and its expansion may require multiple fusion proteins (Danieli et al., 1996; Floyd et al., 2008). Once the fusion pore is sufficiently large, the viral contents may pass into the cytoplasm, permitting viral replication to begin.

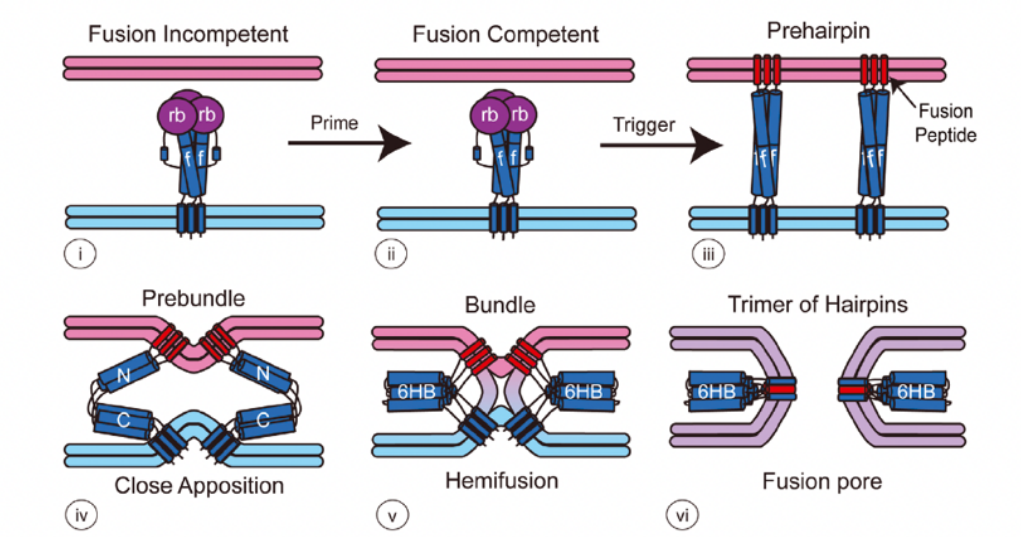

Figure 1.4. **The viral fusion protein mediates the close apposition and merging of virus and host membranes.** Prior to fusion, the viral entry protein (depicted in dark blue [f- fusion subunit] and purple [rb- receptor binding domain]) must undergo a priming step which confers fusion competence to the viral entry protein. Often the priming step is a proteolytic cleavage of the viral entry protein. Once the entry protein is in the presence of necessary factors, the fusion peptide is exposed and can interact with the host membrane (red bilayer). The entry protein then undergoes a conformational change bringing the host membrane and viral membrane (blue) into close proximity until the inner leaflet of the host membrane and outer leaflet of the viral membrane are contiguous (hemifusion). The event can then progress to full fusion in which a fusion pore forms making the inner space of the virus and host cytoplasm contiguous. With formation of a large enough fusion pore, viral contents pass to the cytoplasm completing the entry process. Adapted from White 2016.

Viral Replication

All viruses have structural elements that constitute the viral core underlying the viral envelope and glycoprotein. These repeating subunits of protein often form a spherical shape. More rarely the favored geometry for protein assembly may result in a bullet-shaped or filamentous virus. The primary function of structural proteins is to protect the genetic material inside the virus (Louten, 2016). The genetic material is the blueprint for viral replication and can

consist of negative sense ribonucleic acids (RNA), positive sense RNA, or deoxyribonucleic acids. Facilitating the replication of the genetic code are the RNA or DNA polymerases carried by the virus. The virus then relies on host cell ribosomes to translate the viral genetic material to make new viral proteins (Louten, 2016). Once the viral proteins have been produced, four main steps occur to make a new virion: assembly, envelopment, budding and maturation (Figure 1.3). During assembly, the structural proteins that make up the viral core and other parts of the virus, like the genetic material and polymerases, come together. For enveloped viruses, this assemblage is then is coated with the host membrane (envelopment). To allow budding of the virion and its subsequent release from the cell, either at the plasma membrane or via the secretory pathway, the enveloping membrane must be severed. The virion is then a complete unit and undergoes additional changes (maturation) to become infectious. These changes could involve proteolytic events or other rearrangements of different viral subunits (Rheinemann & Sundquist, 2021). Once the virion is mature it can go on to infect other cells and continue the cycle of entry and replication (Figure 1.3).

1.10 Enveloped viruses and their fusion triggers, including pH

Viral entry proteins are encoded by the viral genome, and viral genome relatedness is used to divide viruses into families and genera (Kuhn, 2021; Louten, 2016). Thus, though viral entry proteins are unique to each virus, there are frequently closely related viruses that have entry proteins with similar

structure and interacting host factors. The viral entry protein, entry pathway and fusion triggers for several families of virus will be described in order to better contextualize the importance of the endocytic pathway and pH in triggering fusion of the viral and host membranes.

Rhabdoviridae: vesicular stomatitis virus

The family *Rhabdoviridae* is made up of two genera of negative sense RNA viruses, *Lyssavirus* and *Vesiculovirus*. The primary human pathogen in the genera *Lyssavirus* is rabies, which is broadly distributed geographically, and if the infection is left untreated typically causes death. For obvious reasons, rabies cannot be studied without special biosafety precautions and is rarely used as a model virus for laboratory studies (Rupprecht & Bleck, 1997). Vesicular stomatitis virus (VSV) is a commonly used model virus that primarily infects livestock (Liu et al., 2021) and is a member of the genera *Vesiculovirus* (Rupprecht & Bleck, 1997). VSV is a commonly used model because it can be used with biosafety protections available to most laboratories (Liu et al., 2021) and has been considered to have a relatively simple, pH-dependent fusion trigger without requiring any preceding proteolytic cleavage events of the viral entry protein.

The viral entry protein of VSV, glycoprotein (G protein), forms a trimer (as reviewed in E. Sun et al., 2013) which binds to LDL receptors at the cell surface, mediating attachment and ensuring that the virus is endocytosed (Finkelshtein et al., 2013; Fischer et al., 1993; X. Sun et al., 2005). The virus is trafficked to a

sufficiently acidic compartment, where the G-protein undergoes a series of conformational changes from an inactive state, to an extended state that interacts with the viral membrane (low-pH triggered active conformation), to a stable post-fusion state that is antigenically distinct from the inactive and active states (Roche et al., 2006, 2007; E. Sun et al., 2013). G-protein is distinct among other viral entry proteins due to the reversibility of the transition between inactive and active states (E. Sun et al., 2013). Low pH is sufficient to trigger membrane fusion mediated by G-protein, but several G-protein trimers are likely needed to mediate virus-host membrane fusion and opening of the fusion pore (illustrated in Figure 1.4) (I. S. Kim et al., 2016). The exact pH reported to trigger the host membrane association or membrane fusion mediated by G protein varies widely in the literature (Beilstein et al., 2020; Carneiro et al., 2001; Eidelman et al., 1984; Fredericksen & Whitt, 1995; J. White et al., 1981). All currently reported values are in reconstituted systems, rather than measured in whole cells. Moreover, the pH values determined may vary based on the component parts of the reconstituted system.

Historically, G protein was assumed to mediate the fusion of VSV with the limiting membrane of the endosome, permitting the virus to infect cells directly from the endosome (Superti et al., 1987). More recently though, VSV was shown to fuse with ILVs in the endosomal lumen as an additional mechanism of entry. After G protein mediates the fusion of VSV with ILVs, the viral nucleocapsid is contained within the ILV. Upon reaching a late compartment of the endocytic

pathway, the ILV can undergo retrofusion with the limiting membrane, allowing the viral contents to enter the host cytoplasm (Le Blanc et al., 2005). A similar mechanism of fusion has been proposed in another family of viruses, *Flavivirus* (Nour et al., 2013). The process of ILV retrofusion occurs even in the absence of virus (Perrin et al., 2021) and relies on the low pH and lipid composition, especially LBPA content, found in late endosomes or endolysosomes (Amini-Bavil-Olyaee et al., 2013; Le Blanc et al., 2005; Perrin et al., 2021).

Arenaviridae: Lassa virus and lymphocytic choriomeningitis virus

The family *Arenaviridae* is made up of two genera of viruses: *Mammarenavirus* and the genus *Reptarenavirus*. *Mammarenaviruses* infect mammals and are further divided into Old World and New World arenaviruses. The Old World arenavirus Lassa (LASV) causes hemorrhagic fever, infecting approximately 300,000 people per year. The New World arenavirus Lymphocytic Choriomeningitis virus (LCMV) infects children and immunosuppressed individuals. Because LCMV is typically not dangerous to healthy adults, it is a commonly used virus to infect mice and conduct immunology and virology studies (Hallam et al., 2018).

The entry protein for all arenaviruses is a trimer of heterotrimeric proteins and requires multiple proteolytic cleavage events to be primed to fusion competence. Each protein in the heterotrimer has a specific function: one interacts with the host receptor (GP1), one drives fusion of the host and virus

membranes (GP2), and another, the stable signal peptide, is essential for the incorporation of the entry protein into viral particles (Hastie & Saphire, 2018; Kunz et al., 2003). For the arenavirus to be internalized, first GP1 must interact with the host receptor. For LASV the host cell-surface receptor is a sugar moiety attached to the protein alpha-dystroglycan (Cao et al., 1998). Once internalized, LASV switches to bind to the endosomal protein LAMP1, which acts as the endocytic receptor for the virus (Jae et al., 2014). LCMV also uses alpha-dystroglycan as a receptor (Cao et al., 1998; Rojek et al., 2008a). The internalization of LCMV is dependent on intracellular cholesterol concentrations but not clathrin-mediated endocytosis or caveolin (Rojek et al., 2008a), whereas LASV has been described to be internalized via micropinocytosis or a clathrin-mediated endocytosis like mechanism (Fedeli et al., 2020; Oppliger et al., 2016; Vela et al., 2007). The transition of arenavirus entry proteins from a pre-fusion state to post-fusion state is triggered by low pH. This transition is irreversible in contrast to VSV (Hastie & Saphire, 2018). In the case of LASV, the endosomal receptor LAMP1 allows fusion to be triggered at a higher pH. Theoretically, this enables escape from the endocytic pathway earlier than the virus would escape in the absence of the receptor (Hulseberg et al., 2018).

Filoviridae: Ebolavirus

The family *Filoviridae* consists of six species of *Ebolavirus*, one species of *Marburg virus*, and one species of *Cuevavirus*, which is more distantly related (H.

Feldmann et al., 2013; T. Goldstein et al., 2018). Ebola ebolavirus (EBOV, formerly Zaire ebolavirus) is notable for its pathogenicity in humans, resulting in significant outbreaks in West Africa between 2013 and the present, 2021 (Jacob et al., 2020). EBOV contains two nucleoproteins, two polymerase complex proteins, a nuclocapsid associated protein (VP24), a matrix protein (VP40), and a glycoprotein (GP) (Watt et al., 2014). These viral proteins are encoded in a negative sense RNA genome. The GP protein protrudes from the cell-derived virus membrane and acts as the entry and fusion protein (H. Feldmann et al., 2013). Furin cleaves GP post-translationally to produce two polypeptide chains: GP1 and GP2 (Volchkov et al., 1998). Fusion is mediated by GP2, which contains an internal hydrophobic fusion loop that, when exposed by low pH and association with necessary host factors, mediates interaction with the host membrane (Adam et al., 2004; Gregory et al., 2011). Due to the high pathogenicity of EBOV it is often studied using pseudoviruses or virus-like particles, a model system that is not pathogenic. Pseudoviruses have structural proteins derived from a non-filamentous virus (typically VSV or a retrovirus) but bear the EBOV GP. Virus-like particles use the structural protein of EBOV, VP40, such that the virus has a filamentous morphology and also bears the EBOV GP. In both cases, the viral genome and other machinery essential for viral replication is absent. Both pseudosviruses and virus-like particles bearing EBOV GP have similar kinetics of infection (Mingo et al., 2015).

EBOV GP can attach to a broad range of factors at the cell surface and is taken into cells by macropinocytosis. Following macropinocytosis, EBOV is enclosed in vesicles that can acquire early endosomal proteins such as Rab5 (Mercer & Helenius, 2009). EBOV is then trafficked to a late endosomal compartment where GP1 can interact with a host factor, Niemann Pick disease type-C1 protein (NPC1) (Mittler et al., 2021; Simmons et al., 2016; Spence et al., 2019). NPC1 is a transmembrane, cholesterol export protein, which receives cholesterol from the soluble lysosomal protein NPC2. GP1 interacts with NPC1 at the same site as NPC1's physiological partner, NPC2 (X. Li et al., 2016). However, the cholesterol exporting function of NPC1 is not required for it to act as the receptor for EBOV (Miller et al., 2012), leading to speculation that the function of NPC1 in EBOV entry is to position GP2 for fusion or to permit additional cleavage events in GP.

During trafficking, EBOV GP must undergo proteolytic cleavage events to render it fusion competent. Required proteases include cysteine proteases cathepsins B and L (Chandran et al., 2005; Schornberg et al., 2006). There are some data to suggest additional proteases and cleavage events may be required, but these additional proteases have not been discovered to date (Fénéant et al., 2019). Low pH triggers interaction of the fusion loop with the host membrane (Adam et al., 2004; Gregory et al., 2011). The fusion loop is most active below pH 5.5 as determined in reconstituted systems (Gregory et al., 2011; J. Lee et al., 2017). The full-length GP has been shown to be stabilized by

low pH in the absence of receptor and other cellular factors. As a stable conformation would likely prevent the GP from mediating fusion, this suggests that, in the context of the full-length protein, low pH must be combined with other factors to trigger fusion (Bortz et al., 2020). Calcium has also been suggested to promote fusion either directly or by enhancing the binding of GP to the host receptor NPC1 (Das et al., 2020; Nathan et al., 2019). Despite much debate in the field over mechanistic roles of host factors, there is general agreement that, in addition to NPC1, host cell proteases, late endosomal ion channels (controlling pH and calcium levels) and host factors involved in endosomal trafficking and maturation are all required to enable EBOV to fuse with the host membrane and enable content release. This common set of factors is required for all ebolaviruses even though the GP sequence differs slightly between individual ebolavirus species (Hoffmann et al., 2016).

Retroviridae: Avian sarcoma leukosis virus

Avian sarcoma leukosis virus (ASLV) is an alpha retrovirus. Retroviruses replicate by infecting cells and achieving the integration of their viral genome into the host genome. From within its site in the host genome, the transcripts for viral proteins are generated. ASLV infects birds and causes lymphoma. ASLV is commonly used as a retrovirus model that is non-pathogenic to humans. Its entry and fusion protein, Envelope (Env) can belong to a variety of viral subgroups (A-E) that individually can interact with one of three different receptors, TVA, TVB or

TVC. TVA is a LDL-receptor family related molecule, with an extracellular domain that shares sequence identity with the LDL-A module and binds to ASLV Env. TVB is a member of the tumor necrosis factor receptor (TNFR) family (as reviewed in Barnard et al., 2006). TVA is of special interest because it has two isoforms, one with a transmembrane domain (TVA950) and one that is lipid anchored (TVA800) (Bates 1993). ASLV is known to be trafficked into the endocytic pathway, where a pH of ~6.0 triggers fusion (Delos et al., 2010; Desai et al., 2017; Melikyan et al., 2005; Padilla-Parra et al., 2012). While the transmembrane receptor undergoes clathrin-mediated endocytosis to be internalized and trafficked to the fusion site, the lipid anchored receptor undergoes a form of lipid-raft dependent endocytosis (Gray et al., 2011; Narayan et al., 2003). Both isoforms of the TVA receptor have been shown to have differing characteristics of trafficking and fusion. When ASLV is allowed to infect lines of cells expressing only one TVA isoform, TVA950, ASLV is about equally likely to fuse within endosomes that move fast or slowly. In contrast, when cells express TVA800, ASLV is more likely to fuse within endosomes that move slowly. In addition, the fusion pore expands more rapidly when the virus fuses in the cell line expressing the transmembrane receptor (Padilla-Parra et al., 2012). These sub-populations of endosomes will be discussed in greater detail in the section that follows and in Chapter 2.

1.11 Endosomal sub-populations in viral entry

Trafficking through the endocytic pathway allows some viruses to reach compartments with the necessary conditions for fusion and, as in the case of EBOV, undergo critical processing events. Sub-populations of early endosomes, the first compartment many viruses encounter after internalization, can mature at differing rates. Influenza virus is preferentially sorted to endosomes that rapidly acquire Rab7, a marker of later more acidic endosomes (Lakadamyali et al., 2006). Influenza virus is a member of the family *Orthomyxoviridae* and is triggered to fuse by pH in the range 5.0-5.7, depending on the strain of influenza (Gerlach et al., 2017; J. White et al., 1981). Lower pH can result in more efficient fusion (Floyd et al., 2008), perhaps because at lower pH more fusion proteins are active. This increases the chance that proximal viral fusion proteins will simultaneously activate, allowing efficient formation of a fusion pore (Otterstrom et al., 2014). Preferential sorting of influenza virus into faster maturing endosomes that reach low pH more quickly may reduce the virus' time to fusion and allow it to infect cells more efficiently. The only other virus that has previously been studied with respect to sorting to subpopulations of endosomes is ASLV. In contrast to the preferential sorting of influenza, ASLV sorts to static and dynamic endosomes in proportion to the abundance of those endosomes (Padilla-Parra et al., 2012). While limited data are available about the mechanism for sorting of ASLV or influenza in specific endosomal subpopulations, physiological cargos may shed some light on the matter. Preferential sorting of

LDL and transferrin to subpopulations of early endosomes originates at the plasma membrane by clustering of the cargos in separate clathrin-coated pits (Lakadamyali et al., 2006).

In addition to subpopulation of early endosomes, there may be multiple sub-pathways within the degradative track of the endosomal system. Viruses may exploit these sub-pathways enabling them to bypass innate immune factors or to enter cells even under unfavorable conditions. The host cell possesses innate immune defenses, some of which reside in the endocytic pathway. Interferons, powerful proteins released by immune cells in the setting of infection, can enhance the expression of viral restriction factors including interferon-inducible transmembrane proteins (IFITMs). IFITM molecules consist of two hydrophobic domains linked by an intracellular domain (as reviewed in Perreira et al., 2013). The topology of IFITMs has been debated (Perreira et al., 2013), but whether the hydrophobic domains are transmembrane or merely embedded in the membrane may depend on the membrane in which the molecule is located (F. Sun et al., 2020). Recent data suggest that the membrane orientation of IFITMs is important as they restrict viral infection by perturbation of the host membrane, blocking expansion of the viral fusion pore and preventing content release (Guo et al., 2021). An additional mechanism of function may be accelerating the trafficking of certain viruses to endolysosomes, potentiating their degradation (Spence et al., 2019). A selection of viruses restricted by IFITMs includes vesicular stomatitis virus, influenza virus and filoviruses (Perreira et al.,

2013; Suddala et al., 2019). New World arenaviruses LASV and Junin virus are known to escape restriction by IFITMs even though like influenza and filoviruses they fuse late in the endocytic pathway (Brass et al., 2009; Suddala et al., 2019). Data show that these viruses primarily colocalize with the isoform of IFITM that predominates in late endosomes, IFITM3, after fusion of host and virus membranes (Spence et al., 2019; Suddala et al., 2019), furthering the possibility that these viruses escape host immune restriction by passing through a special trafficking pathway and/or targeting to a special subset of late endosomes. There remains much work to be done in understanding how and whether specific viruses are sorted to particular pathways, and the advantages that certain pathways may confer to the virus.

1.12 Summary

The endocytic pathway begins at the cell surface and consists of compartments that mature and undergo fusion and fission events. Each compartment of the endocytic system has its own membrane composition and luminal environment. Via a complex series of mechanisms with multiple checks and balances, cargo is targeted for recycling to the plasma membrane, degradation or trafficking to other cellular compartments. Enveloped viruses have proteins on their surface that can bind host receptors at the plasma membrane and, once the virus has encountered appropriate conditions within the endocytic pathway, mediate a fusion event that delivers the virus into the cytoplasm,

causing the cell to become infected. Low pH is an important trigger for the fusion of many viruses. Various probes can be used to measure pH in the endocytic pathway and in the environment of the virus as it is trafficked. Viruses can take unique routes through the endocytic pathway or be targeted to special sub-populations of compartments that may confer the advantage of more efficient fusion or avoidance of host immune factors. In the next chapters, I will describe the development of a novel fluorescent pH probe, the optimization of another, and the use of these probes to better understand critical aspects of viral trafficking and fusion.

Chapter 2. Endosomes supporting fusion mediated by vesicular stomatitis virus glycoprotein have distinctive motion and acidification

Maya Cabot, Volker Kiessling, Judith M White, Lukas K Tamm

Traffic. 2022; 23(4): 221- 234. doi:10.1111/tra.12836

2.1 Abstract

Most enveloped viruses infect cells by binding receptors at the cell surface and undergo trafficking through the endocytic pathway to a compartment with the requisite conditions to trigger fusion with a host endosomal membrane. Broad categories of compartments in the endocytic pathway include early and late endosomes, which can be further categorized into subpopulations with differing rates of maturation and motility characteristics. Endocytic compartments have varying protein and lipid components, luminal ionic conditions and pH that provide uniquely hospitable environments for specific viruses to fuse. In order to characterize compartments that permit fusion, we studied the trafficking and fusion of viral particles pseudotyped with the vesicular stomatitis virus glycoprotein (VSV-G) on their surface and equipped with a novel pH sensor and

a fluorescent content marker to measure pH, motion, and fusion at the single particle level in live cells. We found that the VSV-G particles fuse predominantly from more acidic and more motile endosomes, and that a significant fraction of particles is trafficked to more static and less acidic endosomes that do not support their fusion. Moreover, the fusion-supporting endosomes undergo directed motion.

2.2 Introduction

Viruses infect host cells after binding to host receptors at the cell surface. For most enveloped viruses, infection requires internalization and trafficking through the endocytic pathway. Receptor binding occurs via glycoproteins on the viral surface and conformational changes of these proteins mediate fusion between the viral and host membranes, leading to infection. Some viruses fuse early in the endocytic pathway, while others must be trafficked to late endosomes to encounter conditions required to trigger fusion. These may include processing by proteases, binding to endosomal receptors, as well as favorable conditions of pH, lipid composition, and ionic milieu (J. M. White et al., 2016). Late endosomes are more acidic than early endosomes, and endo-lysosomes and lysosomes are more acidic still. In addition, each progressively more acidic compartment in the pathway has its own lipid and protein components (Huotari & Helenius, 2011). In many cases endosomal pH is the primary fusion trigger, though in some cases there are other essential triggers (J. M. White et al., 2016). Viruses that fuse in

late endosomes include influenza virus and lymphocytic choriomeningitis virus (Pasqual et al., 2011; J. M. White et al., 2016). In contrast, Semliki forest virus (Kielian et al., 1986) and avian sarcoma and leukosis virus (ASLV) fuse in early endosomes (Padilla-Parra et al., 2012).

Early endosomes can be further distinguished as subpopulations with differing characteristics (Kalaidzidis et al., 2015; Perini et al., 2014) and rates of maturation (Lakadamyali et al., 2006). These subpopulations can be important for cargo sorting and fate. While some cargos preferentially sort into faster-maturing and more motile “dynamic” early endosomes, other cargos are preferentially sorted to more slowly maturing and less motile “static” early endosomes (nomenclature as per (Lakadamyali et al., 2006). Influenza virus is preferentially sorted to a subset of motile endosomes (Lakadamyali et al., 2006). In contrast, ASLV non-preferentially sorts to static and dynamic endosomes in proportion to the abundance of those endosomes while reportedly preferentially fusing with less motile, slow-moving compartments in a cell line expressing TVA950, the transmembrane form of the ASLV receptor (Padilla-Parra et al., 2012). Hence among viruses studied with respect to trafficking through subpopulations of endosomes, one virus (influenza) has been reported to preferentially sort to dynamic endosomes, while the other (ASLV) has been reported to preferentially fuse in static endosomes. This stark difference led us to ask whether particles bearing the glycoprotein of another virus, i.e., vesicular stomatitis virus (VSV), fuse in dynamic or static endosomes. We addressed this

question by single particle fluorescence microscopy correlating fusion with the pH state and motility of endosomes in live cells. We also characterized the fate of non-fusing particles. Although we chose to study trafficking and fusion directed by the well characterized VSV glycoprotein (Carneiro et al., 2001; Roche et al., 2006, 2007) as a model, the methods developed in this work should be applicable to study trafficking and fusion of other enveloped viruses at the single particle level in live cells.

VSV is an enveloped virus commonly used as a model for the study of the trafficking and fusion of enveloped viruses. It is a member of the family *Rhabdoviridae*, primarily causes acute illness in hoofed animals, and can cause mild symptoms in humans (Liu et al., 2021). Cell entry and fusion of VSV is mediated by its envelope glycoprotein G. VSV-G is a class III fusion protein known for undergoing reversible conformational changes (Albertini et al., 2012; I. S. Kim et al., 2016). The primary host receptor for VSV is the low-density lipoprotein receptor (LDL-R) (Finkelshtein et al., 2013; Fischer et al., 1993), which has previously been found to sort into dynamic endosomes (Lakadamyali et al., 2006). After binding its receptor, VSV undergoes a mode of clathrin-mediated endocytosis (CME) requiring actin (Cureton et al., 2009; X. Sun et al., 2005), is trafficked through the endocytic pathway encountering progressively lower pH, and is triggered to fuse with an endosomal membrane at low pH (Fredericksen & Whitt, 1995; J. White et al., 1981).

To examine trafficking and fusion mediated by VSV-G and address the question of whether the virus fuses in dynamic or static endosomes, we use murine leukemia virus (MLV) pseudotyped with VSV-G. Our VSV-G pseudotype particles contain gag-mKate2 as a content marker to demonstrate full fusion and a membrane anchored FRET-based ratiometric pH-sensor to monitor changes in acidification as the virus particles are endocytosed and trafficked in live cells. This system allows us not only to correlate fusion with endosomal pH at the single particle level, but also to follow the velocity and directedness of motion of virus-containing endosomes. By using this approach, we describe differing characteristics in the populations of endosomes that support fusion events versus those that do not. Endosomes that are more motile and more readily acidified support VSV-G driven viral fusion events, whereas more static endosomes do not appear to support fusion of VSV-G pseudoviral particles.

2.3 Results

Calibration and characterization of a FRET-based pH sensor in viral particles

Previous work used a FRET-based pH sensor consisting of mTFP1 and eYFP as a chimera with the ICAM1 transmembrane domain (ICAM1-TMD) to monitor pH during the trafficking of MLV bearing the envelope protein from ASLV (Padilla-Parra et al., 2012). The paper's authors identified two key limitations of the mTFP1-eYFP pH sensor: the particles were not observable in the perinuclear region due to noise contributed by cellular autofluorescence exceeding the signal

of the sensor, and the sensor could not reliably detect pH values below 5.2. To improve on these issues, we designed a new ratiometric pH sensor using mTFP1 and mCitrine as a FRET pair (Scott & Hoppe, 2015) attached to ICAM1-TMD (Fig. 2.1A, B). mCitrine is approximately 1.5-fold brighter than eYFP and has a lower pKa of 5.7 compared to 6.9 of eYFP (Griesbeck et al., 2001). Both mTFP1 and mCitrine are translated from a single open reading frame with ICAM1-TMD. The fluorescent proteins are thus expressed in a one-to-one ratio permitting the fluorescence intensity ratio of mTFP1 over mCitrine to be used as a pH indicator (Fig. 2.1B). The use of a ratiometric probe is key for live cell imaging because changes in focal plane affect both emissions wavelengths equally (Canton & Grinstein, 2015), permitting the measurement of pH even when the probe is on a moving object such as a viral particle or endosome. In unfused particles, ICAM1-TMD anchors mTFP1-mCitrine in the membrane of the viral particle topologically oriented toward the extracellular environment or, following endocytosis, into the endosomal lumen. Following fusion, the FRET pair is expected to sense endosomal pH via its luminal orientation with the TMD now embedded in the endosomal membrane.

MLV particles pseudotyped with VSV-G and containing the FRET pH-sensor were produced as described in Materials and Methods. The particles were also labelled with a content marker, Gag-mKate2, which is cleaved to Gag and mKate2 during capsid maturation (Markosyan et al., 2005). To calibrate the sensor, particles were deposited on a poly-lysine coated glass coverslip and

imaged in citrate-phosphate buffers of known pH. Individual, triply labelled particles were selected and the mean emission intensities from 8.9 nm wide spectral bands were extracted from each particle region. Particle regions were background subtracted and the emission intensity ratios of mTFP1 to mCitrine ($I_{494.0\text{-}502.9}$ /$I_{530.0\text{-}538.9}$) were calculated for each pH. The sensor fluorescence ratio undergoes a transition from a high to a low FRET state as the pH is decreased from 7.4 to 4.2 (Fig. 2.1C). Based on the measured fluorescence, the FRET sensor is well-equipped to distinguish pH in the range of 4.5-6.2 but is less discriminating between pH 6.2 and 7.4. At very low pH (4.2-4.5) there is high particle-particle variability in fluorescence ratio (Supp. Fig. 2.1A, B). When buffers of decreasing pH were applied sequentially, most (10/13) individual virus particles' fluorescence ratio responses increased with decreasing pH as expected. However, three of 13 particles were unresponsive or displayed a scattered fluorescence ratio response (Supp. Fig. 2.2A, B). We do not know why the fluorescence of a few particles displayed these unexpected pH dependencies, but one explanation could be that one or the other fluorescent protein is not properly folded or their folding is differently sensitive to pH in these outlier particles.

To assess the performance of the pH sensor over repeated exposures and the variation of the fluorescence ratio for a single particle on a frame-to-frame basis, virus particles were imaged on a coverslip for 16 minutes in neutral live cell imaging buffer before imaging was paused, a buffer of pH 5.2 was

introduced, and imaging was continued (Supp. Fig. 2.2C). While some particles could be observed for many minutes after the pH change, several particles were visible only briefly after the introduction of low pH buffer or were no longer visible at all. As expected, the fluorescence ratio increased with the addition of low pH buffer for all particles still observed after buffer replacement (Supp. Fig 2.2C). The mean values (Supp. Fig. 2.2D) and standard deviations (Supp. Fig. 2.2E) of the fluorescence ratios over the first six frames (in pH 7.4 buffer) were calculated for each of these particles. The median value of the mean ratio for all particles over the first six frames was 0.58, which corresponds according to the calibration curve of Fig. 1C to pH 6.8. The median value of the standard deviation was 0.045, which is equivalent to a range of pH 6.6-7.2 around the median initial ratio of all particles, slightly below the pH 7.4 buffer surrounding the particles. Once the buffer was shifted to pH 5.2, the median fluorescence ratio value of the mean fluorescence ratio for all particles in the six subsequent frames was 1.38, which corresponds to a pH of 5.1 according to the calibration curve. This is approximately the same as the pH 5.2 buffer surrounding the particles, further verifying the accurate readout of the sensor at low pH.

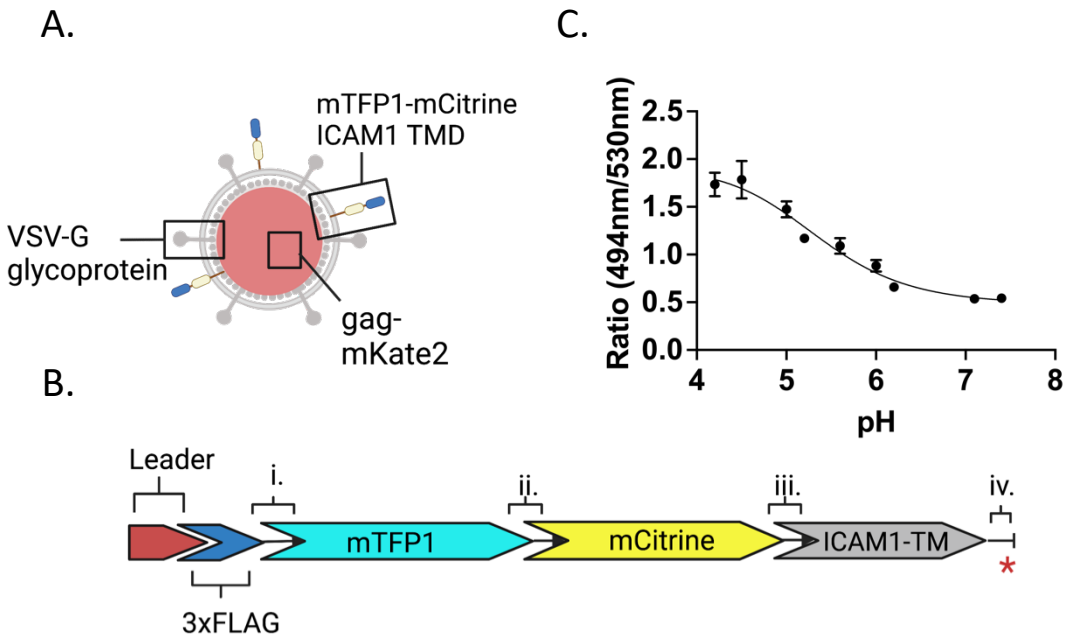

Figure 2.1. Design and calibration of a FRET-based pH sensor to measure cellular trafficking and the pH of fusion of viruses in cells. *A*) Schematic of an MLV particle pseudotyped with VSV-G glycoprotein and bearing a FRET-based pH sensor with mKate2 as a content marker. *B*) Schematic representation of the pH sensor construct. The pre-protrypsin leader sequence (Leader) is followed by 3xFLAG sequences, followed by the fluorescent protein and ICAM1 transmembrane domain sequences. Linkers between components are i., ii., iii., and iv. where iv. separates the first four amino acids of the ICAM1 cytoplasmic domain and the stop codon indicated by the red asterisk. The sequence of linker ii. between mTFP1 and mCitrine is RSTSLQEFGT. *C)* The pH sensitive mTFP1-mCitrine FRET pair on the pseudotyped viral particle (as shown in panel *A*) is calibrated with buffers of known pH on coverslips. The ratio of the fluorescence emission intensities at 494nm/530nm is used as a proxy for FRET efficiency and plotted as a function of pH. The error bars represent the standard errors of the mean (SEM). Numerical values of the mean and SEM and numbers of individual particles evaluated at each pH are listed in Supplemental Figure 1B.

<u>Visualization, pH dependence and time-course of fusion of VSV-G mediated fusion events</u>

Having established the characteristics of the new FRET-based pH sensor in isolated viral particles, we used this sensor to track the measured pH (as

calculated from the calibration curve in Figure 2.1C) of endosomes harboring VSV-G pseudotyped viruses and their eventual fusion by live cell imaging. Parameters to describe these endosomes included their pH, changes in pH, and their displacement and velocity of motion within the cell. Pseudoviral particles were spun onto A549 cells in the cold, a field of view was selected for imaging, and the cold buffer was replaced with warm (37° C) imaging buffer immediately prior to commencing imaging, which was conducted at 37° C. Fusion events were identified by a sudden drop of the mKate2 signal while the mTFP1 and mCitrine signals persisted, as indicated in the representative example shown in Fig. 2.2A by the magenta arrow at 28.3 minutes. Fusion events, initially assessed by direct visualization, were confirmed by quantitation of the raw and background subtracted signals of all three channels (Fig. 2.2B, 2.2C) as described in the Materials and Methods. The displacement and velocity of the particle shown in panel A were plotted as a function of time in Figs. 2.2D and 2.2E, respectively. The displacement and velocity results from this example particle, as well as from many other particles will be described in a later section.

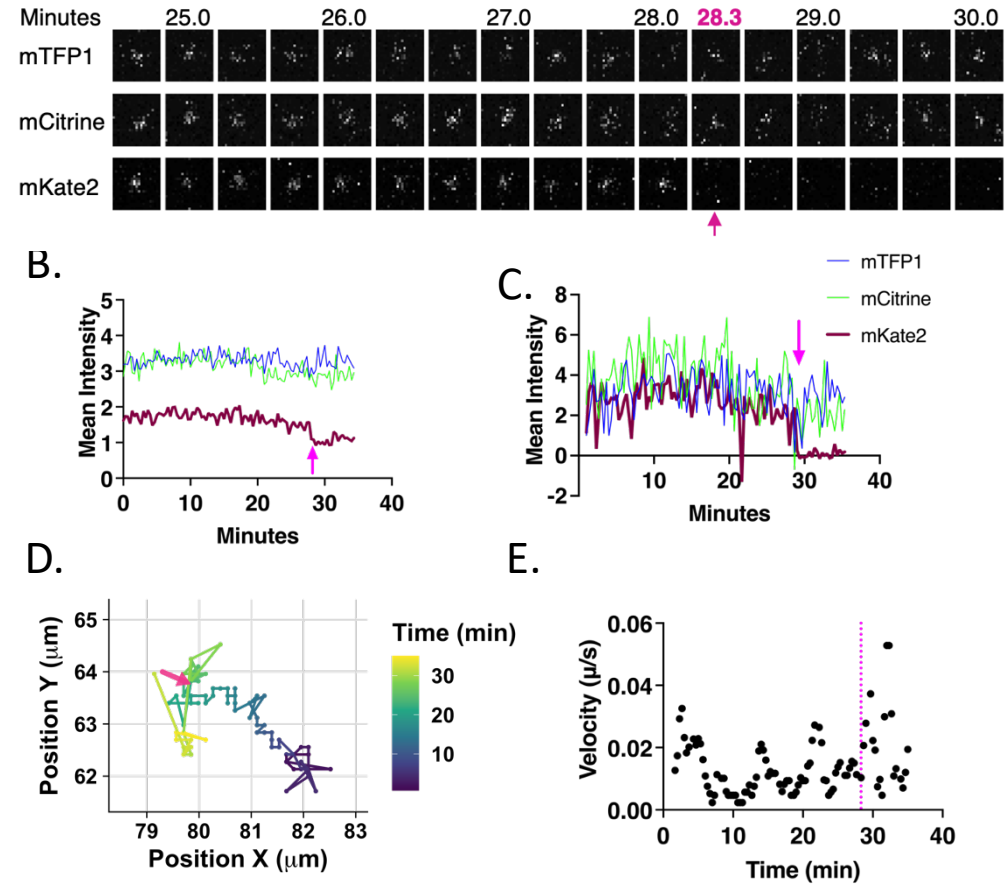

Figure 2.2 Progression of an individual example virus particle from the start of imaging to fusion and beyond simultaneously observed with three fluorescence channels. *A)* Images of the particle in the mTFP1 (494-511nm) (top), mCitrine (521-538nm) (middle), and mKate2 (593-741nm) (bottom) channels. Images are 20s apart and the track is cropped to 10 frames before and 5 frames after fusion. The size of each image is 2.94 x 2.94 μm, centered around the particle centroid determined by tracking. In all images the arrow indicates the time at which fusion ends. *B*) Raw extracted intensity from a 2.94^2 μm^2 box surrounding the particle centroid and plotted over time. *C)* Background subtracted intensity using a 1.96 μm diameter inner circle with an outer 0.28 μm diameter annular region from which the mean intensity was calculated and subtracted from the intensity of the inner region. *D)* Path of the particle over time within a boxed region from the total field of view. The color of the line represents time according to the scale on the right. The arrow indicates the position of the particle at the time that fusion is completed. *E)* Velocity was calculated by taking the distance between the localization of the particles at adjacent points in time and multiplying by the frame rate (1/20s). A 3-frame (one minute) rolling average

of the velocities was taken and plotted as a function of time. The dotted line indicates the time at which fusion is completed.

For each particle undergoing fusion, the ratio of the mTFP1 to mCitrine fluorescence intensity was extracted and plotted at 20 second intervals, the frame rate of imaging, over all frames in which the particle was observed (Fig. 2.3A). The time of fusion, determined as the time of disappearance of the mKate2 signal (Fig. 2.2A, 2.2C), is shown as a vertical dashed line in Fig. 2.3A. Several interesting phenomena of change in fluorescence ratio were observed immediately prior to or following fusion events. In several examples, the pH sensor signal disappeared or experienced significant frame to frame variation within five minutes following fusion (Fig. 2.3A: examples ii., iv., v., ix., xii., and xiv.). This is similar to the phenomenon observed when virus particles were rapidly acidified on a coverslip (Supp. Fig. 2.2C) and may be due to loss of signal from the FRET donor and acceptor, perhaps caused by quenching of the signal due to protonation of the chromophore or irreversible protein unfolding at very low pH (less than pH 4.2). Several fusion events occurred during periods of increasing fluorescence ratio indicating acidification (Fig. 2.3A: examples iii., vi., vii., and xviii.). Even transient shifts to lower pH may trigger viral content release. A decrease in ratio (alkalinization) immediately follows fusion (Fig. 2.3A: examples vi., vii., x., xi., xiii.) for five of the fusion events. Temporary alkalinization of endosomes following fusion could be caused by a leaky fusion

event in which there is a loss of contiguity in the endosomal membrane(Chlanda et al., 2016) allowing the permeation of cytosolic contents into the endosome.

The mean time of fusion (content release), counted from the start of imaging and derived from the 18 events shown in Fig. 2.3A, is distributed primarily in observation times less than 45 minutes with a mean value of 25.2 min (Fig. 2.3B). The mean fluorescence ratio at fusion was 1.24 +/- 0.08 (SEM), which is the equivalent of pH 5.3 (pH 5.2-5.4). The total range of pH values measured at viral fusion extended from a fluorescence ratio of 0.67 (pH 6.4) to 1.78 (pH 4.2) (Fig. 2.3C).

For virus particles encountering progressively more acidic environments as they move along the endocytic pathway, the fluorescence ratio is expected to increase. For 8 of the 18 fusing particles, the change in fluorescence ratio from the first time the particle is observed to the time of fusion was positive as expected, with a mean increase of 0.17 +/- 0.77 over all particles observed (Supp. Fig. 2.3A). Five of the 18 fusing particles had very small fluorescence ratio changes that fell within the expected frame-to-frame variability of the probe (2 SD of frame-to-frame ratio difference for single particles; Supp. Fig. 2.2E) and thus cannot be interpreted as having a meaningful change in pH during the observed time before they fuse (Supp. Fig. 2.3A). Five of the 18 fusing particles demonstrated increasing pH between the time the particle was first observed and the time of fusion. This latter result may both reflect physiologic fluctuations in the pH in the endosome and the possibility that observation of some particles may

have only commenced soon before fusion (Fig. 2.3A), when the particle may already have been in a moderately acidic environment.

Rapid fluctuations in pH during the trafficking of fusing virus particles were a particularly interesting phenomenon observed in several cases (Fig. 2.3A: examples i., iii., xvii.). Similar fluctuations have been observed during trafficking of influenza virus (Lakadamyali et al., 2003, 2006) but were not observed to the same extent during the trafficking of ASLV (Padilla-Parra et al., 2012). For trace i. in Fig. 2.3A, the measured pH decreases from 5.7 to a local minimum of under 4.2 at a rate of at least -0.4 pH units per minute during the four minutes immediately following fusion. The pH is rapidly restored to a calibrated pH of 5.6 at the rate of at least 0.6 pH units per minute during the next two minutes (Supp. Fig. 2.3B). This pattern of rapid acidification followed by alkalinization is also seen in trace xvii. in Fig. 2.3A and is quantified in Supp. Fig. 2.3C. Fluctuations in pH over the course of minutes may reflect proton leak variability over time (Grabe & Oster, 2001; D. E. Johnson et al., 2016) or other transient changes in endosomes. The very rapid rates of acidification following alkalinization are consistent with the previously observed general kinetics of V-ATPase when reacidifying endosomes (D. E. Johnson et al., 2016).

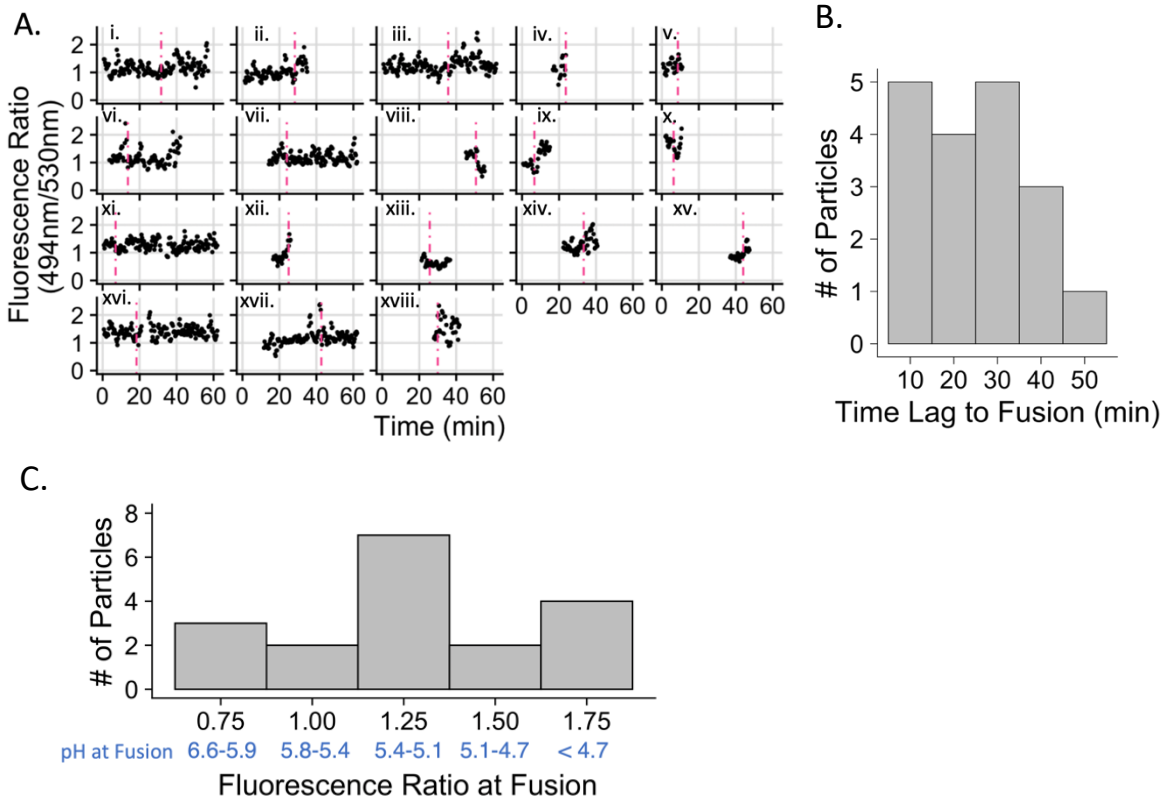

Figure 2.3. Kinetics and pH characteristics of VSV-G mediated viral particle trafficking and fusion. *A*) Fluorescence emission intensity ratio plotted over time for all particles that fuse. The dashed vertical line represents the time of fusion as determined by the spreading or disappearance of the mKate2 signal. *B*) Frequency histogram of the time from the beginning of imaging to the time at which fusion occurs. *C*) Frequency histogram of the 494nm/530nm emission intensity ratios at the time of fusion using a six-frame moving average. The pH range falling within each histogram bin is shown in blue; fluorescence ratios were converted to pH range using the calibration curve (shown in Figure 1C). 18 fusion events were analyzed (out of 88 particles meeting the criteria described in the Materials and Methods) and are represented here (n=18).

<u>Comparison of acidification and properties of motion for fusion permissive and non-permissive endosomes</u>

We next compared the features of fusion permissive endosomes and endosomes that did not permit fusion. The FRET-based pH sensor (Fig. 2.1A, B)

is topologically oriented toward the extracellular/luminal space both while embedded in the viral membrane during trafficking and in the endosomal membrane after fusion, permitting measurement of pH during viral trafficking as well as during and following fusion. Fusion events were identified as described in Figure 2 and in the Materials and Methods in 13 separate experiments conducted on seven separate days. All monodisperse, triple labelled virus particles (mTFP1, mCitrine, gag-mKate2) that were observable for at least 20 frames (~7 minutes) were identified in experiments containing at least one fusion event. Of 88 total particles that were detected and tracked, 18 underwent fusion corresponding to a fusion efficiency of 20.4% for qualified triply labelled particles. We empirically observed a number of significant differences between fusion permissive and fusion non-permissive endosomes.

Fusion permissive endosomes display a higher maximum degree of acidification than fusion non-permissive endosomes. Fusion permissive endosomes achieve a median minimum pH of 4.2 compared to a median minimum pH of 5.3 in fusion non-permissive endosomes (Fig. 2.4A); fluorescence ratios were converted to pH values using the calibration curve of Fig. 2.1C. The pH sensor can best differentiate between pHs in the range of 4.5-6.2 and the upper plateau of the fit for the calibration curve is at pH 4.2, meaning that values at or below 4.2 represent highly acidic values and cannot be interpreted precisely. Despite the greater acidification of fusion permissive endosomes, both categories of endosomes had similar pH values when they

were first observed (pH ~5.5, Fig. 2.4B), and similar values for the most alkaline pH they ever experienced during the whole observation period (pH ~6, Fig. 2.4C). Our observation that most virus particles, regardless of their ability to fuse, appear to start in endosomes with calibrated pH values below seven may be indicative of an initial rapid trafficking period into mildly acidic early endosomes during the one to two minutes required to refocus the microscope after the addition of warm buffer. Prior work found that up to 50% of ASLV viral particles reach a compartment of pH 6.2 or lower within two minutes of the initiation of viral trafficking (Padilla-Parra et al., 2012).

We also calculated the fluorescence ratio difference over the entire time the FRET pair could be observed in a given endosome. According to this analysis, fusion permissive endosomes became more acidified from their starting state than fusion non-permissive endosomes. The median ratio changes were +0.24 and +0.01 units, respectively (Fig. 2.4D). The difference between the initial and final pH was –0.4 units for fusion permissive and –0.1 units for fusion non-permissive endosomes (Fig. 2.4E).

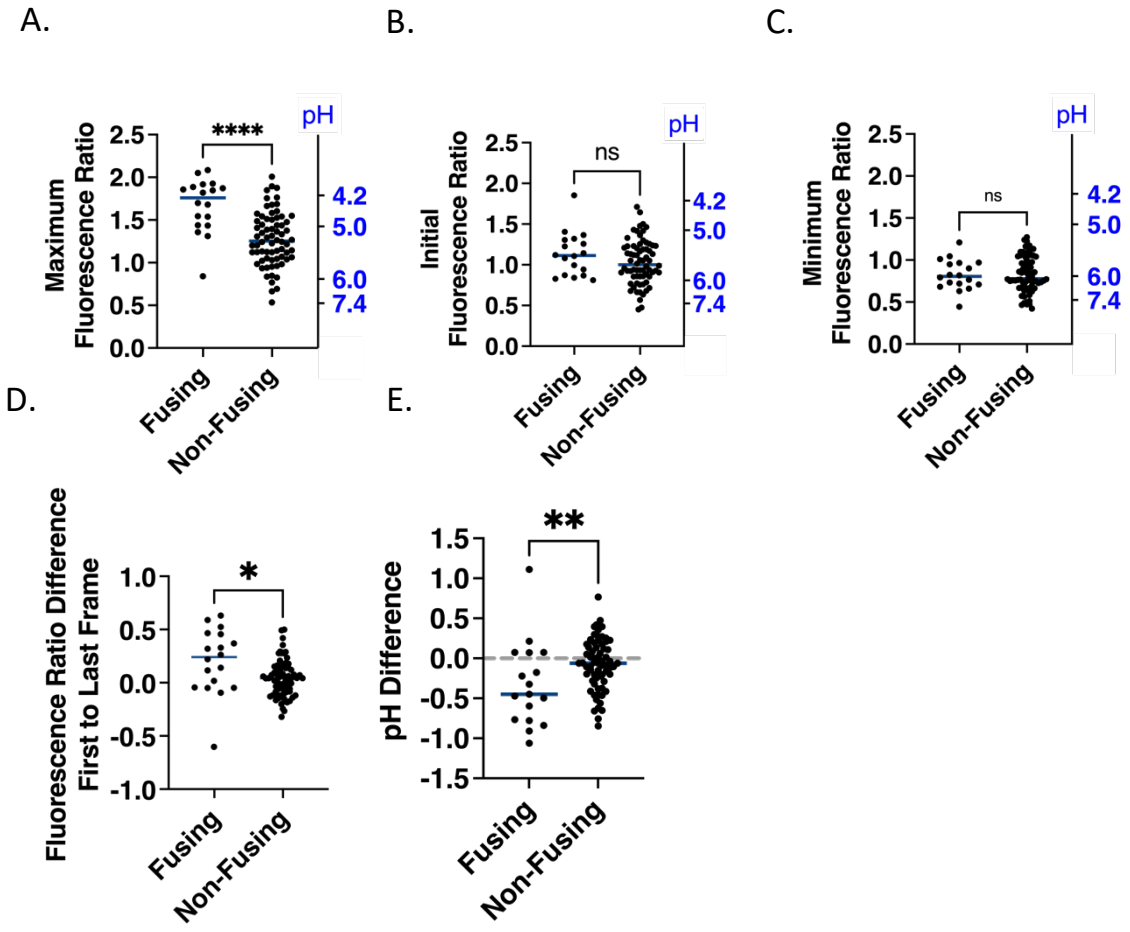

Figure 2.4. Fusion permissive and fusion non-permissive endosomes exhibit different extents of acidification. *A)* Maximum emission intensity ratios (494nm/530nm) achieved in tracks based on a six-frame rolling average for fusion permissive and fusion non-permissive endosomes. The right Y axis displays reference pH values. (Note that the relationship between pH and ratio is not linear; see Figure 1C). All selected particles were non-overlapping with other particles, had apparent diameters less than ~1.5 µm, and were triple labelled. Non-fusing particles are from experiments, in which fusion events were observed in other locations. *B)* Initial emission intensity ratios over the first 6 observable frames for fusion permissive and fusion non-permissive endosomes. *C)* Minimum emission intensity ratios in tracks based on a six-frame rolling average for fusion permissive and fusion non-permissive endosomes. *D)* Difference between emission intensity ratios at the time at which the particle is first observable (start) and the time at which the pH sensor from the particle is last observable (end) for fusion permissive and fusion non-permissive endosomes. *E)* The initial and final emission intensity ratios from panel D converted to pH using the fit of the calibration curve (Figure 1C) and plotted as pH differences over the observable time for fusion permissive and fusion non-permissive endosomes. No change in pH is indicated with a horizontal dashed line. In all panels, points represent the

values for individual particles and horizontal lines represent the median value of each group. Numbers of fusing particles and non-fusing particles are n=18 and n=70, respectively. A Mann-Whitney test (non-parametric assumption) was used to assess the significance of the differences in the distribution of fluorescence ratio values (A-D) or pH (E) ($p<0.05$ = *, $p<0.01$ =**, $p<0.0001$=****, ns, not significant). In E, observations where the initial and final values fell above or below the lower and upper limits of the calibration curve fit were excluded from analysis and the numbers are n=17 for fusing and n=68 for non-fusing particles.

Fusion permissive and non-permissive endosomes displayed different displacements and velocities of displacement during the observed trafficking times in the cell. Velocities were measured from particle localizations in consecutive frames and a three-frame (one minute) rolling average was taken for each time point. While the motions of both fusion permissive and non-permissive endosomes were mostly slow and included stationary segments, leading to median velocities of all segments in a track of ~0.01 μm/s (Fig. 5A), the fastest steps in fusion permissive endosomes had higher velocities (~0.05 μm/s) compared to those observed in non-permissive endosomes (~0.01 μm/s) (Fig. 5B). The total displacement, defined by the distance traveled between the coordinate points at which the particle was first and last observed, was determined for both subpopulations of endosomes. The median total displacement of fusion permissive endosomes was higher than that of non-permissive endosomes (Fig. 5C). This result is somewhat surprising in light of the similar median velocities of the two subpopulations of endosomes, but suggests that the high maximum velocities found in fusion permissive endosomes make an outsized contribution to their total displacement. Finally, FRET signals from

tracks of fusion permissive and non-permissive endosomes could be observed for a similar length of time (Fig. 5D), demonstrating that the difference in total displacement and maximum velocity did not depend on the total time for which the particle was observed.

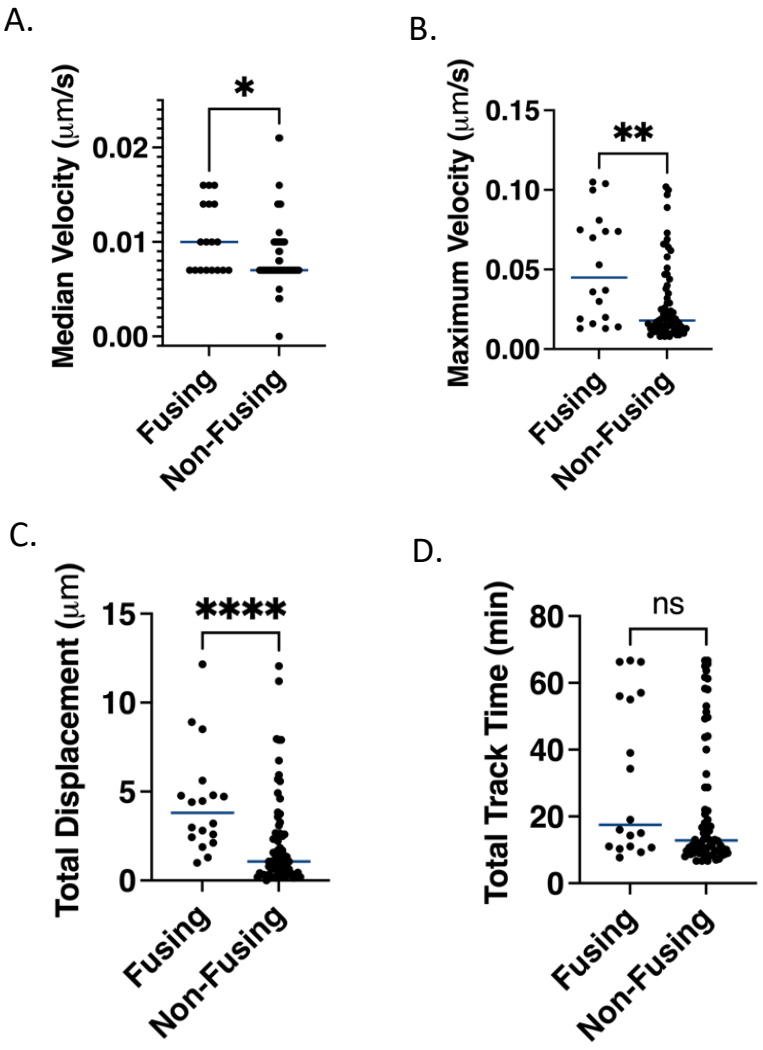

Figure 2.5. Fusion permissive endosomes have higher maximum velocities and travel further than fusion non-permissive endosomes. *A)* Median velocities from all segments in a given track for fusion permissive and fusion non-permissive endosomes. The median value for each endosome is calculated based on a 3-frame (1 minute) rolling average of the velocities of all segments in a given track. *B)* Maximum velocities determined as the highest velocity of for any segment based on a 3-frame rolling average as in A) for fusion permissive and fusion non-permissive endosomes. *C)* Total displacements calculated from

the distance between the coordinate points at which the FRET sensor signal is first and last observed for fusion permissive and fusion non-permissive endosomes. *D)* Total track lengths, i.e. times that the FRET sensor signal was observable calculated as the time difference between when particles are first and last observed for fusion permissive and fusion non-permissive endosomes. In all panels, points represent the values for individual particles and the horizontal lines represent the medians. A Mann-Whitney test (non-parametric assumption) was used to assess the significance of the differences in the distribution of all values ($p<0.05$ = *, $p<0.01$ =**, $p<0.0001$=****, ns, not significant).

Mean squared displacement and trajectory analysis of fusion permissive and non-permissive endosomes

Given the different maximum velocities and total displacements between fusion permissive and non-permissive endosomes, a mean-squared displacement (MSD) analysis was conducted to determine whether the two subpopulations of endosomes exhibit different modes of motion. We used plots of MSD versus time to distinguish between random (diffusive) and directed motion (Qian et al., 1991; Saxton & Jacobson, 1997). To facilitate this analysis, we took a randomly chosen 18-member subset from the fusion non-permissive endosomes such that equal numbers of the two subpopulations of endosomes were analyzed. The MSD (μm^2) at each time step up to 400 seconds (6.7 minutes) was calculated and plotted for the 18 fusion permissive and 18 non-permissive endosomes (Supp. Fig. 2.4A, B). For better visualization, we also averaged the MSD values for all 18 tracks in each set at each time lag and plotted the averaged MSD at each time lag (Fig. 2.6A). This averaged MSD plot is dramatically different for fusion permissive and non-permissive endosomes, with fusion permissive-endosomes showing an upwards bending curve indicative

of directed motion, while the fusion non-permissive endosomes exhibited a more linear MSD vs. time relationship indicating free (Brownian) diffusion (Fig. 2.6A). As expected, there is higher variability at longer time steps since these are derived from fewer measurements (Qian et al., 1991). The same trend observed in the averaged data can be seen in many curves of individual endosomes (Supp. Fig. 2.4A, B).

The MSD data from 17 out of 18 fusion tracks could be reasonably fit with a model for directed motion (Equation 1 in Materials and Methods) with the velocity coefficient *v* as one of the fitting parameters. The particles were binned according to their velocity coefficients and moved with an average velocity coefficient of 0.0027 μm/s (Fig. 2.6B). The velocity coefficients plotted for the fusion-permissive endosomes are consistent with previously published values for slow directed motion of endosomes containing influenza virus along microtubules or microfilaments (L. Xia et al., 2021). The difference in characteristics of motion and acidification between fusion permissive and non-permissive endosomes are indicative of two distinctive populations of endosomes, one of which undergoes acidification and trafficking, and one of which is relatively static on the time-scale of trafficking and fusion of MLV particles bearing VSV-G (Figure 2.7).

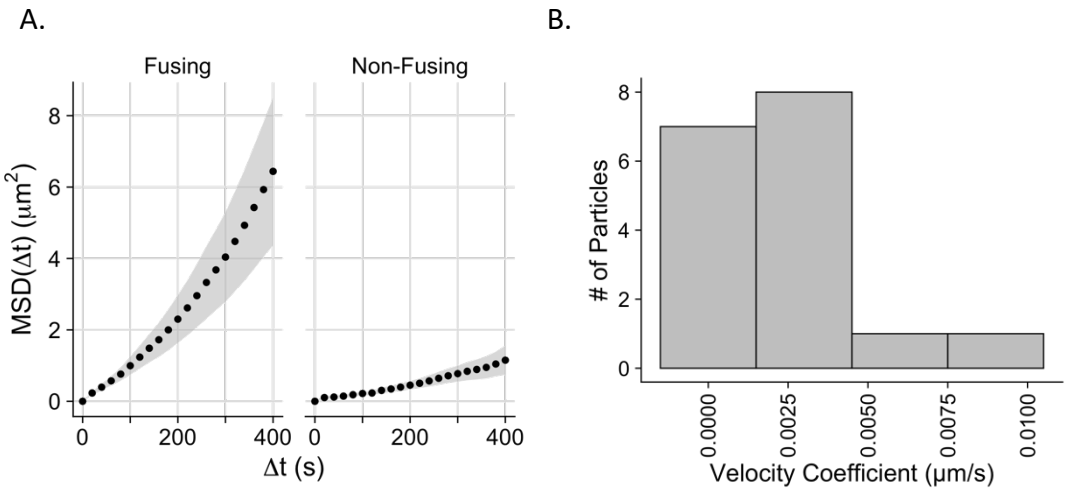

Figure 2.6. Motion analysis reveals behavior consistent with directed motion in fusion-permissive endosomes. *A)* Mean square displacements (MSD) (μm^2) plotted vs. time step Δt for endosomes harboring fusing and non-fusing virus particles. Each data point represents the mean MSD of 18 endosomes containing fusing or non-fusing particles respectively, at each time step. The grey envelopes represent the standard errors of the mean for all particles in the plotted data set at Δt. *B)* Distribution of velocities (*v*) of directed motion of fusing virus particles. To test for a component of directed motion, the MSD of fusing particles was fit with Equation 1 in Materials and Methods. Time steps up to 60% of the total length of the track were fit. 17/18 of the fusing particle MSD curves could be fit with this model; one curve had a decrease in MSD values at higher values of Δt such that it could not be fit with Equation 1.

A.

Characteristic	Fusion Permissive Endosomes	Fusion non-permissive endosomes
Acidification	Greater	Lesser
Displacement	Higher	Lower
Maximum Velocity	Higher	Lower
Directed motion	Common feature	Uncommon feature

B.

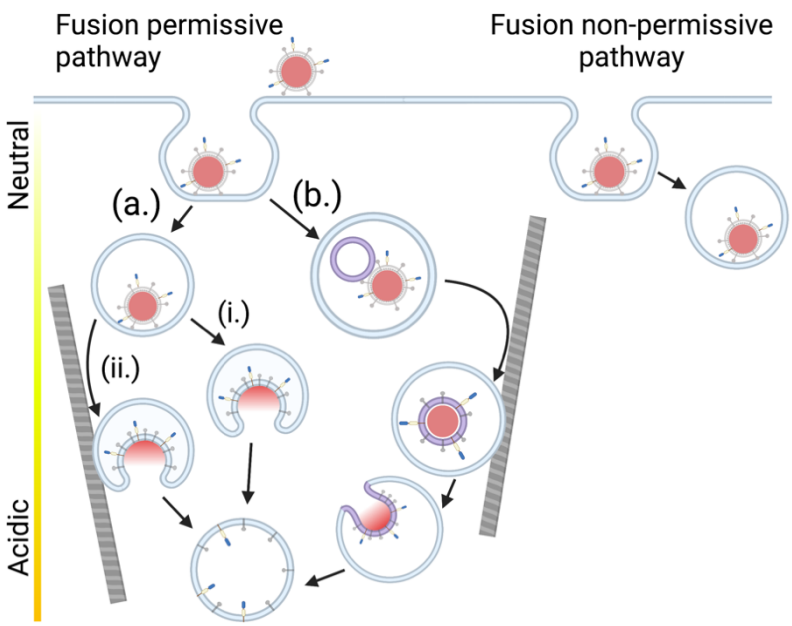

Figure 2.7. Summary of characteristics for fusion permissive and fusion non-permissive endosomes with a model for viral particle trafficking during cell entry. *A)* Summary of characteristics of fusion permissive and non-permissive endosomes based on the single virus particle tracking and fusion data presented in Figures 2.4-6. *B)* Model of trafficking of VSV-G pseudotyped viral particles in fusion permissive and non-permissive endosomes. In this model, fusion is associated with the maturation of the subpopulation of fusion permissive endosomes, many of which also undergo directed motion, likely along elements of the cytoskeleton. The sorting of particles to fusion permissive or non-permissive endosomes does not appear to be preferential (see Discussion). Three fusion scenarios are displayed: In path (a) the virus fuses directly with the limiting endosomal membrane; in path (i) the virus fuses prior to directed motion of the endosome or in an endosome that does not undergo directed motion; in path (ii) the virus fuses after the endosome containing it undergoes directed motion. In path (b) the virus undergoes fusion with an intralumenal vesicle, which then undergoes retrofusion with the limiting membrane of the endosome in a

more acidic compartment. The ILV-containing compartment also may or may not undergo directed motion prior to fusion. Components of the viral particle are as represented in Figure 2.1A.

2.4 Discussion

In this study, we have investigated the fusion of single virus particles mediated by the surface glycoprotein VSV-G in whole, live A549 cells and discovered that two subpopulations of endosomes with different characteristics of acidification and intracellular motion play a role in the fate of individual viral particles. Endosomes that did support fusion of internalized viruses were more acidic, more motile and underwent directed motion to a greater extent than endosomes that did not support fusion (Fig. 2.7A). Based on our findings, we propose a model whereby the sorting of viral particles into more dynamic endosomes disposes particles to undergo fusion; conversely the sorting of virus particles to a more static subpopulation of endosomes traps these particles in locations where they are strongly disinclined to fuse (Fig. 2.7B).

Distinctive pools of endosomes and viral fusion

The presence of different pools of early endosomes has previously been established (Kalaidzidis et al., 2015; Miaczynska et al., 2004; Perini et al., 2014) with some less motile early endosomes maturing more slowly, as defined by a longer time lag to the acquisition of Rab7, and some more motile early endosomes maturing more rapidly (Lakadamyali et al., 2006). Maintenance of these separate populations of dynamic and static early endosomes is dependent

on intact microtubules and the early endosomal tethering complex CORVET, while sorting of cargo into subpopulations relies on differential clustering of the cargo at the cell surface (Lakadamyali et al., 2006; Perini et al., 2014). The significance of these separate pools to viral infectivity has only begun to be studied, with differing results as to whether viruses are more likely to be sorted to or fuse from dynamic or static early endosomes (Lakadamyali et al., 2006; Padilla-Parra et al., 2012). We found that viral particles pseudotyped with VSV-G had a fusion efficiency (as indicated by content release) of approximately 20%. Fusion permissive endosomes moved a median 3.8 μm during their entire observation times (Fig. 5C) with a mean velocity of 0.16 μm/min (Fig. 6B). They also decreased their pH on average by -0.4 units during the entire observation time (Fig. 4E) and reached an average pH of 5.3 immediately before fusion (Fig. 4C). Most of the remaining 80% of particles, consisting of the non-fusing subset, were contained in endosomes that had a lower motility and lower overall acidification than endosomes bearing particles that fused. For comparison, endosomes bearing virus particles that did not fuse moved on the median only 1.0 μm (Fig. 5C), moved diffusively with no discernible component of directed motion (Fig. 6A), and lowered their pH on average only by -0.1 units during the entire observation time (Fig. 4E). Only 10 of the 70 fusion non-permissive endosomes achieved a change in pH above the median change in pH for fusion-permissive endosomes (Fig. 4E).

The sorting of viruses and physiological cargoes to subpopulations of early endosomes may rely on a number of factors including cargo size and qualities of the receptor. The static subpopulation of endosomes is in the majority (65%) and the minority of endosomes are dynamic (35%) in BSC-1 cells. In the same cells, influenza virus is preferentially sorted to the dynamic endosome subpopulation as compared to static endosomes. When bound with its endogenous ligand, LDL, LDL-R, which also serves as the VSV-G receptor, is preferentially sorted to dynamic endosomes as well (Lakadamyali et al., 2006). In contrast to influenza virus, ASLV pseudotyped viral particles were found to sort predominately (70%) to less motile endosomes in CV-1 cells expressing the transmembrane receptor for ASLV, TVA950 (Padilla-Parra et al., 2012). The 70% of ASLV sorted to less motile endosomes is consistent with the overall proportion (65%) of static endosomes (Lakadamyali et al., 2006). This suggests that ASLV is sorted to static and dynamic subpopulations in proportion to the abundance of each endosome subpopulation, without preference for either subpopulation. In our current study, VSV-G pseudotyped particles are also sorted without a clear preference for dynamic endosomes.

The indiscriminate sorting of VSV-G pseudotyped particles as compared to the preferential sorting of LDL-bound LDL-R to dynamic endosomes may be due to the smaller size of LDL compared to MLV particles. MLV particles are approximately five times larger in diameter than LDL, the physiological cargo for LDL-R (Jeon & Blacklow, 2005; Yeager et al., 1998). The importance of cargo

and viral particle size with respect to trafficking has previously been demonstrated. VSV particles required an actin dependent mechanism of clathrin-mediated endocytosis as compared to small, defective viral particles that were otherwise similar (Cureton et al., 2009). The MLV particles bearing VSV-G used in the present study are more spheroid in comparison to the bullet shape of VSV. They are ~25% smaller in length than the maximum dimension of VSV particles, but they are almost twice as wide (Cureton et al., 2010; Yeager et al., 1998), suggesting that they, like VSV, are large enough to potentially undergo clathrin-mediated endocytosis in a different manner than relatively small cargo such as LDL. Smaller particle size has also been shown to have important downstream effects in motility; smaller cargo are more likely to undergo fast directed motion (Aoyama et al., 2017). Binding avidity for ligands to receptors has also previously been shown to affect cargo fate (Ghaffarian & Muro, 2014). Therefore, it is possible that the number of glycoproteins on a single viral particle that bind to multiple LDL-Rs in a single clathrin coated pit could also determine to which type of endosome the internalized virus is directed.

In general accordance with our findings that fusion non-permissive endosomes did not achieve the same extent of acidification as fusion permissive endosomes, endosomes containing ASLV particles that failed to fuse showed a pH distribution shifted toward more neutral pH values compared to fusing particles (Padilla-Parra et al., 2012). However, while ASLV was observed to undergo an initial period of acidification to a pH of approximately 6.2-6.0 and then

stay close to that pH, we observed continued further acidification as well as significant physiological fluctuations in pH in endosomes bearing VSV-G viral particles (Fig. 3A, 4C-E). One limitation of the prior study, as identified by the authors, with respect to measuring pH during trafficking of ASLV particles, was difficulty in observing pH values below 6.0 due to cellular autofluorescence and, potentially, the higher pKa of the pH sensor used in that study (Padilla-Parra et al., 2012). We did not observe significant cellular autofluorescence and utilized a FRET acceptor fluorescent protein that was 1.5-fold brighter than the acceptor protein used in the previous work. Moreover, mCitrine, used in our work as the acceptor fluorescent protein, has a pKa of 5.7 (Griesbeck et al., 2001), permitting measurements down to pH 4.2 in live cell imaging.

Determining the compartment identity of both fusion permissive and non-permissive populations of endosomes would be fertile ground for future study. While the current experimental system has the advantage of a ratiometric pH probe in combination with a content marker, allowing the measurement of both pH and content release, the combination of fluorophores occupies a broad spectral range (approximately 475-750 nm emission wavelength). Recently developed near infrared fluorescent proteins (Matlashov et al., 2020) may offer an exciting opportunity to express fluorescent chimeras of compartment markers (such as APPL1, EEA1, Rab5, Rab7 or Rab11) that will not interfere with imaging of the FRET-based pH probe and viral content marker described in this study. One intriguing possibility is that fusion non-permissive endosomes recycle viral

particles to the cell surface, a phenomenon recently described for Zika and influenza viruses (Owczarek et al., 2019; Z.-G. Wang et al., n.d.) thus providing an additional layer of defense to the host cell.

Characteristics of VSV-G mediated fusion

Viral internalization and trafficking through the endocytic pathway are key requirements for productive fusion and infection by most enveloped viruses (J. M. White et al., 2016). We identified individual full fusion events based on content release of mKate2 (Fig. 2A-C, Fig. 3A). By simultaneously tracking the pH sensors on individual particles prior to, during, and following fusion, we were able to quantify pH changes as well as the pH at which full fusion occurred. The mean lag time from initiating trafficking via addition of warm medium to fusion was 25 minutes for the 18 fusing particles observed (Fig. 3B). Although the time course of fusion for viral particles may depend on cell type and viral model, it is interesting that our results are substantially similar to at least three previously published studies, i.e., similar values of approximately 20-35 minutes were obtained in bulk assays for half-maximal infection or fusion of viral particles bearing VSV-G (Le Blanc et al., 2005; Mingo et al., 2015; Saeed et al., 2006). This indicates that the FRET-based pH sensor does not appear to significantly change the kinetics of trafficking and/or fusion. The heterogeneity of the time course of fusion seen in our single particle experiments likely not only reflects biological variabilities of individual particles, but likely also reflects the

heterogeneity of maturation of the endosomes harboring the viral particles, leading to a quite broad range of times to achieve fusion.

To our knowledge, this is the first single-particle measurement of the pH of VSV-G mediated full fusion in intact cells. Our data suggest that most full fusion and content release events occur at a mean pH ranging from 5.2 to 5.4 (Fig. 3C) in whole cells. Interaction of VSV-G with liposomes, reflecting an early stage of fusion, requires a pH trigger reported to be anywhere from approximately 4.0 to 6.0 (Carneiro et al., 2001; Eidelman et al., 1984) although the biggest structural changes in the VSV-G protein occurs between pH 5.5 and pH 6.5 (Carneiro et al., 2001). Cell-cell fusion mediated by G protein expressed in the plasma membrane showed half maximal fusion at approximately pH 6.0-6.2 (Fredericksen & Whitt, 1995; J. White et al., 1981), though the extent of cell-cell fusion has been demonstrated to be greater at pH 5.5 (Beilstein et al., 2020). The efficiency of VSV fusion (lipid mixing) with a supported lipid bilayer is also greatest at pH 5.5 (I. S. Kim et al., 2016). Differences in the target membrane with which VSV-G fuses and ionic conditions in the endosome likely influence the fusion behavior of internalized viruses and environmental conditions in the endosome may differ significantly from these earlier model systems used to study membrane binding and fusion.

Previous findings suggest that VSV-G mediated virus entry includes an intermediate step of fusion whereby viral particles first fuse with intraluminal vesicles (ILVs) within endosomes (Le Blanc et al., 2005). The endosomes

containing these virus-bearing ILVs then mature, acidifying further, and acquiring lysobisphosphatidic acid (LBPA). In the presence of the appropriate lipid composition and pH, ILVs then undergo retrofusion with the limiting membrane enabling the release of viral contents in the cytoplasm (Le Blanc et al., 2005) (Fig. 7B). The findings that VSV-G may fuse with intraluminal vesicles is further supported by the fact that anionic lipids, such as LBPA, promote VSV-G content release (Matos et al., 2013; Roth & Whittaker, 2011) and these lipids are potentially enriched in ILVs (Kobayashi et al., 1998). The lower average pH of content release determined in our experiments compared to the interaction of VSV-G with plasma membranes (e.g., for cell-cell fusion) reported at higher pH could be explained by the proposed mechanism of viral content release requiring ILV retrofusion in the late endosome. Many of the content release events we observe may therefore represent retrofusion events that may require a lower pH than the initial fusion with ILVs and are known to depend on the lipid composition of the late endosomes (Amini-Bavil-Olyaee et al., 2013; Le Blanc et al., 2005; Perrin et al., 2021). The small number (3/18) of content release events we observe at greater than pH 6.0 (Fig. 3C) may represent direct virus fusion with the limiting membrane of the endosome. It is possible content release via retrofusion is the predominant mechanism while fusion with the limiting membrane only predominates when the retrofusion mechanism has been blocked in some way or is not advantageous within a given cell or endosome. This is supported by data showing that content release is markedly less efficient

when ILVs cannot be formed or trafficked, but that some content release still occurs under these conditions (Le Blanc et al., 2005; Pasqual et al., 2011).

General considerations of FRET-based pH sensors to track viruses and study membrane fusion

The FRET-based pH sensor consisting of mTFP1 and mCitrine enhanced our ability to observe the trafficking of viral particles to low pH compartments and the pH of endosomes following viral fusion. Important was the lower pKa and higher emission intensity of mCitrine compared to FRET donors in previously used sensors. This system in conjunction with a third soluble content probe included in the viral particle to measure content release (full fusion) should be useful to follow the trafficking and fusion of other viruses. Improved far red fluorescence proteins such as mCardinal (Chu et al., 2014) or the recently developed FR-MQV (Mukherjee et al., 2020) could further enhance signal over noise, improving particle tracking and perhaps allowing identification of more fusion events in every field of view. The mTFP1-mCitrine sensor could also be used in future experiments to describe pH and motion of individual physiological cargos during trafficking, thereby solidifying the role of distinctive populations of endosomes on the fate of specific cargoes.

Important to the success of the current study was also the software developed to extract the traces of trafficking particles and their fusion events. Summing the fluorescence from three spectrally well-defined channels and

defining appropriate surrounding backgrounds around moving particles in live cells was critical for identifying fusion events (Fig. 2, 3). In addition, this software enabled trajectory analysis to distinguish different modes of motion of organelles or viruses in cells (Fig. 6).

The current study should also serve as a helpful illustration of the virtue and limitations of current pH sensing and tracking methods. As illustrated in many of our figures, the spread of biological variations of individual particles and the uncertainties of the measured parameters can be quite large. Careful calibration of the probes and analytical methods including defining the appropriate statistical descriptions of error is important. Despite these challenges, it is possible to extract meaningful new biological data from single particle tracking and pH measurements in cells as demonstrated in the present work. We expect that the continued development of new technologies in microscopy will further improve signal-to-noise and enable the tracking of many particles in the same field of view at high time resolution, thereby increasing assay throughput.

2.5 Materials and Methods

Cell lines

A549 cells came from the lab of Judy White and were verified by ATCC Human Cell Line STR Profiling Service. A549 cells were grown in Ham's F12 Nutrient Mixture with 10% FBS v/v and 100 units/mL penicillin, 100 units/mL

streptomycin, 0.25 micrograms/mL amphotericin B. U2OS and HEK293T17 cells were grown in high glucose DMEM supplemented with 10% FBS v/v, 2mM L-Glutamine, 1 mM sodium pyruvate, 100 units/mL penicillin, 100 units/mL streptomycin, 0.25 micrograms/mL amphotericin B.

Plasmids and cloning

To construct the FRET-based pH sensor, the mTFP1-mCitrine fragment was synthesized by GENEWIZ. The linker between the two constituent fluorescent proteins was RSTSLQEFGT. The gene fragment was then inserted in the place of ecto-pHluorin (EcpH) in EcpH-TM, a gift from Gregory Melikian (Addgene plasmid # 85389; http://n2t.net/addgene:85389; RRID: Addgene_85389).(Miyauchi et al., 2011) The mTFP1-mCitrine gene fragments and EcpH-TM were separately digested using HindIII HF and EcoRI HF (New England Biolabs) according to manufacturer instructions for 1 hr. Digestions were gel purified; then EcPh-TM and the insert were ligated with T4 ligase (NEB). The ligation reaction was heat inactivated and transformed into DH5α competent cells (NEB). Colonies were selected on LB-carbenecillin plates. Plasmids were initially screened by digestion and then the sequence of the open reading frame was verified with primers corresponding to sequences in CMV (forward), TFP (forward), hGH poly(A) (reverse).

Additional plasmids used included Gag-mKate2 (a gift from Gregory Melikian, Emory University), Murine leukemia virus (Friend strain) gag-pol

plasmid (a gift from Jean Millet at Cornell University and Jean Dubuisson at the Centre National de la Recherche Scientifique in Lille), pTG-luc (a gift from Gary Whittaker at Cornell University and Jean Dubuisson at the Centre National de la Recherche Scientifique in Lille), VSV-G plasmid (a gift from Michael Whitt at the University of Tennessee).

Preparation of pseudovirus

VSV-G bearing MLV pseudovirus with the FRET-based pH sensor and gag-mKate2 content marker was prepared by transfecting HEK293 T17 cells in Optimem-I using polyethylenimine and a 4:2:0.75:2:3 ratio: pTG-luc:pCMV gag-pol:gag-mKate2:VSV-G:mCitrine-mTFP1-ICAM1. HEK293 T17 cells were seeded at a density of ~$5x10^6$ cells/well in a 6 well tissue culture dish 24 hours prior to transfection. Optimem-I medium was replaced after 4-6 hours with high-glucose DMEM supplemented with 10% FBS. Supernatant was collected after 48 hours and purified by low-speed centrifugation, passage through a 0.45 μM filter, and centrifugation at $1.04x10^5 \times g$ through a 25% sucrose-HM cushion. The supernatant and the cushion were aspirated to the pellet, which was resuspended in HM buffer (130 mM NaCl, 20 mM HEPES, 20 mM MES, pH 7.4) at ~140x concentration relative to the initial volume of viral supernatant. Resuspended pseudovirus was stored in aliquots at -80° C.

The infectivity of generated pseudoviruses was evaluated by luciferase assay as described previously.(Hulseberg et al., 2019) Briefly, A549 target cells

were seeded at $2.5x10^4$ cells/well in a 96 well plate and infected by spinning at 4° C. Cells were prepared according to Britelite plus Reporter Gene Assay system (PerkinElmer). The assay was read on a GloMax Explorer (Promega). The pseudovirus preparation used to generate data contained in Figures 1-6 was found to be infectious (Supp. Fig. 5A). Additional viral preparations were found to be similarly infectious (Supp. Fig. 5B) and have comparable calibration curves (Supp. Fig. 5C).

Particle and experimental analysis criteria for calibration and live cell imaging

Stringent quantitative selection criteria were applied to ensure that the pH readout was uniform between calibration and live cell imaging, as well as that tracking would be accurate. Only particles with fluorescence from gag-mKate2 (content marker), mTFP1 (FRET donor) and mCitrine (FRET acceptor) were included in analysis of calibration experiments and live cell imaging. In addition, only particles less than approximately 1.5 μm in apparent diameter were included in the analysis as larger spots were considered to be part of aggregates.

Live cell imaging was performed on 27 plates of cells on 11 separate days. In each plate of cells, a single field of view was imaged, comprising one individual experiment. Of these 27 individual experiments, only 13 individual experiments conducted on 7 separate days had ideal conditions in which the field of view had 5-20 viral particles visible in the collected image series and a viral content release event was observed in the field of view. For four of the individual

experiments conducted, more than one fusion event was observed in the field of view. Individual experiments with too many particles in the field of view were excluded because individual particles couldn't be differentiated and tracked during trafficking.

For the 13 plates retained for analysis, the criteria described above for particle selection was applied (triply labelled, less than 1.5µm in apparent diameter). As an additional measure to avoid including particles where tracking was ambiguous in the analysis, particles were excluded if they could be observed in the same 2.94 μm^2 area as another particle at any time while they were tracked. Only particles that could be observed for at least 20 frames (6.67 minutes) were included in the analysis. From a total observation of 5041 particle tracks from the 13 individual experiments, 930 tracks were retained based on the applied criteria of the particle/endosome being tracked for at least 20 frames. After the additional particle inclusion criteria (listed above) were applied, 88 tracks remained. Within these 88 tracks, 18 fusion events occurred. Intensity and trajectory analysis were conducted for all 88 tracks.

Calibration and evaluation of FRET-based pH sensor

6-8 microliters of suspended pseudoviral particles labelled with the FRET-based pH sensor, mCitrine-mTFP1-ICAM1, and the content label, gag-mKate2 were spun for 20 min at 4° C and 200xg onto poly-L-lysine 0.1% V/V (Sigma-Aldrich) coated 35mm imaging dishes with a #1.5 glass insert (Mattek), such that

there were ~5-20 particles per field of view. The particles were observed on a laser scanning confocal microscope (LSM880, Carl Zeiss) at 37° C with a 63x (1.4 NA) oil immersion objective. The pH sensor was excited with an Argon laser at 458nm and the content label was excited at 561nm. Emissions intensities were collected in 15 × 8.9nm-width spectral bands between 472nm and 606nm using the GaAsp spectral detector of the microscope. In addition, emissions above 606nm were collected in a photomultiplier tube detector and that intensity was assigned to mKate2.

Mean fluorescence emission intensities at each wavelength were extracted from the region of each triple labelled, detected particle in each field of view and background subtraction was performed.

The donor intensity relative to the acceptor intensity was quantified by measuring the ratio of the intensities from the two respective bands according to $I_{494.0\text{-}502.9}/I_{530.0\text{-}538.9}$. The mean and standard deviations of all evaluated particles for a given prep at a given pH were plotted and fit with a sigmoidal function in GraphPad Prism 9.

Live cell imaging

A549 cells were seeded 24-32 hours prior to imaging at a concentration of approximately $1x10^5$ cells/dish onto a 35mm imaging dish with #1.5 glass slide insert (Mattek) coated with fibronectin. Prior to addition of virus, cells were chilled on ice for 10 minutes, then washed with cold HEPES imaging buffer (Life

Technologies) supplemented with 4.5 mg/mL glucose. 8-12 µL of pseudoviral particles were spun onto cells for 20 minutes at 4° C and 200 × *g*. A single pseudovirus preparation was used to generate the data derived from live cell imaging and displayed in Figures 2-6. Based on the similar infectivity and pH sensor calibration of viral particles from different preparations (Supp. Fig. 5 B,C), we expect that live cell imaging data from additional pseudovirus preparations would produce very similar results to those shown in Figures 2-6. Cells were washed in 2 mL of cold imaging buffer, placed on the microscope with the stage warmed to 37° C and the field-of-view for imaging was selected. After field-of-view and focus were set, viral trafficking was initiated by removal of 4° C imaging buffer and replacement with 37° C imaging buffer. A one to two-minute period of re-focusing followed the addition of 37° C imaging buffer and time zero in all experiments is the initiation of imaging after this initial time lag.

Excitation and detector configurations were the same as described for calibration and evaluation of the FRET-based pH sensor. An additional photomultiplier detector was used to generate a pseudo-DIC image of the cells using the transmitted light from the 458nm excitation. Frames were taken every 20s for at least one hour in a z-stack of 13 planes with 0.535nm between each plane. The image size was (800 x 800 pixel^2) with a pixel resolution of 0.141 nm/pixel and an optical zoom of 1.2x. The Definite Focus feature of the microscope was used every 5 frames to avoid vertical drift.

Analysis of live cell imaging

Unless otherwise noted, particles were tracked in 2D using a maximum intensity Z-projection of the integrated intensities from emission bands 494-502 nm, 530-538 nm, and 593-741nm. The cell area was masked for analysis using the pseudo-DIC image to exclude particles directly adhered to the glass insert of the imaging dish. Particles were tracked using the TrackMate (Tinevez et al., 2017). Particles were detected using a Laplacian of Gaussian segmentation and an expected minimum particle radius of 700-800 nm and an intensity threshold appropriate to the individual experiment. The simple Linear Assignment Problem (LAP) tracker was used with a maximum search distance of 2 nm for consecutive frames and a search radius of 3 nm for missed frames with a maximum of 2 missed frames permitted. Tracks with less than 4 spots were eliminated. In cases where a particle was visible but below the selected threshold for 2 or more frames, tracks were manually connected. Manual connection of particle localizations was only performed in cases where based on the sparseness of particles we had a high degree of confidence the particle identified by the tracking program at two separated time points was the same.

Tracking results were compiled into tracks and intensities from 494.0-502.9 and 530.0-538.9 were extracted using the MATLAB (R2018a, MathWorks). The mean intensity of the background at all extracted emissions intensities was subtracted from the mean intensity of the particle area, with the background region being a 2 pixel-width annular region around each 14 pixel (1.96μm)

diameter circular particle region. This data was used to calculate fluorescence ratios.

An in-house designed MATLAB (R2020b, MathWorks) application extracted and stored image regions of 21x21 pixel dimensions around each tracked particle and from 3 spectral channels. This data was then visualized and analyzed to identify fusion events, displacements and motion by custom built software written in LabView (National Instruments). Emissions collected from wavelengths 494-511 were assigned to channel 1, 521-538 to channel 2, and 593-741nm to channel 3. The extracted image regions corresponding to the trajectory of each file were read into LabView. Fusion was identified as a well-defined decrease of the mKate2 signal over 1 minute or less while signal corresponding to the FRET pair persisted. Only well-centered particles in the extracted region that had an approximate apparent diameter of less than 1.5 μm were considered for fusion analysis and only particles satisfying the same criteria were selected for the comparison set of non-fusing particles.

The velocity coefficient (v), representing the velocity of directed motion apart from drift or diffusion, was obtained using a directed-motion model of mean-squared displacement (MSD, ρ)

(Equation 1) $$\rho(\tau) = 4 D\tau + v^2 \tau^2$$

where D is the observed diffusion coefficient and τ is the time lag. Only time lags less than 60% of the total length of the entire tracks were used to fit to equation 1 because of the degree of imprecision in time lags that are long relative to the length of the observation time of the particle (Qian et al., 1991).

pH values were determined from the measured fluorescence emission intensity ratios $I_{494.0\text{-}502.9}/I_{530.0\text{-}538.9}$ using a standard table calculated from the fit in the calibration experiment of Fig. 1C (see Statistical Analysis and Data Fitting).

Statistical analysis and data fitting

Particle localization and emissions intensity data for all experiments was initially aggregated in R Studio (v. 1.1.453, R Studio Team 2020). Velocity, total displacement, fluorescence intensity ratio change, and related values were calculated in R Studio unless otherwise indicated. Statistical analysis was conducted in GraphPad Prism (Version 9.1.2 for Mac) and compared with the distributions of groups without an underlying assumption of parametric distributions (Mann-Whitney test). The two-tailed P-values were calculated and the summary values are reported in the relevant figures.

2.6 Supplemental Figures

A.

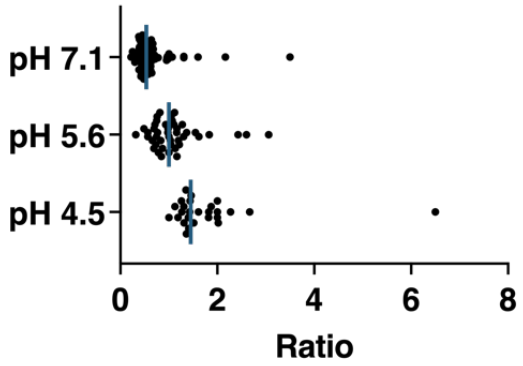

B.

pH	Mean Ratio	SEM	n
4.2	1.73	0.12	32
4.5	1.79	0.20	27
5.0	1.48	0.08	39
5.2	1.17	0.04	45
5.6	1.09	0.08	44
6.0	0.88	0.06	37
6.2	0.66	0.04	48
7.1	0.63	0.05	86
7.4	0.74	0.05	84

Supplemental Figure 2.S1. The pH sensitivity of the mTFP1-mCitrine FRET pair. *A)* Fluorescence intensity ratio data for individual virus particles from the experiment in Figure 2.1C is plotted at three pH values where each dot represents the emissions intensity ratio (494-502nm)/(530-538nm) for one particle. Blue bars represent the median ratio value of all particles at that pH. *B)* The fluorescence intensity ratio values (494nm/530nm) from the plot in Figure 2.1C. The number of individual particles at each pH varied in part because particles lifted from the coverslip or, in some cases, did not fluoresce above background at standard imaging settings at low pH. All data in A and B are from a single preparation of virus.

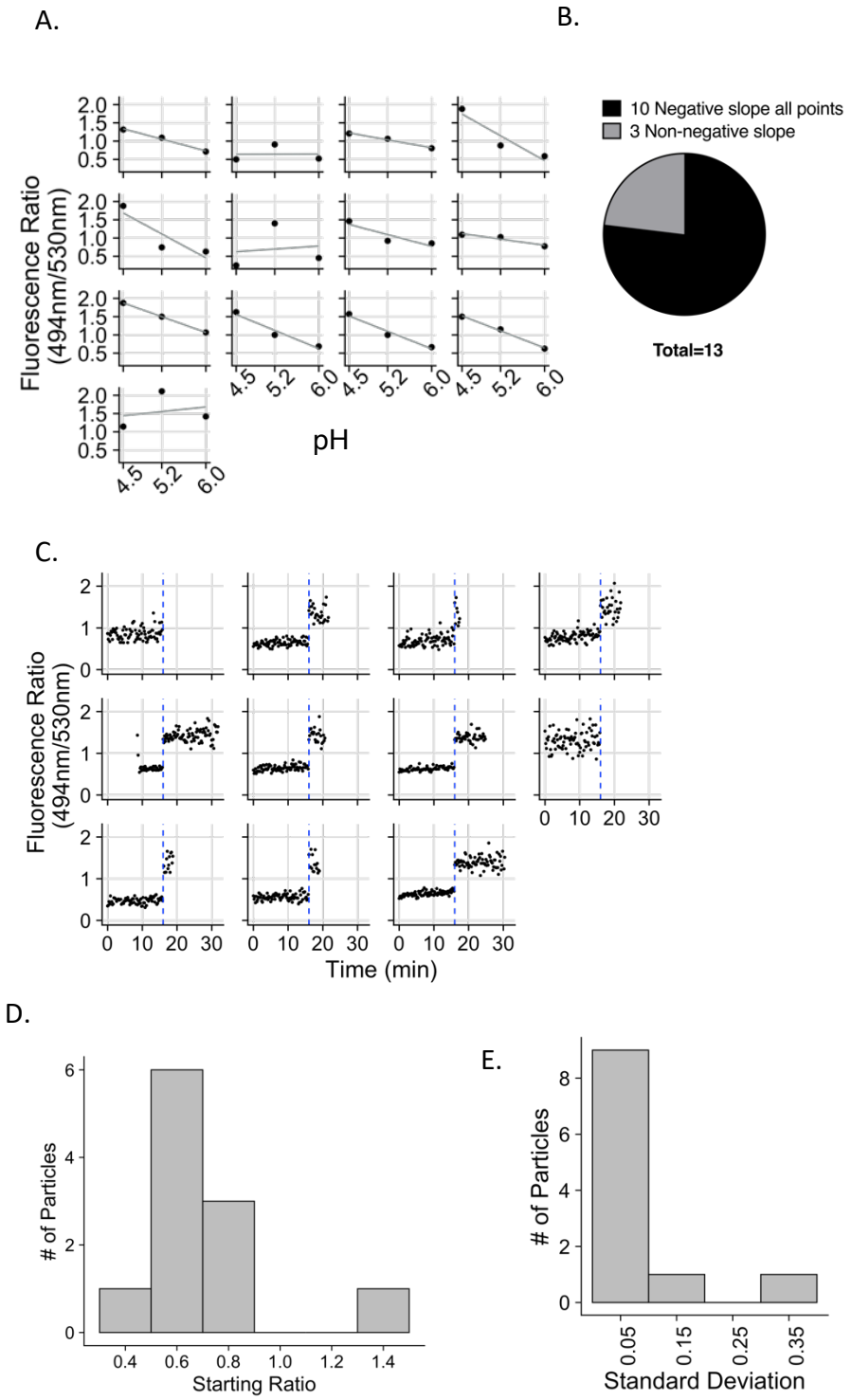

Supplemental Figure 2.S2. Variability of fluorescence behavior and pH response of viral particles with the mTFP1-mCitrine FRET pH sensor on coverslips. *A)* Particles spun onto a poly-lysine coverslip were imaged in three buffers of known pH consecutively applied and the 494nm/530nm emission

intensity ratio of 13 individual particles was determined. *B)* Proportion of particles in A that show the expected progression of increasing ratio with decreasing pH for all points (negative slope) versus proportion of particles that do not show this expected behavior (non-negative slope). *C)* Particles spun onto a poly-lysine coverslip were imaged in pH 7.1 buffer every 12s. After 16 min, pH 5.2 buffer was added as represented by the vertical dashed line. 494nm/530nm fluorescence intensity ratios are graphed over time. *D)* Distribution of the emission intensity ratio (494nm/530nm) of the experiment in panel A averaged over the first 6 frames. *E)* Distribution of standard deviations of the 494nm/530nm fluorescence intensity ratios over the first 6 frames of each experiment in panel C, representing frame-to-frame variability for individual particles.

A.

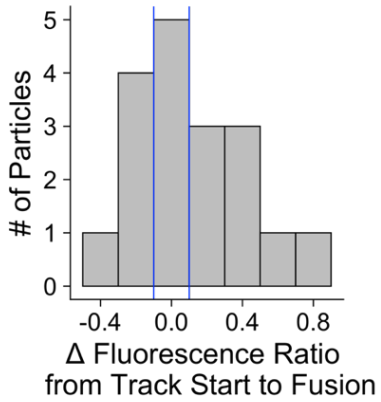

B.

Time (minutes)	Fluorescence Ratio (494nm/530nm)	pH	Δ pH per minute	Δ pH per minute, to and from local minimum
33.0	1.0	5.6		↓
36.0	1.6	4.7	-0.30	↓
36.7	2.0	Less than 4.2	At least -0.75	At least -0.38
39.0	1.1	5.5	0.56	At least 0.56

C.

Time (minutes)	Fluorescence Ratio (494nm/530nm)	pH	Δ pH per minute	Δ pH per minute, to and from local minimum
36.3	0.99	5.7		↓
38.0	1.14	5.4	-0.14	↓
40.0	1.81	less than 4.2	At Least -0.61	At least -0.40
41.3	1.52	4.8	0.49	↓
42.3	1.05	5.6	0.72	At Least 0.59

Supplemental Figure 2.S3. Additional acidification characteristics of endosomes harboring viral particles that fuse. *A)* Frequency histogram of the difference of 494nm/530nm emission intensity ratios between the mean of the six frames over which the particles are first observed (start) and the time at which the particles fuse (fusion). Blue lines denote the "zero" bin that contains particles within the band of frame-to-frame variability of the FRET sensor, i.e. particles displaying insignificant ratio changes. *B)* Quantification of a rapid fluctuation in pH in a fusion permissive endosome beginning about 5 minutes following fusion

of the viral particle. The fluorescence ratio over the entire observation time is depicted in Fig. 2.3A panel i. *C)* Quantification of a pH fluctuation in an endosome occurring in a time window 5-10 minutes prior to the fusion of the viral particle. The fluorescence ratio over the entire observation time is depicted in Fig. 2.3A panel xvii. For B and C, when fluorescence ratio values fell above the upper limit of the calibration curve, the pH was less than 4.2 but the exact value of the pH could not be determined. The values listed in the right are for the rate of pH change per minute over the entire time segment leading to the highest ratio (lowest pH value) and over the time period of re-alkalization to baseline.

A.

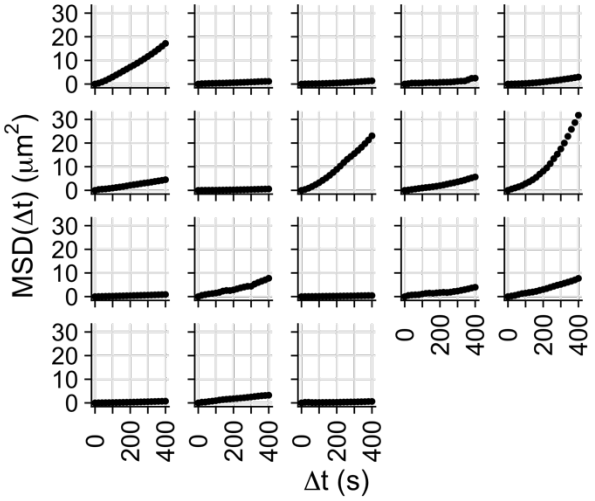

B.

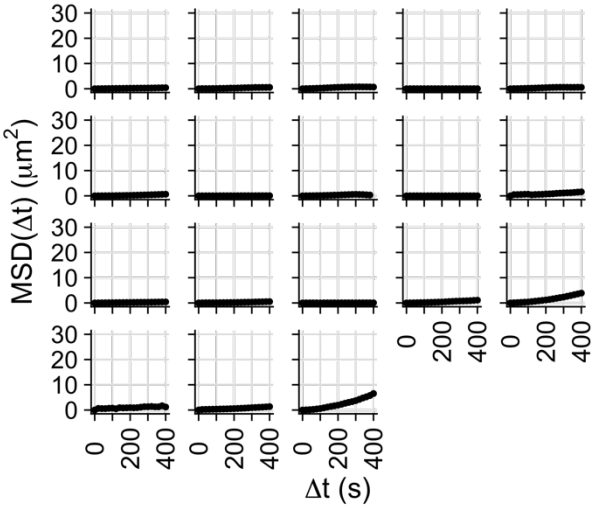

Supplemental Figure 2.S4. Motion analysis for individual endosomes harboring fusing and non-fusing viral particles. *A)* The mean squared displacement (μm^2) was calculated from particle localizations generated from tracking and plotted up to a maximum time step of 400 seconds for all fusion-permissive endosomes. The smallest time step is 20 seconds. *B)* Same as A., for fusion non-permissive endosomes. The averaged data from panels A. and B. are presented in Figure 2.6A.

A.

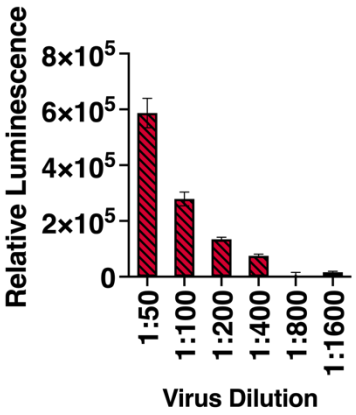
Relative Luminescence
8×10^5
6×10^5
4×10^5
2×10^5
0
1:50
1:100
1:200
1:400
1:800
1:1600
Virus Dilution

B.

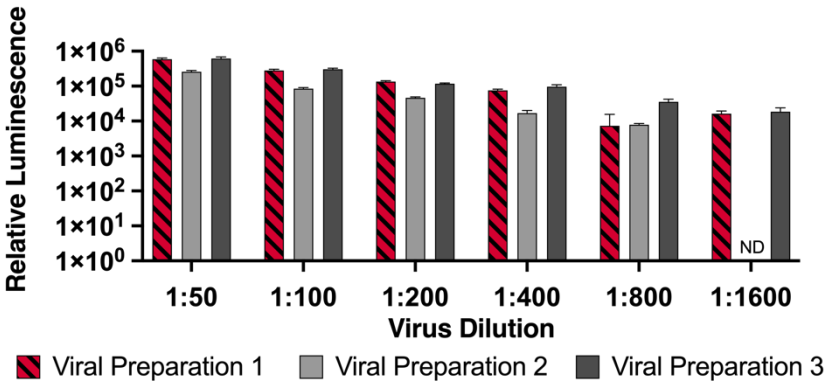
Relative Luminescence
1×10^6
1×10^5
1×10^4
1×10^3
1×10^2
1×10^1
1×10^0
ND
1:50
1:100
1:200
1:400
1:800
1:1600
Virus Dilution
Viral Preparation 1
Viral Preparation 2
Viral Preparation 3

C.

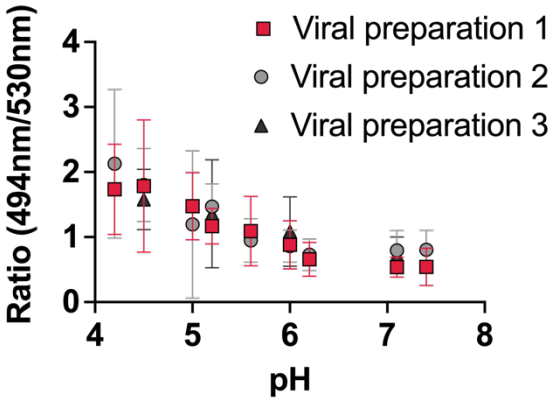
Ratio (494nm/530nm)
4
3
2
1
0
4
5
6
7
8
pH
Viral preparation 1
Viral preparation 2
Viral preparation 3

Supplemental Figure 2.S5. Infectivity and calibration curves of viral particles pseudotyped with VSV-G, bearing the pH sensor mTFP1-mCitrine and the content marker Gag-mKate2. *A)* The infectivity of pseudovirus used in imaging experiments from which the data displayed in Figures 1-6 originates. *B)* Infectivity data as in panel A (shown as red striped bars) alongside infectivity data for two other viral preparations produced using the same procedure as for the preparation in panel A. For viral preparation 2, the 1:1600 dilution was not assessed (indicated by ND). Data in (B) is plotted on a log scale. (A-B) Cells were infected as described in the Materials and Methods and the level of infection was measured by luciferase assay. Relative luminescence units, where a higher value indicates a greater degree of infection, are plotted for several viral dilutions. Data represent average luminescence units ± 1SD, measured in triplicate, from one experiment. *C)* Calibration curves of the pH-sensitive FRET pair for the three viral preparations whose infectivities are shown in panel B. The calibration values are depicted as red squares for the viral preparation whose infectivity is shown in panels A and B (Viral Preparation 1) and whose calibration is also shown in Fig. 2.1C. For viral preparation 3, data was collected at pH 4.5, 5.2, 6.0 and 7.1 only. Error bars represent 1 SD of the fluorescence ratios of individual particles found in each pH condition. For each pH condition, at least 32 individual particles were measured.

Chapter 3: Determination of the pH of Ebola Virus Fusion in Live Cells by Correlative Assay

3.1 Abstract

Ebola virus (EBOV) is a negative sense RNA virus presenting a serious risk to human health. The virus has a complex mechanism of entry into host cells. It is internalized and trafficked to an acidic late endosome (LE), where its glycoprotein (GP) is proteolytically processed and binds to its host cell receptor (NPC1) before fusion ensues. Studies that have reconstituted the fusion of EBOV GP or isolated portions of EBOV GP with artificial membranes or cell plasma membranes have yielded an estimated fusion pH of less than 5.5. While providing very valuable information on the pH of fusion of EBOV, these studies provide only partial insight on the conditions of fusion within live cells as key factors from the endosomal milieu, for example NPC1 or endosomal lipids, were not present. To gain further insight into the pH of EBOV fusion from within endosomes, we employed EBOV models with full-length GP to determine the pH dependence of EBOV fusion in live cells. We employed a novel endosome pH sensor, mNectarine-Lamp1, and correlated inhibition of viral entry by bafilomycin, an agent blocking viral entry by alkalinizing the LE lumen, with pH of the LE lumen (measured with mNectarine-LAMP1) upon treatment with the same concentrations of bafilomycin. With this approach, we determined that the

majority of EBOV particles fuse in U2OS cells below pH 5.7. The methodology presented could be used to determine the pH dependence of fusion in live cells for other enveloped viruses that enter cells through an endosomal pathway.

3.2 Introduction

Ebola virus (EBOV) is an enveloped virus with a high degree of pathogenicity and has been responsible for a significant public health burden in West Africa over recent years. Because the virus can persist in animal populations as well as immune privileged human tissues such as the eye and testes, future outbreaks are virtually inevitable (Jacob et al., 2020). EBOV is a member of the family *filoviridae*, named for the filamentous shape of individual viral particles (D. F. and H. Feldmann, 2015). EBOV contains two nucleoproteins, two polymerase complex proteins, a nucleocapsid associated protein (VP24), a matrix protein (VP40), and a glycoprotein (GP) (Watt et al., 2014), which are encoded in a negative-sense RNA genome (H. Feldmann et al., 2013). The EBOV GP is the portion of the virus that interacts with the host cell. A complex series of steps renders GP competent to mediate fusion of the virus with the host cell (Fénéant et al., 2019; J. M. White et al., 2016).

EBOV attachment to the cell is mediated by the interaction of GP or the viral envelope with proteins in the plasma membrane including lectins and TIM/TAM family members (Nanbo et al., 2010). The virus is then internalized via a macropinocytosis-like mechanism (Nanbo et al., 2010; Saeed et al., 2010) and

is trafficked to an acidic intracellular compartment, the late endosome (Simmons et al., 2016), where the viral glycoprotein (GP) is primed for fusion by proteolytic cleavage conducted by the cysteine proteases cathepsins B and L (Chandran et al., 2005; Schornberg et al., 2006). Low pH induces a change in the conformation of a key portion of the glycoprotein that enables fusion of the host and viral membrane, resulting in the release of viral contents into the cell cytoplasm and infection of the cell (Bär et al., 2006; Gregory et al., 2011; J. Lee et al., 2017). For fusion to occur, the virus must associate with its receptor, Niemann Pick disease type-C1 protein (NPC1) (Côté et al., 2011; Miller et al., 2012; Mittler et al., 2021; Spence et al., 2016). The portion of GP that binds NPC1 is known as GP1, while GP2 is responsible for mediating fusion with the host membrane (J. M. White et al., 2016). The mechanism served by NPC1 in EBOV fusion is not fully elucidated, but it may reposition GP2 in a manner that is favorable for fusion or allow other as yet unknown proteases to more efficiently act upon GP (Fénéant et al., 2019; J. M. White et al., 2016).

The role of late endosomal pH in the fusion of EBOV has been widely discussed and debated. Low pH is known to cause important structural changes in GP that result in the exposure of the fusion peptide, a moderately hydrophobic portion of GP2 that inserts itself into the lipid bilayer of the host membrane to initiate fusion (Gregory et al., 2011; J. Lee et al., 2017). However, a recent study has introduced new questions by demonstrating that low pH may stabilize the overall structure of GP, potentially opposing fusion (Bortz et al., 2020). It is

possible that low pH only induces conformational changes favoring fusion in the presence of other cellular factors such as full length NPC1 and appropriate levels of calcium (Das et al., 2020; Nathan et al., 2019), further emphasizing the need to study the pH of EBOV fusion in a cellular context. Therefore, we sought to fill the knowledge gap as to the pH of fusion of EBOV in live cells. To determine the pH of fusion, we performed an assay correlating endosomal pH with the ability of the virus to infect cells. We expressed a previously described fluorescent pH sensor mNectarine (D. E. Johnson et al., 2009), as a chimera with Lamp1, a resident late endosomal transmembrane protein, in U2OS cells. By imaging the mNectarine-Lamp1 pH sensor in live cells, we then measured the pH in late endosomes under both physiological conditions and when endosomes were alkalinized using bafilomycin, a vacuolar ATPase (V-ATPase) inhibitor. We concurrently determined the inhibitory concentration of bafilomycin for the infectivity of virus-like particles (VLPs) bearing EBOV GP in U2OS cells. We estimated the required pH for EBOV fusion in live cells by correlating these two measurements (Supp. Fig. 3.1).

3.3 Results

Expression and localization of mNectarine-Lamp1

To determine the pH of fusion for EBOV, we sought to develop a pH probe specifically targeted to the subset of late endosomes where EBOV fuses. A red fluorescent protein, mNectarine (D. E. Johnson et al., 2009), was cloned as a

chimera with Lamp1. mNectarine is derived from a mFruit construct combining mutations in mCherry2 and mTangerine and was generated using multiple rounds of error-prone PCR for mutagenesis and selection for enhanced fluorescence emissions intensity (D. E. Johnson et al., 2009). Lamp1 was chosen to both target and anchor mNectarine in the endosomal membrane because it had previously been described to reside in the same cellular compartments as NPC1 (Macías-Vidal et al., 2014; Xie et al., 2011). In addition, Lamp1 has also been shown to colocalize with TPC2 (Ruas et al., 2014), a protein that is be required for efficient EBOV entry (Sakurai et al., 2015). Moreover, many EBOV particles undergo lipid mixing with the host membrane in Lamp1+ compartments (Spence et al., 2016). The construct was engineered with a signal sequence preceding mNectarine such that mNectarine was translated into the luminal space of the endosome. mNectarine was linked directly to Lamp1. The design of the construct also preserved the late endosomal targeting sequence of Lamp1 (Rohrer et al., 1996) (Fig. 3.1A).

The mNectarine-Lamp1 chimera was expressed in U2OS cells and the localization of mNectarine-Lamp1 was evaluated. U2OS cells were chosen for their flat morphology, making them utile for microscopy, and their previous use in studies of EBOV entry (Spence et al., 2019). To confirm that mNectarine-Lamp1 localizes to compartments in which EBOV undergoes fusion, mNectarine-Lamp1 was co-expressed with NPC1-eGFP or TPC2-GFP, both of which mark compartments where EBOV fuses (Simmons et al., 2016). Less than one in 20

cells surviving transfection highly expressed both fluorescent chimeras. Sample images are shown for cells co-expressing mNectarine-Lamp1 and TPC2-GFP or NPC1-eGFP (Fig. 3.1 C, D). Object-based colocalization was conducted for nine cells co-expressing mNectarine-Lamp1 and NPC1-eGFP. An object-based approach was used because the variable relative abundance of mNectarine-Lamp1 and NPC1-eGFP in each cell rendered pixel-by-pixel measurement of co-localization less meaningful (Comeau et al., 2006). Endosomes positive for mNectarine-Lamp1 were segmented and the distribution of signal intensity of NPC1-GFP within this population of endosomes was measured. A control area from within the cell body was also measured and plotted for comparison (Fig. 3.1E). The data demonstrates that the signal of NPC1-eGFP is substantially higher in mNectarine-Lamp1 positive compartments than in a control area, suggesting that many endosomes containing mNectarine-Lamp1 also contain NPC1. Further, most mNectarine-Lamp1 colocalizes with TPC2-GFP. In a sample of 11 cells, the Manders coefficient (M1) that measures the proportion of mNectarine-LAMP1 that overlaps with TPC2-GFP is 0.99, with a maximum possible score of 1 indicating total overlap (representative image in 3.1 C). Thus, colocalization data suggests that mNectarine-Lamp1 localizes to the EBOV fusion compartment.

A.

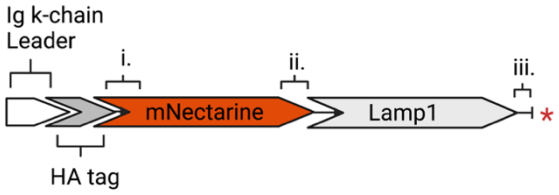
Ig k-chain
Leader
i.
ii.
iii.
mNectarine
Lamp1
HA tag

B.

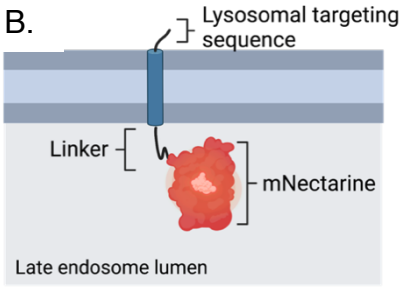
Lysosomal targeting
sequence
Linker
mNectarine
Late endosome lumen

C.

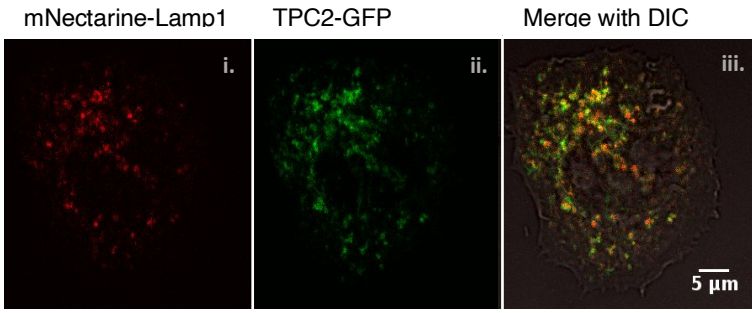
mNectarine-Lamp1
TPC2-GFP
Merge with DIC
i.
ii.
iii.
5 µm

D.

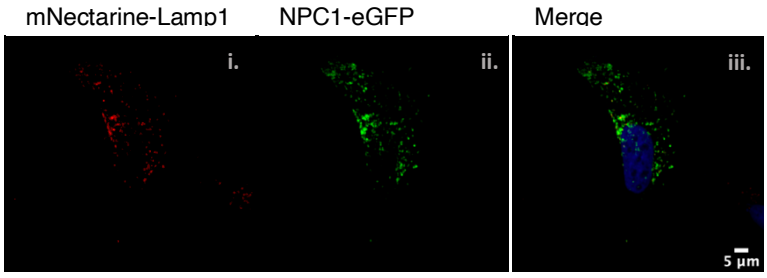
mNectarine-Lamp1
NPC1-eGFP
Merge
i.
ii.
iii.
5 µm

E.

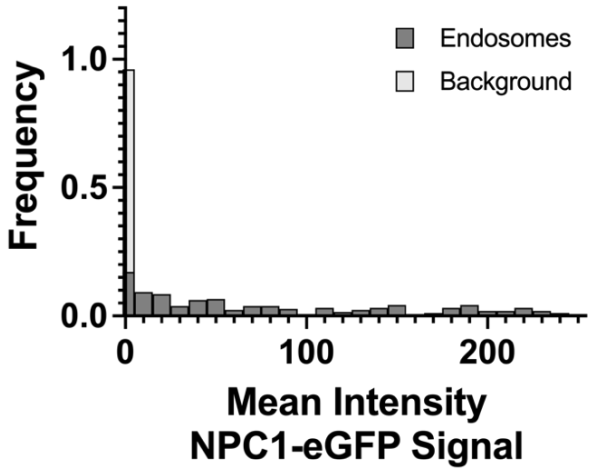
Endosomes
Background
Frequency
1.0
0.5
0.0
0
100
200
Mean Intensity
NPC1-eGFP Signal

Figure 3.1. mNectarine-Lamp1 localizes to late endosomes and senses luminal pH. *A)* The open-reading frame of the mNectarine-Lamp1 construct consists of a leader sequence to ensure translation into ER lumen (topologically analogous to extracellular space or endosomal lumen), an HA tag, a short linker (i.), mNectarine, a linker region (ii.) and Lamp1 including its lysosomal targeting sequence (iii.). The stop is indicated by the asterisk. *B)* Once translated, the polypeptide is directed to the endosome by the lysosomal targeting sequence of Lamp1. mNectarine resides in the endosomal lumen. *C)* Images of a U2OS cell co-expressing mNectarine-Lamp1 and TPC2-GFP with (i.) mNectarine-Lamp1 in red, (ii.) TPC2-GFP in green, and (iii.) images of both overlaid with a DIC image of the cell. *D)* Images of a U2OS cell co-expressing mNectarine-Lamp1 and NPC1-eGFP with (i.) mNectarine-Lamp1 in red, (ii.) NPC1-eGFP in green, and (iii.) images of both overlaid with DAPI stain for the cell nucleus. *E)* The co-localization of mNectarine-Lamp1 and NPC1-eGFP (representative image in D) was evaluated using an object-based approach for a sample of nine cells. The mean NPC1-eGFP fluorescence intensity in each late endosome, as identified from the fluorescence of mNectarine-Lamp1, was plotted. A negative control comparison set of endosome regions that would not be expected to contain a significant amount of NPC1-eGFP (see Materials and Methods, *Analysis of imaging experiments*) was plotted for comparison.

Calibration of mNectarine-Lamp1

The mNectarine-Lamp1 probe was calibrated in-situ using buffers of a known pH containing ionophores that permitted the equilibration of the endosomal pH with the buffer solution in which the cells were bathed. Images of a single cell bathed in a series of buffers with decreasing pH demonstrate that the intensity of emissions from mNectarine decreases with decreasing pH (Fig. 3.2 A). To quantify the pH response of mNectarine for individual cells, the perimeter of each cell was defined using a differential interference contrast (DIC) image of the cell. The thresholded mean fluorescence intensity within each cell above was then computed and plotted for a series of pH buffers ranging from 4.5 to 7.5. These full calibration curves were completed for four cells (Supp. Fig. 3.2)

and a representative curve is shown in Fig. 3.2 B. The calibration curves shown for mNectarine-Lamp1 in whole cells (Supp. Fig. 3.2) yield a calculated pKa of 6.1-6.3 for mNectarine-Lamp1. This is slightly lower than the pKa determined from a previously described calibration curve obtained for mNectarine alone purified from *E. coli* (pKa = 6.9) and analyzed in buffers of known pH using a spectrofluorometer (D. E. Johnson et al., 2009).

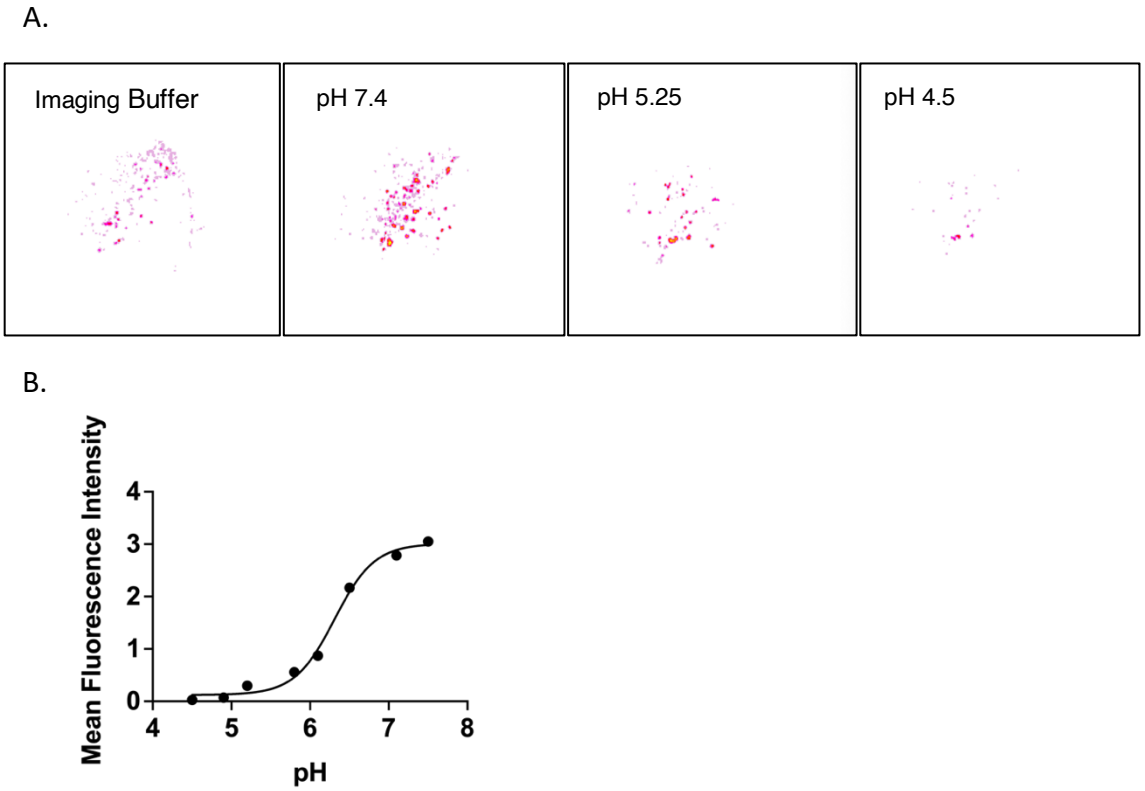

Figure 3.2. mNectarine-Lamp1 fluorescence intensity decreases with decreasing pH. *A)* An image of a U2OS cell expressing mNectarine-Lamp1 was collected in imaging buffer. Subsequently buffers of pH 7.4, 5.25 and 4.5 containing ionophores were added and images were collected. All images are displayed on the same 16-color scale with white indicating zero intensity, then pink to yellow indicating increasing intensity. *B)* The calibration curve of a single

cell fit was with a sigmoidal curve. The mean fluorescence intensity in a single plane of the cell body (region defined by DIC image of the cell) was determined in buffers of known pH containing ionophores and plotted over the pH of the applied buffers. The calibration data was not generated from the cell depicted in panel A. Additional calibration curves are shown in Supp. Fig. 3.1.

Correlative assay to determine the pH of full fusion for Ebola virus

Having established the localization and the pH response of the mNectarine-LAMP1 sensor, the change in late endosomal pH in response to varying concentrations of bafilomycin was determined. These data regarding late endosomal pH were used in conjunction with data from assays assessing entry of EBOV VLPs to estimate a pH of fusion mediated by EBOV GP (Supp. Fig. 3.1). To assess late endosomal pH, U2OS cells expressing mNectarine-Lamp1 were pre-treated with DMSO (vehicle for bafilomycin, mock treatment), 10 nM, 15 nM bafilomycin and 25 nM bafilomycin (Figure 3.3A). The mean fluorescence intensity of mNectarine-Lamp1 was determined on a per cell basis. In comparison to the mock treated control group, cells treated with bafilomycin had increased fluorescence of mNectarine-Lamp1 indicating that the endosomes had become more alkaline as expected. Each individual cell underwent a calibration procedure in-situ using two buffers of known pH after initial imaging. The buffers contained ionophores permitting equilibration of the endosomal lumen. The fluorescence intensity value of mNectarine-Lamp1 in the calibration buffers was used in conjunction with the initial measured fluorescence intensity of mNectarine to calculate the mean late endosomal pH within each cell.

The distribution of mean endosomal pH for individual cells was relatively narrow for mock treated cells (median = 4.7, interquartile range = 4.6-5.1) and broadened with 10 nM bafilomycin (median = 5.6, interquartile range = 5.2-6.4) or 15 nM bafilomycin treatment (median = 5.8, interquartile range = 5.5-6.4) (Figure 3.3A). Treatment with 25 nM bafilomycin again narrowed the distribution of pHs observed on a per cell basis and severely alkalinized late endosomes (median pH = 6.4, interquartile range = 6.2-6.5). The median pH value of approximately 4.7 determined for late endosomes in mock treated cells matches well with previously published data describing late endosomal pH (D. E. Johnson et al., 2016; R. J. Lee et al., 1996; Linders et al., 2022; Mundy et al., 2012; Ohkuma & Poole, 1978; Tycko et al., 1983), further supporting the use of the sensor to provide a late endosomal readout.

The effects of alkalinizing late endosomes on the infectivity of EBOV VLPs were also determined. VLPs have the filamentous morphology of live EBOV and bear EBOV GP but lack the required components for replication, rendering them non-pathogenic. Cells were pretreated with bafilomycin, VLPs were applied, and cytoplasmic entry assays were conducted in U2OS cells. The entry assays were used to assess what proportion of individual cells were infected in the presence of a given concentration of bafilomycin. Five entry assays were conducted on separate days (Supp. Fig. 3.3) and the results averaged to generate an inhibition curve (Figure 3.3B). To generate the inhibition curve, the proportion of cells infected in each increasing concentration of bafilomycin was normalized to the

percent of cells infected in the 0 nM bafilomycin condition. The relative entry was plotted over a range of bafilomycin concentrations. Sigmoidal fitting was performed on the inhibition curve (Figure 3.3B) and the concentration of bafilomycin that inhibited 50% of EBOV VLP entry was found to be 13 nM.

The results of the mNectarine-Lamp1 assay to measure late endosomal pH and the EBOV VLP entry assay were tabulated together to estimate the pH required to trigger EBOV GP mediated fusion (Figure 3.3C). The inhibition of viral entry in the presence 10 nM and 15 nM bafilomycin, the concentrations used to perturb endosomal pH, was 36 and 53%, respectively. The correlating median late endosomal pH in each condition is 5.6 and 5.8, respectively. The first quartile endosomal pH in each condition is approximately 5.2 and 5.5, respectively, and the minimum late endosomal pH in a single cell is 5.0. The 50% inhibitory concentration of 13 nM (calculated from a fit of the inhibition curve) falls between 10 nM and 15 nM, equivalent to a late endosomal pH of ~5.7. We therefore estimate that a pH under 5.7 facilitates EBOV fusion. Although the pH best supporting EBOV fusion may be slightly lower (see Discussion).

A.

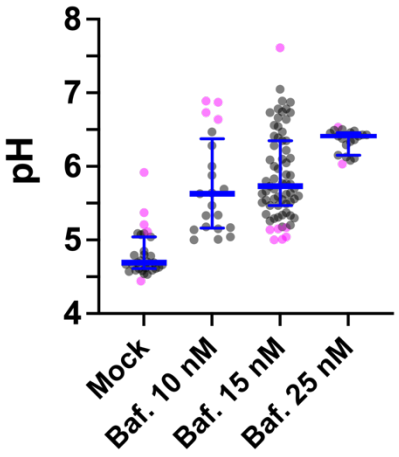

B.

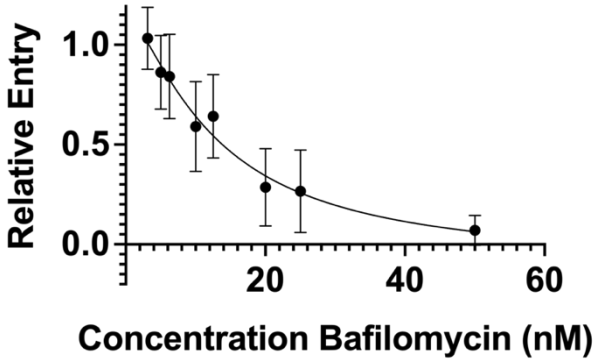

C.

Bafilomycin (nM)	Median pH	Percent Inhibition
0	4.7	0%
10	5.6	36%
15	5.8	53%
25	6.4	84%

Figure 3.3. Correlative data describe the relationship between inhibition of viral entry and the mean pH in late endosomes on a per-cell basis. *A)* The mean pH of late endosomes was determined in U2OS cells expressing mNectarine-Lamp1 and treated with bafilomycin or mock treated with DMSO. The mean emissions intensity from mNectarine-Lamp1 was taken in individual cells and those cells were then treated with buffers of a known pH. The pH of each cell was determined using own-cell calibration data and calculated pH values that fell above or below the pH values of the two calibration buffers are plotted in pink. Data points that fall between the pH values of the two calibration buffers are plotted in black. The first quartile, median and second quartile are plotted as blue bars. 31 individual cells were measured for the mock treatment condition, 21 for 10 nM bafilomycin, 67 for 15 nM bafilomycin, and 19 for bafilomycin 25 nM. *B)* Entry assays of EBOV VLPs into U2OS cells were conducted in the presence of varying concentrations of bafilomycin. Cells were

pretreated for 1 hour in bafilomycin and the indicated concentration of bafilomycin was maintained during the course of the assay. 5 biological replicates (with 3-4 technical replicates per concentration of bafilomycin per assay) were measured and the results averaged. Error bars are 1SD of biological replicates. A sigmoidal curve was fit to the results. *C)* The median pH and percent inhibition (calculated from sigmoidal fit in B) tabulated together.

V-ATPase inhibition and the trafficking of virus-like particles

Endosome acidification is a key part of the endosomal maturation program and bafilomycin treatment alkalizes late endosomes by inhibition of the V-ATPase, which pumps protons into the endosomal lumen (Bowman et al., 1988; Yoshimori et al., 1991). For EBOV to enter cells, it must be trafficked to mature endosomes where it encounters NPC1 and other requisite factors to trigger fusion (J. M. White et al., 2016). Evidence in the literature regarding the effect of bafilomycin treatment on trafficking of cargo from the plasma membrane to endosomes is equivocal (Bayer et al., 1998; Matsumoto & Nakanishi-Matsui, 2019; Stenbeck & Horton, 2004). To determine whether the inhibition of entry of EBOV in the presence of bafilomycin may be due in part to loss of trafficking of EBOV in addition to endosomal alkalization, we examined the co-localization of EBOV VLPs with the fusion compartment marker and viral receptor NPC1.

The co-localization of EBOV VLPs with NPC1 was compared in the presence and absence of bafilomycin after zero hours of trafficking and two hours of trafficking, the point at which maximal infection or colocalization with NPC1 is anticipated (Mingo et al., 2015; Spence et al., 2016). Colocalization of the EBOV VLPs, bearing a fluorescently labelled structural protein (mCherry-

VP40), and NPC1, detected by immunofluorescence, was assessed by fluorescence microscopy and quantitated using a Manders coefficient. Nocodazole (400 µM), which depolymerizes microtubules and severely limits the trafficking of EBOV VLPs to late endosomes (Mingo et al., 2015), was used as a negative control for colocalization of NPC1 and EBOV-VLP at 2 hours. Bafilomycin treatment (15 nM) substantially reduced the colocalization of NPC1 and EBOV-VLP compared to the mock treated condition (DMSO, bafilomycin vehicle), though the reduction was not as severe as with treatment by nocodazole (Figure 3.4, Supp. Fig 3.5). The reduction in expected trafficking of EBOV-VLP to a compartment containing NPC1, requisite for EBOV fusion, may cause some of the reduction in EBOV entry in the presence of bafilomycin (Figure 3.4, Fig. 3.3 B), introducing a confounding factor in the correlative assay.

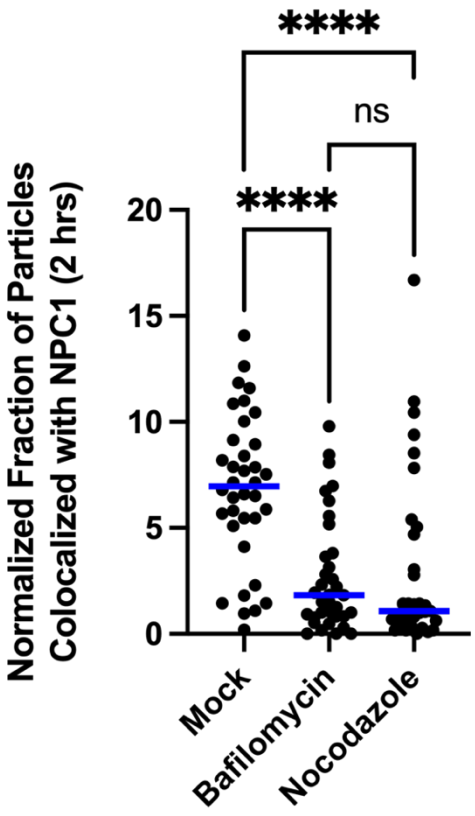

Figure 3.4. Bafilomycin inhibits the trafficking of EBOV VLPs in U2OS cells. EBOV VLPs were applied to U2OS cells and the effect of mock (DMSO), bafilomycin (15 nM) or nocodazole treatment (400 μM) on VLP trafficking to the EBOV fusion compartment (NPC1+) was assessed by immunofluorescence. Colocalization was calculated on a per-pixel basis and represents the overlap of thresholded VP40-mCherry signal from the VLPs with immunostained NPC1 (marked by Alexa-488). The colocalization of VLPs with NPC1 after 2 hours of trafficking for each cell was normalized to the mean value of colocalization at 0 hours over all cells in the same treatment group. This normalization was intended to compensate for differences in initial binding. 36 cells were assessed for the mock treatment, 35 for bafilomycin treatment and 33 for nocodazole treatment. The data are derived from experiments conducted on two separate days. A Kruskall-Wallis test (non-parametric multigroup statistical test) identified a statistically significant difference between mock treatment and both bafilomycin and nocodazole treatments (****, $p < 0.0001$; ns, no significance).

3.4 Discussion

Considerations in the use of a correlative assay to determine the pH of EBOV fusion

All measurements in the correlative assay used to estimate the pH required to trigger fusion mediated by EBOV GP were conducted on a per cell basis. Using a fluorescent sensor that specifically localized to late endosomes (Figure 1C-E), we determined the pH of late endosomes in a median U2OS cell to be ~4.7. Treatment with bafilomycin in concentrations of 10 nM and 15 nM raised the mean late endosomal pH in a median U2OS cell to 5.6 and 5.8 respectively (Figure 3.3C). Relative to the entry of EBOV VLPs into untreated cells, the entry of VLPs is inhibited by bafilomycin treatment with a 50% inhibitory concentration of 13nM. Because the assay is correlative, with pH and entry evaluated in separate experiments, it is uncertain where infected cells fall within the distribution of mean (per-cell) late endosomal pH compared to uninfected cells (Figure 3.3C). If we assume that cells falling within a specific part of the pH distribution are not preferentially entered, we can infer that the threshold pH for 50% efficient entry is 5.7. On the other hand, findings in reconstituted systems show that pH less than 5.5 best supports fusion (Bär et al., 2006; Gregory et al., 2011; J. Lee et al., 2017), suggesting that the subset of cells with the lowest mean late endosomal pH favor entry. If cells with more acidic late endosomes preferentially support fusion, most fusion events that still occur under 15nM bafilomycin treatment (close to the IC50 of 13nM) would be in cells with a mean

endosomal pH between 5.0 (lowest observable mean endosomal pH) and 5.6 (the median of the mean endosomal pH).

Aside from some uncertainty regarding through which subset of cells fusion occurs, it is not possible to know through what subset of endosomes entry occurs. Previous work has shown that late endosomes in fact have heterogenous pH (D. E. Johnson et al., 2016). It may be that even in the presence of bafilomycin treatment, endosomes have heterogenous pH. The particles that undergo fusion may do so preferentially through the most acidic endosomes, as only a few particles may have to enter a given cell for the cell to be counted as infected in the entry assay. It is also possible that particles enter through endosomes that have a combination of sufficiently low pH and other characteristics such as a specific concentration of calcium (Das et al., 2020; Nathan et al., 2019) or that some unknown factor promoting EBOV fusion (Fénéant et al., 2019; J. M. White et al., 2016) defines the endosomal subpopulation through which the particles enter. The question of what subset of cells or endosomes support entry can only be fully resolved by live cell imaging in which pH and fusion can simultaneously be observed. As described in Chapter 2, endosomes that supported viral content release mediated by the vesicular stomatitis virus fusion protein (VSV-G) were more acidified and motile than endosomes that did not mediate fusion events. If we conducted experiments using a similar system as in Chapter 2 to determine the EBOV pH of fusion, it is

possible that we would observe a unique subpopulation of endosomes that support fusion events and are characterized by acidification or motion.

Inhibition by bafilomycin of the trafficking of EBOV virus-like particles

The inhibition of trafficking of EBOV VLPs by bafilomycin introduces a confounding factor in the interpretation of the entry assay relative to pH data. The structure of the correlative assay assumes that loss of entry is due to alkalization of late endosomes rather than secondary factors. The failure of EBOV VLPs to co-localize with NPC1 in the setting of bafilomycin treatment is somewhat surprising based on previous findings that EBOV VLPs co-localize with NPC1 to the same or greater extent with bafilomycin treatment as opposed to mock treatment (Mingo et al., 2015). The effects of bafilomycin may be cell line and concentration dependent as other work has reported varying consequences for trafficking (Bayer et al., 1998; L. S. Johnson et al., 1993; Mingo et al., 2015; Stenbeck & Horton, 2004). While a fluid phase marker was shown to traffic normally in HeLa cells treated with 20nM bafilomycin, 200nM bafilomycin inhibited trafficking of the marker (L. S. Johnson et al., 1993). In osteoclasts, a specialized cell type that is rich in secretory lysosomes, treatment with just 25nM bafilomycin inhibited uptake of a fluid phase marker by 35% (Stenbeck & Horton, 2004). The use of HeLa or BSC1 cells in lieu of U2OS cells may eliminate the effect of bafilomycin on EBOV VLP trafficking (L. S. Johnson et al., 1993; Mingo et al., 2015) at the concentrations described in this study (0-15nM).

Testing a different agent by which to alkalinize endosomes may also permit normal trafficking of viral particles. Bafilomycin inhibits the V-ATPase, which interacts with molecules driving endosomal maturation (De Luca & Bucci, 2014; Matsumoto & Nakanishi-Matsui, 2019) and thus bafilomycin may inhibit trafficking by a mechanism other than alkalization of the endosomal lumen. Ammonium chloride directly alkalinizes endosomes as a weak base and while it may somewhat inhibit the maturation of endosomes, the effect is not as pronounced as with bafilomycin treatment (Clague et al., 1994; Ukkonen et al., 1986). Recently, a novel set of nanoparticles was designed to buffer endosomes to specific known pH values (pH 4.4-7.1) and additionally use fluorescence to indicate which endosomes are at or below the clamped pH. The nanoparticles enter the cells by fluid phase uptake (C. Wang et al., 2015). Some evidence exists to show that buffering the endocytic pathway through the use of nanoparticles still permits normal physiological functions as the treatment of cells with nanoparticles of pKa 4.4 did not block autophagosome maturation (C. Wang et al., 2017). When cells were treated with nanoparticles of pKa 6.2, compartments bearing Rab5, an early endosome marker, eventually acquired LAMP2, a late endosome and lysosome resident protein, indicating normal endosome maturation (C. Wang et al., 2015). The effect of the application of nanoparticle buffers of any pKa on the trafficking of cargo to late endosomes has not been investigated directly however and would need to be elucidated prior to using nanoparticle buffers as a means of perturbing viral fusion.

Advancing the correlative assay for pH of fusion with ratiometric pH sensors

A correlative approach to determining the pH of viral fusion in whole cells offers the advantage of being relatively high throughput. For numerous less-studied viruses, the assay could be applied as a high-throughput method for estimating what pH is sufficient for fusion. Since only one curve would need to be generated describing the correlation between endosomal pH and the concentration of an alkalinizing agent used, each virus under investigation would simply require an entry assay to determine the inhibitory concentration of the alkalinizing agent.

The use of the assay as a high throughput method for determining a pH threshold for the fusion of many viruses could be made even more robust by the replacement of mNectarine with a ratiometric fluorescent pH sensor. A ratiometric pH sensor was not used in this study because we initially planned to use the sensor in conjunction with additional sensors or viral labels. This required we minimize the fluorescence emissions range of the pH sensor as most ratiometric pH sensors that function well at low pH consist of multiple fluorophores. For the purposes of solely advancing the correlative assay though, a ratiometric pH sensor would be ideal. The readout of ratiometric pH sensors is unaffected by the expression level in individual cells (see Chapter 2) (Canton & Grinstein, 2015) and thus a generic calibration curve relating a fluorescence emissions intensity ratio to pH could be used for all cells. The recently described pHLARE is a ratiometric pH sensor that is targeted to late endosomes via Lamp1

and is sensitive to pH variations between 4.5 and 6.5 (Webb et al., 2021), a range highly relevant to the fusion of pH-triggered enveloped viruses (Lozach et al., 2011; J. M. White et al., 2016) and could enhance the robustness of the correlative assay.

Alternative approaches to determining the pH of EBOV fusion

Single particle approaches provide definitive information regarding the fusion of individual viral particles to construct a distribution of the pH at which fusion events occur. To monitor pH, a sensor may either be anchored in the endosomal membrane (as described in this Chapter) or the viral membrane (as described in Chapter 2). Fusion for individual particles can then be monitored via release of fluorescently labeled viral contents (as described in Chapter 2) or changes in fluorescence of a lipid label in the viral membrane (Simmons et al., 2016; Spence et al., 2016; L.-J. Zhang et al., 2020). The disadvantage of single particle approaches is that live cell imaging experiments with single particle tracking are technically challenging and are relatively low throughput. We attempted to use the assay described in Chapter 2 consisting of a pseudovirus particle with a content marker and FRET based pH sensor to also determine the pH of EBOV fusion. Unfortunately, the particles generated bearing EBOV GP were quite dilute and yielded low infectivity when assayed by a luminescence assay (10,000 RLU or less compared to greater than 500,000 RLU for VSV-G, see Chapter 2 for VSV-G data). It is possible that, as discussed in Chapter 2 and

Appendix A, alternative model viral systems, such as vesicular stomatitis virus pseudotypes may improve viral infectivity and/or allow the production of more concentrated viral particles (Hulseberg et al., 2018; Schornberg et al., 2006). In addition, improvements in imaging technology and labeling schemes may allow the measurement of pH at the time of fusion of EBOV particles.

3.5 Materials and Methods

Cloning and plasmids

The leader-mNectarine-Lamp1 construct was cloned into the pcDNA3.1 (Invitrogen) vector by a multistep process that used assembly in pDisplay (Invitrogen) followed by digestion of the open reading frame and ligation into pcDNA3.1. The protocol is detailed below. pBAD-mNectarine was a gift from Robert Campbell (Addgene plasmid # 21717 ; http://n2t.net/addgene:21717 ; RRID:Addgene_21717) (Johnson 2009). pRK5-LAMP1-FLAG was a gift from David Sabatini (Addgene plasmid # 71868 ; http://n2t.net/addgene:71868 ; RRID:Addgene_71868) (Wang 2015).

Primers (Table 3.1) were designed for amplification of mNectarine and Lamp1 such that sequence overlap was generated between these two fragments and pDisplay. pDisplay was digested with SmaI (New England Biolabs) to generate a linear fragment and gel purified by kit (Qiagen, catalogue #28706). An assembly of the pDisplay backbone and mNectarine and Lamp1 inserts was conducted using NEBuilder HiFi Assembly (New England Biolabs). A 3:3:1 molar ratio of mNectarine insert to Lamp1 insert to linearized vector was used and the

assembly reaction was incubated for 30 minutes at 50° C. The reaction product was transformed into XL 10 Blue competent cells (Agilent). Colonies were selected on carbenicillin (Sigma-Aldrich) plates. DNA was prepared from single colonies and screened by restriction digest of the assembled fragment using BglII and PstI (New England Biolabs). Colonies positive for the assembled insert of mNectarine-Lamp1 were amplified by PCR (primers in Table 3.1) along with the leader sequence derived from pDisplay, generating the desired open reading frame and cleavage sites for NotI and BamHI (New England Biolabs). The amplified fragment of leader-mNectarine-Lamp1 was cleaned on a QIAquick column (Qiagen) and digested by NotI and BamHI. pcDNA3.1 was also digested by NotI and BamHI and purified on an agarose gel. The insert was ligated into pcDNA3.1 using T4 ligase (New England Biolabs). The ligation was transformed into DH5α competent cells (Life Technologies). The construct was verified by sequencing and is referred to as mNectarine-Lamp1.

Plasmids used for expression of TPC2-GFP and NPC1-eGFP were from Origene (cat # RG209023) and David Castle at the University of Virginia, respectively.

Table 3.1. Primers for sequence amplification

Target	Orientation	Sequence
mNectarine	Forward	CCCAGCCGGCCAGATCTCCCGTGAGCAAGGGCGAGGAG
mNectarine	Reverse	CCGCCGGATCCTCCCTTGTACAGCTCGTCCATGC
Lamp1	Forward	GCTGTACAAGGGAGGATCCGGCGGAGGTTCTGGTGGTGCAATGTTTATGGTGAAAAATG
Lamp1	Reverse	GACCTGCAGCCGCGGATCCCCTAGATAGTCTGGTAGCC
open reading frame in pDisplay	Forward	GCGACGGGATCCGGAATTCGGCTTGGGGATATCCACC
open reading frame in pDisplay	Reverse	CGTATGCGGCCGCCCTGCAGCCGCGGATCC

Cell Culture

U2OS cells (from Dorothy Schafer, University of Virginia) and HEK293T17 cells (from Judith White, University of Virginia) were grown in high glucose Dulbecco's Modified Eagle Medium (DMEM) supplemented with 10% FBS v/v, 2mM L-glutamine, 1 mM sodium pyruvate, 100 units/mL penicillin, 100 units/mL streptomycin, 0.25 micrograms/mL amphotericin B (all from Gibco Life Technologies).

Preparation of virus-like particles

Virus-like particles (VLPs) bearing Ebola virus glycoprotein were prepared as previously described (Shoemaker et al., 2013). Briefly, 293T17 cells were transfected with plasmids for VP40, β-lactamase-VP40, mCherry-VP40 and the Ebolavirus glycoprotein. Supernatant from the cells was harvested and clarified. The supernatant was then placed over a sucrose cushion and the virus-like particles pelleted by ultracentrifugation. The virus-like particles were then resuspended and frozen at -80 °C for further use. The infectivity of each

preparation was determined using the β-lactamase/CCF2 method described below (*Virus entry assays*).

Expression of fluorescent chimeras

mNectarine-Lamp1 was expressed in U2OS cells. The cells were transfected by electroporation in a Nucleofector 2b device (Amaxa). Cells used for transfections were 70-85% confluent and had been passaged less than 30 times. U2OS cells were lifted by trypsin, gently pelleted, resuspended in PBS and counted. $1x10^6$ cells were spun down, washed with 5 mL of PBS and spun down again. The cells were then resuspended in 100 µL of electroporation solution, 1 µg of purified mNectarine-LAMP1 cDNA was added, and the mix was gently pipetted into a cuvette for electroporation (Ingenio, Mirus Bio, catalogue #50121). The cells were electroporated using program X-001. 500µL of warm culture medium was added to the cuvette and the cell mixture was transferred to a single well of a prepared 6-well plate containing warm medium. After approximately 16-24 hours the transfected cells were lifted, counted and transferred to a fibronectin coated slip or plate for imaging (see sections below).

For co-transfection experiments, the same electroporation protocol above was conducted but the DNA mixture used was modified. For co-transfection of TPC2-GFP or NPC1-eGFP and mNectarine-Lamp1, 0.9 µg of each DNA was used per electroporation reaction. Cells co-transfected with NPC1-eGFP and

mNectarine-Lamp1 were fixed with 4% paraformaldehyde and stained with DAPI prior to imaging.

Live cell imaging and v-ATPase inhibition experiments

Transfected cells (see *Expression of mNectarine-Lamp1* section above) were seeded onto fibronectin-coated 35 mm dishes with a #1.5 glass slip insert (Mattek) at a density of $1.2x10^5$ cells per dish. Cells were imaged 18-24 hours after seeding on a LSM880 scanning confocal microscope (Zeiss). Growth medium was exchanged for Live Cell Imaging Solution (Invitrogen) containing 4.5 mg/mL glucose prior to imaging. A heated stage was used to maintain the temperature of the cells at 37 °C. mNectarine was excited at 561 nm and emissions were collected from 565-680 nm in a photomultiplier tube detector. In addition, signal was collected to generate a pseudo-DIC image that could be used to define the cell perimeter. A 40x/1.4 NA DIC oil immersion objective (Zeiss) was used to collect the 1024x1024 pixel images.

For experiments in which cells were treated with bafilomycin to inhibit V-ATPase and alkalize the endosomes, growth medium containing the indicated concentration of bafilomycin (Sigma-Aldrich, 20 μM working solution in DMSO) was exchanged onto the cells ~1.5 hours prior to imaging. The same concentration of bafilomycin was maintained throughout the experiment by application of imaging buffer containing bafilomycin. For the mock treatment condition, 0.2% (v/v) DMSO was added to imaging buffer.

Calibration of mNectarine and photobleaching analysis

Cells were prepared as described above in the section *Live Cell Imaging*. After each experiment, mNectarine was calibrated *in situ* on a per-cell basis using a 2-point calibration curve. Pairs of buffers were used rather than a full calibration curve to minimize photobleaching following the initial period of imaging the experimental condition. For each mock or bafilomycin treatment condition, a pair of buffers was used such that the intensity of mNectarine when bathed in those buffers encompassed the approximate range of intensities observed in the experimental condition. The pairs of buffers used for each experimental condition are listed in Table 3.2.

To perform the calibration *in situ*, pairs of buffers with known pHs were prepared with the following composition: 143 mM KCl, 5 mM glucose, 1mM $MgCl_2$, 1 mM $CaCl_2$, 20 mM MES or sodium acetate or HEPES, 10 µM nigericin and 5 µM monensin (Sigma-Aldrich). After the initial imaging period, the Live Cell Imaging Solution was removed, the well of the dish was gently rinsed with 500 µL of the calibration buffer, and 1 mL of

calibration buffer was applied. The first calibration buffer was applied for a period of at least 10 minutes to allow the ionophores to reach full effectiveness and allow the pH inside of the endosomes to fully equilibrate with the pH of the bathing buffer. Subsequent buffers were incubated for at least 5 minutes prior to imaging.

Additional buffers at pH 7.5, 7.1, 6.5, 6.1, 5.8, 5.2, 5.0, 4.5 were prepared to generate the full calibration curves of mNectarine-Lamp1 (as shown in Figure 3.2 B, Supp. Fig. 3.2). When completing a full calibration curve, buffers were applied in the order from high pH to low pH.

Photobleaching analysis was conducted in whole cells to ensure that taking several Z-stacks of cells when collecting the in-situ calibration curve would not affect pH determination. Bleaching was approximately linear (Supp. Fig. 3.4). Based on the determination of bleaching using a laser power of 1.5%, it was decided to use a lower laser power for live cell imaging to minimize photobleaching. The laser power used varied slightly based on whether the cells were treated to alkalinize late endosomes. In all cases the same laser power was used for both the initial data collection (imaging buffer) and calibration. When endosomes were highly alkalinized resulting in a bright signal from mNectarine, a lower laser power was used for collection and calibration. The laser power used was always below 1.2% and, in most cases, ranged from 0.3-1%. No correction was performed for photobleaching.

Table 3.2. pH buffers for calibration of mNectarine-Lamp1

Condition	High pH buffer	Low pH buffer
Mock Treatment	5.1	4.5
Bafilomycin 10 nM	6.5	5.0
Bafilomycin 15 nM	7.1	5.2
Bafilomycin 25 nM	6.5	6.1

Virus-like particle entry assays

Entry assays were conducted as previously described (Mingo et al., 2015; Shoemaker et al., 2013). Briefly, U2OS cells were seeded at a density of $4.5x10^4$ cells per well in a 96 well plate. Cells were seeded from plates that were no less than 70-90% confluent. Cells were pretreated for one hour at 37° C with the indicated concentration of bafilomycin. Virus-like particles were bound to cells by spinning (250 × g) at 4° C in the presence of the indicated concentration of bafilomycin. VLPs used in these experiments had previously been assayed for infectivity. An amount of virus was applied such that on average 17% of cells were infected in the mock condition. After infection, cells were transferred to a 37° C incubator for 3 hours. Entry was then stopped by washing samples once with loading buffer (phenol red free DMEM supplemented with 2 mM L-glutamine, 2.5 mM, probenecid, 25 mM HEPES, and 200 nM bafilomycin). A β-lactamase substrate, CCF2, was then loaded into cells by incubation in the dark for 1 hour. Cells were fixed and analyzed for cleavage of CCF2 by use of flow cytometry (as previously described, Shoemaker et al., 2013).

Virus-like Particle Trafficking Assay

A viral trafficking assay was used to assess the progress of VLPs to the fusion compartment in the presence of bafilomycin, nocodazole or mock treatments in Figure 4. VLPs bearing a fluorescently labeled structural protein (VP40-mCherry) were used as in the virus entry assays. The colocalization of these VLPs with immunostained NPC1 was assessed. Higher co-localization at

longer timepoints indicated that more viral particles had been internalized trafficked to the fusion compartment.

U2OS cells were seeded onto fibronectin coated #1 coverslips contained in a 24-well plate at a density of 3.2-3.5x10^4 cells/well such that the cells were no more than 70% confluent at the commencement of the trafficking assay. 24-36 hours after seeding cells were chilled on ice for 10 minutes. Cells were pretreated with DMSO, 15nM bafilomycin or 400 µM nocodazole. Purified VLPs were diluted in Opti-MEM (Gibco) with a concentration of 0.2% (v/v) DMSO, bafilomycin or nocodazole such that the pretreatment conditions were maintained. The VLPs were diluted such that the concentration of VLPs per well would be expected to yield ~30% infection based on infection data for a given viral preparation (see *Virus-like Particle Entry Assays*). The VLP mixtures were applied to the pre-chilled cells and spun for 1 hr at 4° C at 250xg. Samples in the 0 hr condition were immediately placed on ice, rinsed in PBS and fixed in 4% paraformaldehyde. Samples in the 2 hr condition were warmed to 37° C and incubated in 5% CO_2 for two hours, after which they were rinsed and fixed. The overall immunofluorescence protocol was performed as previously described (Mingo et al., 2015). Briefly, all samples were permeabilized and blocked using a saponin/bovine serum albumin solution (10% heat inactivated Supplemented Calf Serum (HyClone), 0.05% saponin (Sigma S-1252), 10 mM glycine pH 7.4, 10 mM HEPES pH 7.4). Immunofluorescence staining was then conducted for NPC1 using an anti-NPC1 primary antibody (1:500; Abcam, ab134113) and anti-rabbit Alexa Fluor-488 as the secondary antibody (1:1500; Invitrogen). Coverslips were

mounted using Prolong Gold (Invitrogen), sealed and underwent confocal scanning imaging (LSM880, Zeiss).

Collected images were analyzed in FIJI (ImageJ) using JACoP (Bolte & Cordelieres, 2006). The automatic thresholding function was used and the Manders value for co-localization of VLPs with NPC1+ immunostained compartments was calculated. Higher Manders values represent a greater overlap of signal above threshold from the two channels with a maximum value of one. To account for any differences in virus binding between treatment conditions, Manders (M1) values after two hours of trafficking for each field of view in each treatment were normalized to the mean Manders value in the corresponding zero-hour time point for the same treatment. Only assays in which the nocodazole was shown to inhibit trafficking relative to mock treatment were included in the analysis.

Analysis of imaging experiments to assess late endosomal pH

For live cell imaging experiments, the cell body was masked based on the pseudo-DIC image. As above, the analysis was conducted using FIJI. The mean emission intensity between 565 and 680 nm was assessed within the region of the cell body. To evaluate the background signal, the emission intensity of mNectarine and/or cellular autofluorescence outside discrete punctate areas representing endosomes but within the cell body was assessed in mock treated cells. Based on the mean signal intensity from the background area, a threshold was applied on a per experiment basis (sets of cells in a single condition

collected on the same plate). Threshold intensity values ranged from ≤3-10 (in a 255 value, 8-bit image). The same analysis procedure was applied to generate intensity values for the *in situ* calibration curve. A mean pH of the late endosomes in each cell was calculated by converting the mean, thresholded intensity within the cell body to a pH by interpolation using the 2-point calibration curve (see *Calibration of mNectarine*).

Analysis of imaging experiments to assess co-localization of mNectarine-Lamp1 with cellular markers

The colocalization of mNectarine-Lamp1 with TPC2-GFP was determined in FIJI using a Manders coefficient as described above in the section *Viral trafficking assay*.

Object-based colocalization for mNectarine-Lamp1 was determined in FIJI by identification of mNectarine-Lamp1 endosomes and the quantitation of mean NPC1-eGFP fluorescence intensity in each endosome. This approach was used instead of a Manders coefficient because the variable relative abundance of mNectarine-Lamp1 and NPC1-eGFP in each cell rendered pixel-by-pixel measurement of co-localization less meaningful (Comeau et al., 2006). Endosomes were identified by use of a binary image generated using an automated Otsu threshold on the image generated by emissions from mNectarine-Lamp1 only. Then the particle analysis function was used to generate regions of interest (ROI) representing endosomes. These ROI were applied to the image of NPC1-eGFP and the mean intensity within each ROI

quantified and plotted as a distribution. A comparison data set (negative control for colocalization) was taken by taking the mNectarine-Lamp1ROIs from one cell and applying them to the image of NPC1-eGFP in a different cell, such that the ROI set would not be expected to solely or even primarily sample endosomes. The mean intensity values of NPC1-eGFP in this control set was considered to be background or coincidental.

Data Analysis

Plots were generated in R Studio and Prism 9 (GraphPad). Statistical significance was evaluated by a Kruskall-Wallis test.

3.6 Supplemental Figures

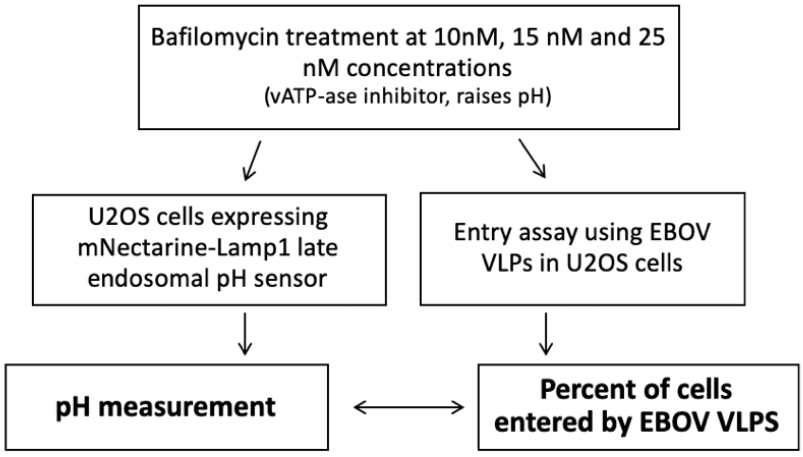

Supplemental Figure 3.1. Schematic representation of a correlative assay to estimate the pH of EBOV fusion. Bafilomycin was used to alkalinize the endosomes of U2OS cells and the change in late endosomal pH and the entry of EBOV VLPs was measured. The correlating change in pH and inhibition of entry was used to estimate a pH of fusion.

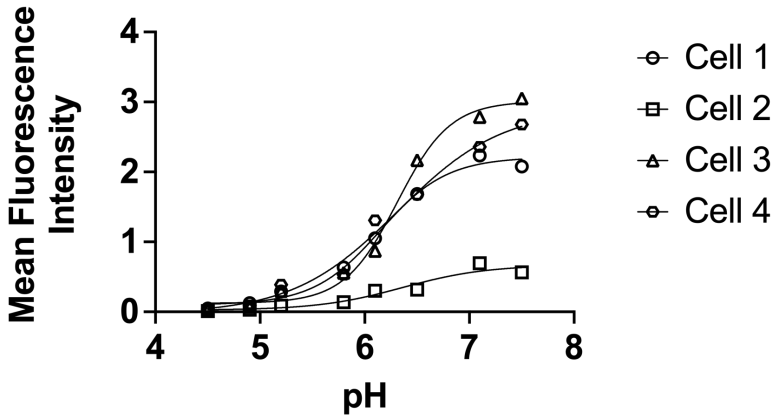

Supplemental Figure 3.2. mNectarine-Lamp1 calibration curves for four individual cells. Calibration curves of mNectarine-Lamp1 were collected in several cells. Data was collected, analyzed and fit as described in Figure 2B. The calibration curve depicted in Figure 2B is Cell 3 above.

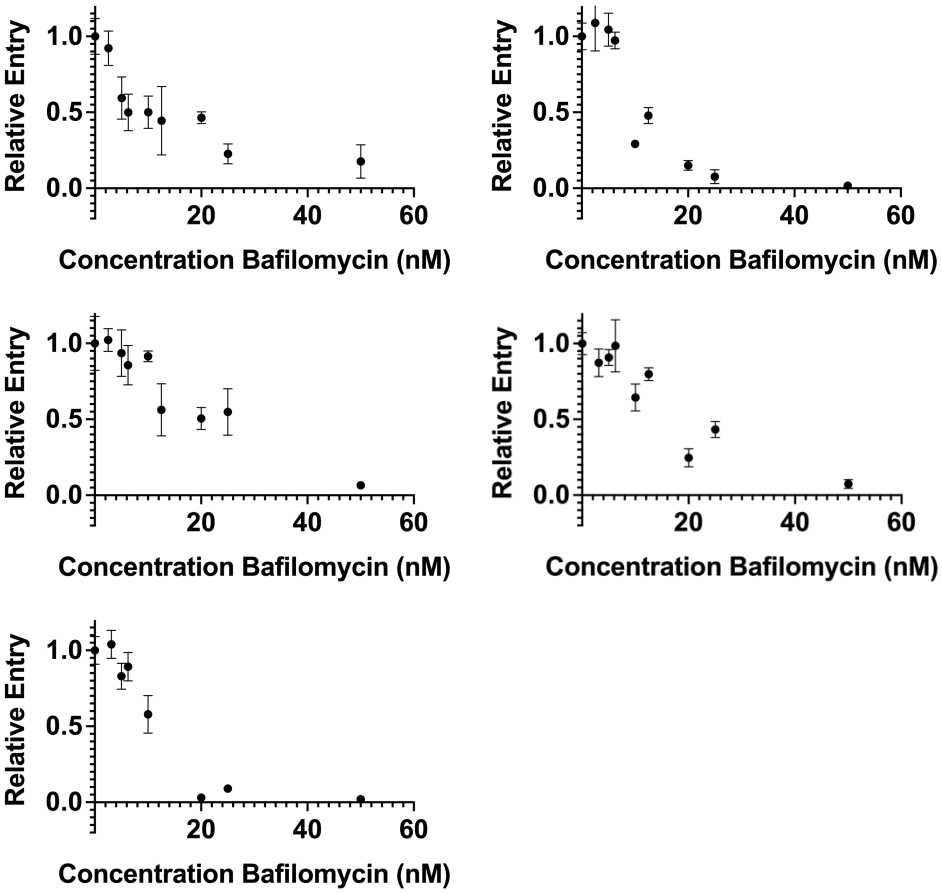

Supplemental Figure 3.3. Individual entry assay data of EBOV VLP into U2OS cells treated with bafilomycin. U2OS cells were pretreated with bafilomycin for 1 hour and EBOV VLPs were applied. The data averaged from 5 biological replicates in Fig. 3B is plotted by individual assay. Error bars in each plot represent one standard deviation of 3-4 technical replicates for the individual assay.

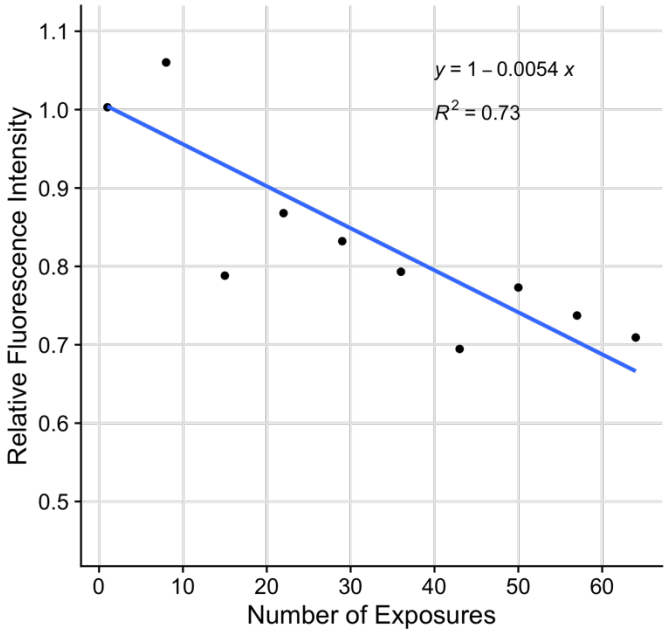

Supplemental Figure 3.4. Bleaching data for mNectarine-Lamp1 in whole cells. A mNectarine-Lamp1 expressing cell (representative of typical fluorescence intensity of a cell used in live cell imaging experiments) was serially exposed using the same imaging parameters as live cell experiments. The laser power was set slightly above that used for most live cell imaging experiments (1.5%, vs. a typical power of 0.3-1%). Exposures were collected in seven plane Z-stacks and the mean fluorescence intensity from the brightest plane was determined, normalized to the initial fluorescence intensity and plotted. A linear decrease in fluorescence intensity was observed with continued exposure.

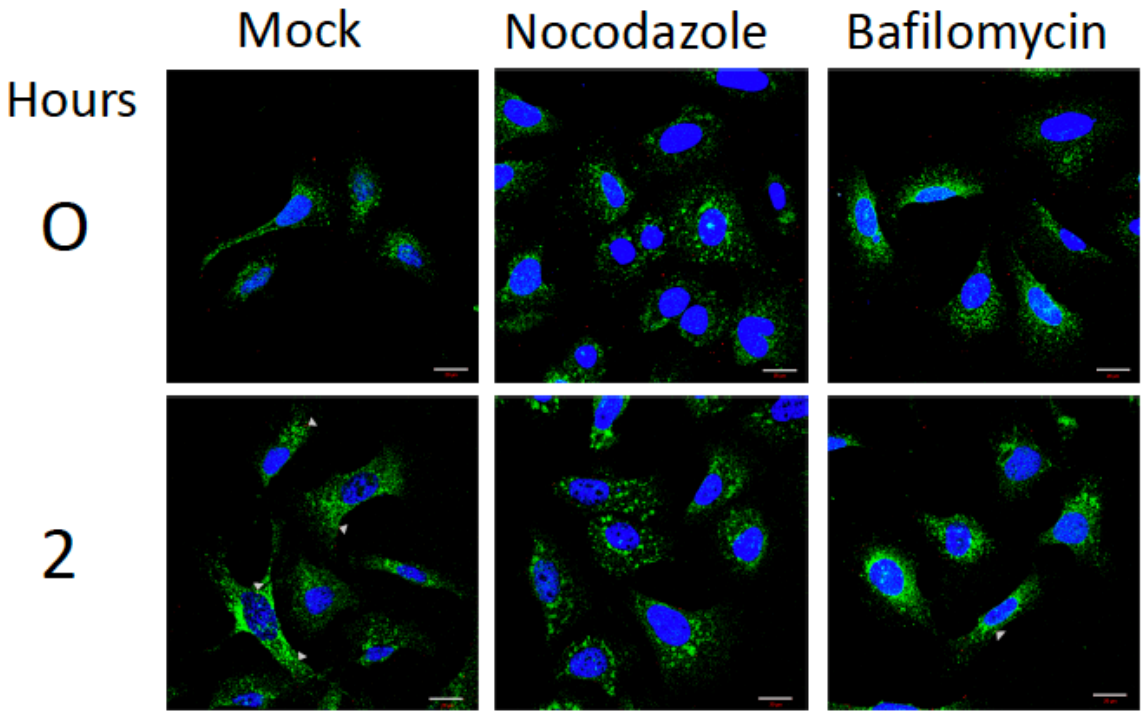

Supplemental Figure 3.5. Sample images from virus-like particle trafficking assay. Images from the virus-like particle trafficking assay from which co-localization data in Figure 3.4 is derived. Immunostained NPC1 is indicated in green, VLPs are in red and DAPI labelling of the nucleus is in blue. Viral particles that co-localize with NPC1 are indicated by grey arrowheads. After two hours of trafficking, four particles co-localize with NPC1 in the mock condition, one co-localizes in the bafilomycin treatment condition and none colocalize in the nocodazole treatment condition. A 20 µm scale bar is in grey in the lower left. Virus-like particles are <1 µm in size.

Chapter 4: Discussion and Outlook

4.1 An overview of subpopulations of endosomes and opportunities to advance the field

While the endocytic system has canonically been divided into broad categories of compartments with similar functional roles or associated proteins, the endocytic system is in reality far subtler and more complex. Over the past 20 years, studies have from time to time directly addressed or hinted at the role or existence of specific subpopulations of endosomes. These studies have largely been enabled by imaging approaches with sufficient spatial and time resolution to study individual endosomes (D. E. Johnson et al., 2016; Suresh et al., 2021). The functional roles of subpopulations of early or late endosomes in cargo trafficking or cell physiology are addressed in a handful of publications (Cao et al., 1998; Kalaidzidis et al., 2015; Lakadamyali et al., 2006; Miaczynska et al., 2004; Padilla-Parra et al., 2012; Perini et al., 2014). Several of these studies focus on separate populations of early endosomes and their role in advancing degradative cargo to late endosomes while enabling recycling cargo to reach the plasma membrane more efficiently (Kalaidzidis et al., 2015; Lakadamyali et al., 2006; Miaczynska et al., 2004). Subpopulations of endosomes may also play a role in growth signaling, sensing cargo in early endosomes and affecting a transcriptional response (Cao et al., 1998; Miaczynska et al., 2004).

The picture of how heterogeneity of compartments within the endocytic system affects cellular physiology is far from complete even in the face of the interesting studies cited above. Factors that have hindered more rapid advancement in the field over the past decades include technical challenges inherent in imaging single endosomes, disparate approaches and definitions of endosomal subpopulations between studies and a lack of attention toward the subject due to its technical and conceptual complexity. In the study of trafficking, much focus has historically been placed on protein markers of compartment identity (such as Rabs, see Chapter 1.2). This approach has utility since it can act as a uniform standard for compartment identity between various studies, but has limits in usefulness for understanding subpopulations of endosomes and their role in cellular processes. Tying functional identity, such as lumenal pH, protease activity, motility and whether a given compartment acts as a site of viral fusion, to compartment identity as determined by protein marker will better contribute to understanding the impact and relevance of endosomal subpopulations to cellular physiology As will be discussed in following sections covering new research directions and methods, developments in imaging technology and fluorescent proteins may enable further studies of endosomal subpopulations and promote a more nuanced and detailed view of the endocytic system.

4.2 Connecting subpopulations and sub-pathways of endosomes to innate immune mechanisms

Viruses may exploit endosomal subpopulations and sub-pathways either to advance more efficiently to endosomal compartments where they can fuse or to evade host immune factors. Several papers have described how different viruses may bypass specific populations of endosomes (Oppliger et al., 2016; Pasqual et al., 2011; Quirin et al., 2008; Rojek et al., 2008b; Spence et al., 2019; Suddala et al., 2019) In one example, influenza virus entry into host cells is restricted by the innate immune factor IFITM3 (localized primarily in late endosomes) while the entry of Lassa virus is not (Brass et al., 2009; Feeley et al., 2011; Spence et al., 2019; Suddala et al., 2019; X. Sun et al., 2016). Both influenza and Lassa require a low pH characteristic of late endosomes to trigger fusion. While influenza co-localizes with IFITM3 prior to fusion, blocking downstream steps in infection, Lassa virus particles do not co-localize with IFITM3 until after they have undergone hemifusion (lipid mixing of the viral envelope and host membrane, see Figure 1.4) (Suddala et al., 2019). It seems that Lassa virus escapes IFITM3 restriction by avoiding trafficking through compartments containing IFITM3. Whether other viruses escaping IFITM similarly take special endocytic sub-pathways and whether this pathway originates from any particular subpopulation of endosomes remain to be determined. Subpopulations of endosomes and the early events in virus internalization likely contribute to determining what sub-pathway viruses are

trafficked along and whether they are able to avoid innate immune restriction in endosomes.

A more complete picture of the role of endosomal subpopulations in downstream events in trafficking and host restriction of viral entry has been hampered in part by definitions of endosomal subpopulations (discussed here) and imaging constraints (discussed later). Based on viral markers, compartment markers and imaging modalities, studies addressing endosomal subpopulations in viral entry (Chapter 2) (Lakadamyali et al., 2006; Padilla-Parra et al., 2012) all used slightly different definitions of endosomal subpopulations. This variability between studies makes it hard to directly compare the role of viral entry proteins in mediating the sorting of viral particles to subpopulations of endosomes. A unifying and comprehensive study using a single pseudoviral model (with MLV pseudovirus as described in Chapter 2 as one example) bearing various viral glycoproteins (such as Lassa, influenza and VSV) is needed to resolve the role of viral entry proteins in sorting of viral particles to endosomal subpopulations and of the role of endosomal subpopulations in viral fusion. Multiple functional readouts for endosomal subpopulation, such as kinetics and extent of viral acidification, viral particle velocity and protease activity, could be examined for each viral entry protein using the same viral system. In conjunction and/or in separate experiments, endosomal subpopulations could be described in terms of their protein markers (Rabs and similar common markers). Such a direct comparison between viruses would be technically challenging and labor

intensive, but more thoroughly define the role of viral entry proteins in mediating the sorting of particles to different endosomal subpopulations. The study could be extended to determine whether early sorting events of viral particles to endosomal sub-populations drive particles into specific endosomal sub-pathways.

4.3 Future studies into the fate of non-fusing viral particles

Most studies of viral trafficking focus on the particles that do fuse (Lakadamyali et al., 2003; Simmons et al., 2016; Spence et al., 2016), rather than the fate of viral particles that do not fuse. In Chapter 2, we described a sub-population of endosomes that do not support viral fusion mediated by VSV-G. Based on the constraints of our study, we were not able to determine the fate of these non-fusing particles but future studies may be able to approach this question. Functionally, the endosomes that did not support fusion were less motile and less acidified over an approximately one-hour observation period compared to endosomes that did support fusion mediated by VSV-G. Since we did not monitor the particles indefinitely, it is possible that non-fusing particles do go on to fuse eventually as the endosomes in which they are contained will eventually mature. This outcome seems unlikely based on bulk data demonstrating VSV-G mediates trafficking and fusion of most VSV-G viral particles within 1 hour of infection (Mingo et al., 2015; Saeed et al., 2006). Conversely, the long dwell time of non-fusing particles in early endosomes may

facilitate viral degradation (Johannsdottir et al., 2009) and these more static endosomes may protect the cell from viral infection. Imaging techniques that preserve cells and are less phototoxic than scanning confocal microcopy (Chapter 2), such as spinning disk confocal, could enable the observation of the fate of non-fusing viral particles over the course of hours and answer the question of whether particles that do not fuse initially are degraded or go on to fuse after an extended observation.

Another possibility is that these fusion non-permissive endosomes eventually recycle non-fusing particles to the cell surface (Owczarek et al., 2019; Z.-G. Wang et al., 2022). Additional imaging experiments using markers of specialized endocytic compartments will be needed to resolve this question. If non-fusing viral particles are observed to co-localize with a fluorescent marker for Rab11, a key membrane associated protein of recycling endosomes (Wandinger-Ness & Zerial, 2014), that would tend to indicate non-fusing particles are eventually returned to the plasma membrane. Further compartment markers such as Rab5, APPL1 and EEA1 could be used to determine whether non-fusing viruses colocalize with any specific subpopulation of early endosomes (Kalaidzidis et al., 2015; Perini et al., 2014).

While viruses do not need to be very efficient to cause infection since they can hijack cellular machinery to copy themselves many times over, mechanisms in the endosomal pathway that result in the recycling or degradation of some proportion of viral particles could buy the host time to mount an immune

response by decreasing the initial number of particles infecting a given cell. A lower initial number of particles infecting a collection of cells could delay rapid increases in the viral load within the whole organism. Thus, understanding the fate of non-fusing viruses may enable a better understanding of the factors determining viral fusion efficiency and could contribute to an understanding of cargo-sorting within the endocytic system as a potential innate defense against viral infection.

4.4 Future studies of the role of viral particle size and avidity for cellular receptors in sorting to endosomal subpopulations

Plasma membrane receptors are sorted for recycling or degradation based on amino acid sequences and/or structural motif in their cytoplasmic domains (Mellman, 1996) as well as into which lipid domains they partition (Diaz-Rohrer et al., 2014). As viruses bind to and are internalized with plasma membrane receptors, it might be expected that they are sorted with these receptors. In Chapter 2, we describe that the sorting of viral particles bearing VSV-G differs from that of the VSV receptor, LDL-R. While LDL-R bearing its physiological cargo, LDL, has previously been found to preferentially sort to dynamic endosomes (Lakadamyali et al., 2006), viral particles bearing VSV-G were sorted to static and dynamic endosomes approximately in proportion to the expected abundance of these endosomes (Chapter 2).

The difference in behavior between the physiological ligand and viral particles may be due to avidity and particle size. It would be interesting to carefully control the average active number of VSV-G molecules per particle and thus measure avidity effects on the sorting of the virus to endosomal subpopulations and downstream effects on viral trafficking. In principle, such a study might be possible by treating a viral preparation with various concentrations of an antibody (or antibody fragment) against VSV-G and using antibody-treated particles to infect cells. A similar approach has previously been used to relate fusion protein stoichiometry and fusion kinetics of influenza with an artificial membrane (Otterstrom et al., 2014), though the approach would require some re-engineering to work in whole cells.

The effect of particle size in sorting could be examined by generating size-controlled nanoparticles bearing a lipid bilayer (or host-derived membrane) and a viral glycoprotein. Nanoparticles of known size functionalized with viral glycoproteins have previously been reported in the literature (H.-W. Chen et al., 2016), and the technique could be re-engineered to label the nanoparticles with various labels, facilitating their tracking in live cell imaging. Understanding how viral particle size affects sorting to subpopulations of endosomes may help describe the mechanistic basis of differential sorting of specific viruses to various endosomal subpopulations as viruses vary in their size and morphology (Louten, 2016, p. 201).

4.5 Developments in fluorescent proteins and sensors

Studying the trafficking of individual viruses in the endocytic pathway using fluorescence microscopy often relies on fluorescent proteins to observe markers of cellular compartments (Lakadamyali et al., 2006; Spence et al., 2016, 2019; Z.-G. Wang et al., 2022) or viral content release (Chapters 2) (Padilla-Parra et al., 2012; Simmons et al., 2016; Sood et al., 2017). To assess content release, viral structural proteins are typically expressed as a chimera with a fluorescent protein, enabling incorporation of the fluorescent protein into the virion (Sherer et al., 2003). In other cases (Chapter 2) (Miyauchi et al., 2011; Padilla-Parra et al., 2012), fluorescent proteins or biosensors can be incorporated into the virion membrane to measure conditions in the compartments through which the viruses are trafficked. Key technical issues of concern in these approaches include the brightness of fluorophores and avoiding spectral overlap between probes that might be used simultaneously, such as a viral content marker, lipid label and compartment markers. Recent developments in fluorescent proteins and labeling with synthetic fluorophores such as quantum dots may open possibilities to accurately monitor several aspects of trafficking and fusion simultaneously.

As described in Chapter 2, challenges in using fluorescent biosensors in the viral membrane include brightness of the biosensor, the range of pHs that can accurately be measured and the compatibility of the spectral occupancy of the biosensor with the use of additional fluorescent markers. A recently described

fluorescent pH sensor, pH-Lemon offers a slightly improved range of sensitivity with the ability to distinguish pH values falling in the range 4.4-7.0 (Burgstaller et al., 2019). pH-Lemon is FRET-based and ratiometric and consists of Tq2-eYFP. One possible variation of pH-Lemon (Burgstaller et al., 2019) would be to use mCitrine as an acceptor in place of eYFP. mCitrine is brighter than eYFP and has a lower pKa than eYFP (Griesbeck et al., 2001) such that in combination with Tq2 it could provide reliable pH measurements below pH 4.5. The trade-off to replacing eYFP with mCitrine could be lower sensitivity of the sensor near neutral pH. The construction of pH-Lemon also gives a hint about how the pH sensing FRET pair mTFP1-mCitrine (Chapter 2) might be further optimized. In pH-Lemon, the fusion of N-terminus of the donor to C-terminus of the acceptor was found to slightly increase the dynamic range of the pair (Burgstaller et al., 2019). A similar approach could be tried with mTFP1-mCitrine, reorienting the C-terminus of mCitrine to the N-terminus of mTFP1.

Another recently reported pH sensing method uses the fluorescence lifetime imaging of RpHLuorin2, a ratiometric pH probe derived from green-fluorescent protein (GFP), to address the problem of spectral occupancy. Fluorescence lifetime imaging of RpHLuorin2 enables accurate measurement of pH values as low as 5 with excitation at only 488nm and counting photons with wavelength 502nm to 530nm (Linders et al., 2022). By use of RpHLuorin with fluorescence lifetime imaging, compartment markers or viral content markers emitting in the red, far red and near infrared bands of the light spectrum could all

be used while also monitoring pH. Both of the described sensors could be anchored in the viral membrane with a non-viral protein such as ICAM1 (Chapter 2).

Other studies have used lipid labelling to track viral trafficking and lipid-mixing events (Lakadamyali et al., 2003, 2006; Spence et al., 2016, 2019). New labels using the conjugation of quantum dots, extremely bright fluorophores that are highly resistant to photobleaching, to viral membrane lipids or to proteins that bind viral membrane lipids may provide a brighter readout and the ability to monitor pH (Z.-G. Wang et al., 2022). One disadvantage of conjugating quantum dots to lipids in the viral membrane or using lipid-binding proteins conjugated with quantum dots is that they are large compared to a fluorescent protein (Hink et al., 2000; Wichner et al., 2017) and may perturb the viral envelope or interact with the viral fusion protein. A possible solution is to express a transmembrane protein (such as ICAM1 as described in Chapter 2) with a special amino acid sequence inserted (such as a SNAP tag) that could then be recognized by a functionalized quantum dot (Petershans et al., 2011; Wichner et al., 2017, p. 2). This would avoid direct interaction between the quantum dot and the viral envelope, which for some viruses has a critical role in mediating attachment and fusion (Richard et al., 2015). Another solution would be to use a synthetic dye that is smaller in size than a quantum dot and is conjugated to recognize SNAP tags (for example SNAP-surface Alexa dyes, NEB). The use of quantum dots as biosensors and markers of hemifusion could enable monitoring of viral particles

at high temporal and spatial resolution, enhancing understanding of trafficking kinetics, modes of motion and potentially sub-populations of endosomes that contain viral particles.

4.6 Developments in the spatio-temporal resolution of microscopy to enhance study of viruses and the endocytic system

Studies of viral trafficking in whole cells may be dramatically enhanced by the use of new imaging technologies such as lattice light sheet microscopy (B.-C. Chen et al., 2014). Lattice light sheet microscopy relies on illuminating the sample with a specially structured beam of light at an angle that is perpendicular (B.-C. Chen et al., 2014) or oblique (Sapoznik et al., 2020) to the objective lens that collects emissions signal. The latticed sheet of light can be “dithered” or repeatedly swept over a single cell to collect many x-y planes at a high rate of speed (100s per second)(B.-C. Chen et al., 2014). The advantages of lattice light sheet are a relatively low exposure of sample to photons compared to scanning confocal imaging, offering reduced photobleaching and toxicity, with high time and spatial resolution. The technique has not yet been published in an application studying virus trafficking and entry but promisingly has been used for monitoring phagocytosis (Vorselen et al., 2021), clathrin-mediated endocytosis (Sapoznik et al., 2020), macropinocytosis (Quinn et al., 2021) and other physiological phenomena (Chou et al., 2021; Geoghegan et al., 2021) that must be monitored at high spatial resolution in live cells to derive biologically

interesting data. For the purposes of monitoring viral entry, as described in Chapter 2, the high time resolution would help resolve some of the problems with differentiating particles, thus increasing assay throughput.

4.7 Conclusions

The study of endocytic subpopulations and sub-pathways is a rich area that has been and will continue to be enabled by advances in biochemistry and imaging technology. Defining endosomal subpopulations by their functional attributes (such as acidification, motility and protease activity) is especially useful to understanding their role in physiological processes. The role of endosome subpopulations in viral fusion is of great interest because of the potential to shed light on the role of the endocytic pathway in targeting some viral particles for recycling or degradation and thus mediating a means of host defense. In addition to the nature of the receptor to which a viral particle binds, the size of the particle and avidity of the particle for the viral receptor may play a role in the sorting of the particle to a particular endosomal subpopulation. More clearly defining the nature of endosomal subpopulations will make it easier to compare the results of studies examining the sorting of different viruses or physiological cargos to these endosomal subpopulations and would aid the field.

Appendix A: The comparison of the characteristics of FRET-based pH sensors and the optimization of the preparation of viral particles bearing FRET-based pH sensors

A.1 Introduction

Many enveloped viruses are triggered to undergo fusion by low pH in the endocytic pathway (Chapter 2, Chapter 3, White 2016). The pH of viral fusion can be measured by separately assessing viral infection and the pH of endosomes (Chapter 3) or by attaching a pH sensor directly to the viral particle that also contains a marker for content release (Chapter 2). When the pH sensor is attached to the viral membrane or the pH of individual endosomes are measured, a ratiometric pH probe is required. For a ratiometric pH probe, changes in focal plane of the probe, such as when a viral particle moves along the Z-axis inside the cell, affect the intensities of the two emission wavelengths of the probe equally. On the other hand, emission wavelengths and their intensities are affected differentially by changes in pH. This enables the accurate measurement of pH in spite of any motion of the probe (Canton & Grinstein, 2015). In some cases, ratiometric pH probes consist of a single fluorophore with differential sensitivity to pH with respect to the intensity of two emission

wavelengths (Mahon, 2011; Sankaranarayanan et al., 2000). Other ratiometric probes consist of two separate fluorophores, one pH sensitive and one insensitive, typically linked to dextran or another substrate that undergoes fluid uptake or endocytosis. The emission intensity from the pH sensitive component can be normalized to the pH insensitive component (D. E. Johnson et al., 2016). A genetically encoded pH sensor targeted to late endosomes by the transmembrane protein Lamp1 also uses two separate fluorophores, one in the endosomal lumen to sense endosomal pH and one in the cytosol (with a pKa well below typical cytosolic pH) to act as a pH insensitive constant (Webb et al., 2021).

Förster resonance energy transfer (FRET)-based pH sensors rely on the ratio of emission intensities from two component fluorophores with differential sensitivity to changes in pH that are expressed as a single polypeptide chain in a 1:1 ratio. The donor fluorophore (lower excitation wavelength) is excited and resonantly transfers energy to the acceptor fluorophore (higher excitation wavelength). As the acceptor fluorophore is quenched by protonation due to decreasing pH, the emission intensity corresponding to the acceptor decreases and the emission intensity of the donor increases. With progressively lower pH the ratio of fluorescence intensity of the donor to the acceptor is expected to increase. One advantage of FRET-based pH sensors is that their response to pH can be fine-tuned and optimized for use in specific pH ranges by swapping out one or the other of the component proteins for a protein with a different pKa/pH

sensitivity (Esposito et al., 2008). Such sensors have been used in several cases where a wide range of pH must be measured and targeting of the probe to a specific organelle or incorporation into a viral particle is desired (Burgstaller et al., 2019; Padilla-Parra et al., 2012) (Chapter 2).

Previous work using a FRET-based pH sensor to measure pH during viral trafficking in the endocytic pathway used the FRET pair mTFP1-eYFP expressed as a chimera with ICAM1, which was then incorporated into the viral envelope (Padilla-Parra et al., 2012). As the authors of this study noted, observing pH values below 6.0 was challenging due to cellular autofluorescence; the relatively high pKa of eYFP may have been a contributing factor (Griesbeck et al., 2001). Many viruses fuse late in the endocytic pathway, in compartments with a pH less than 6.0 (Table A.1). To enable the study of later fusing viruses we engineered a FRET-based pH sensor with a FRET acceptor, mCitrine, having lower pKa and higher brightness than eYFP (Table A.2). The mTFP1-mCitrine FRET pair was expressed as a chimera with ICAM1, which was incorporated into the membrane of MLV viral particles (see Chapter 2). In this Appendix, we characterize the mTFP1-mCitrine sensor, including its brightness and pH response, in comparison to mTFP1-eYFP. We also compare the effect of fluorescent labelling on the infectivity of viral particles. Finally, we describe the importance of using a non-spectrally overlapping viral content marker as we found spectral overlap and interference between viral content markers with the FRET-based pH sensor.

Table A.1. pH of fusion for several enveloped viruses. To determine the range of pH sensitivity for a sensor to measure the trafficking and fusion of enveloped viruses, the literature was surveyed and a table of fusion pH values prepared. Most values derive from reconstituted systems. The ASLV value is in bold because it is the only direct measure of viral content release in conjunction with pH in live cells that we are aware of. The measurement of pH values 5.0-6.2 is essential for a pH sensor to be used measuring pH experienced by enveloped viruses during trafficking and fusion.

Virus	pH of fusion	Method
VSV	~6.2	Cell-cell fusion (J. White et al., 1980)
SFV	~6	Cell-cell fusion, liposome fusion (J. White et al., 1980; J. White & Helenius, 1980)
ASLV	**5.8-6.1**	**Direct measure w/FRET pair (Padilla-Parra et al., 2012)**
Lassa	5.5	Cell-cell fusion (Hulseberg et al., 2018)
Influenza (WSN)	<5.5	Hemolysis (Maeda & Ohnishi, 1980)
Influenza (A0PR8)	5.0-5.5	Hemolysis (Maeda & Ohnishi, 1980)
Influenza (Japan)	5.2	Cell-cell fusion (Gething et al., 1986)

Table A.2. Characteristics of component fluorescent proteins for pH-sensing FRET pairs. The key characteristics of component fluorescent proteins were tabulated from the literature (Griesbeck 2001, Ai 2006). mCitrine is brighter and has a lower pKa than eYFP but similar peak excitation and emission wavelengths.

Protein	Ex.	Em.	pKa	Quantum Yield	Brightness
eYFP	513	527	6.9	0.61	50.9
mCitrine	516	529	5.7	0.76	58.5
mTFP1	462	492	4.3	0.85	54

A.2. Results and Discussion

Comparison of mTFP1-mCitrine-ICAM1 and mTFP1-eYFP-ICAM1 FRET-based pH sensors

Based on the comparative properties of eYFP and mCitrine (Griesbeck et al., 2001), mTFP1-mCitrine was expected to be brighter and to FRET efficiently at lower pH levels compared to mTFP1-eYFP. Pseudoviral particles bearing Lassa virus glycoprotein, one of the FRET-based pH sensors described above and the viral content marker Gag-mKate2 were prepared. Prepared pseudoviral particles bearing either mTFP1-eYFP-ICAM1 or mTFP1-mCitrine-ICAM1 were adhered separately to coverslips in imaging dishes such that they could be imaged in a series of citrate-phosphate buffers of known pH. Individual, triply labelled particles were selected and the mean emission intensities from 8.9 nm wide spectral bands were extracted from each particle region. These spectral emissions intensities were plotted for particles bearing either mTFP1-eYFP-ICAM1 (Figure A.1 A, top) or mTFP1-mCitrine-ICAM1 (Figure A.1 A, bottom). At all pH values, mTFP1-mCitrine is relatively brighter (under identical imaging conditions) compared to mTFP1-eFYP. One unusual feature is that mTFP1 signal remains fairly steady from pH 5.2 to pH 4.5 in the mTFP1-mCitrine construct, while mCitrine is slightly decreased (loss of FRET without a commensurate increase in donor fluorescence). This could be because at pH 4.5 mTFP1 begins to be quenched, even though it is not transferring energy to

mCitrine to as great an extent as at high pH and the direct quenching balances any increased intensity from mTFP1 due to loss of FRET.

As an approximation of FRET efficiency, the ratio of the emission intensity from mTFP1 (494nm) over eYFP or mCitrine (530nm) was calculated for individual particles. Particle regions were background subtracted and the emission intensity ratios of mTFP1 to mCitrine ($I_{494.0\text{-}502.9}/I_{530.0\text{-}538.9}$) were calculated for each pH. The sensor fluorescence ratio undergoes a transition from a high to a low FRET state as the pH is decreased from 7.4 to 4.2 (see Chapter 2). The distribution of ratios calculated from individual particles in buffers of known pH was plotted (Figure A.1 B). Both sensors follow the expected pattern as the center of the distribution of the particle ratios increases with decreasing pH. The spread of ratios for individual particles with mTFP1-eYFP at pH 4.5 is quite broad. Fluorescence intensity ratio data derived from the experiment shown in Figure A.1 B as well as additional data collected from particles in additional buffers of known pH was plotted in Figure A.1 C to construct calibration curves of mTFP1-eYFP and mTFP1-mCitrine. Particles bearing mTFP1-eYFP show a greater variability in ratio at low pH compared to particles bearing mTFP1-mCitrine. The transition of mTFP1-eYFP is steeper than mTFP1-mCitrine from low-high pH. The approximate pH response of both is the same near neutral pH. Based on the sigmoidal fit of the data the pKa of mTFP1-eYFP was 5.3 (5.0-5.5, 95% confidence interval) and the pKa of mTFP1-mCitrine was 5.5 (5.3-5.9, 95% confidence interval). The pKa of particles bearing mTFP1-

mCitrine and the fusion protein of vesicular stomatitis virus was found have a similar pKa of 5.7 (see Chapter 2).

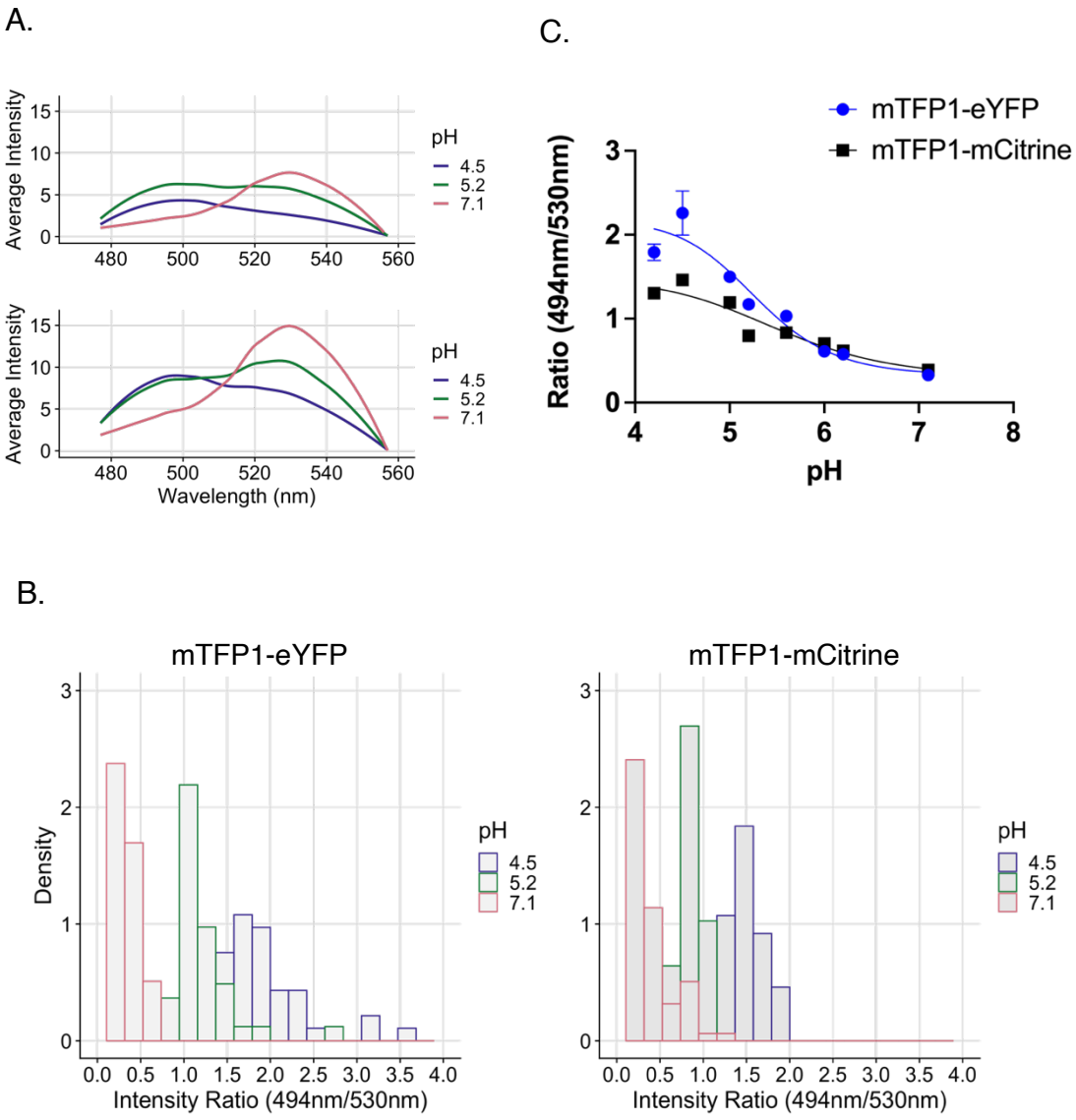

Figure A1.1. mTFP1-mCitrine is brighter than mTFP1-eYFP and provides a more reliable readout at low pH. MLV viral particles bearing mTFP1-eYFP-ICAM1 or mTFP1-mCitrine-ICAM1 and Lassa virus glycoprotein were adhered to a coverslip and observed using a confocal microscope with equipped with spectral detector. The particles were excited at 488 and the emissions spectrum was observed in 8.9 nm bands. Particle regions were identified and the mean fluorescence emissions intensities extracted for each particle. A background region was taken and the fluorescence intensities from the background region was subtracted from all particle regions. *A)* The integrated emissions intensity of

all observed particles at each pH (pH 4.5 = purple, 5.2 = green, 7.1 = pink) was plotted to generate an emissions spectrum for mTFP1-eYFP (top) and mTFP1-mCitrine (bottom). The smoothed curve represents a series of local fits of a polynomial curve (loess) to the data. *B)* The distribution of fluorescence intensity ratios from individual particles in three buffers of known pH. The ratio of the background subtracted emissions intensity at 494nm and at 530nm was taken. The distributions of the ratio at each of the three pHs was plotted for particles with mTFP1-eYFP (left) and mTFP1-mCitrine (right). *C)* The mean fluorescence intensity ratios for particles in buffers of known pH (determined as B) were plotted. The error bars represent the SEM of all the particles measured at a given pH. (A-C) Integrated intensities and ratio distributions come from 30-75 particles per pH.

Further optimization of probe brightness and sensitivity would benefit the development of an optimal pH probe to investigate the trafficking and fusion of enveloped viruses. Ideas for optimization include inverting the position of FRET donor and acceptor relative to ICAM1 and trying different N-terminus to C-terminus orientations of both donor and acceptor. The FRET based pH probe pH-Lemon, consisting of Tq2 and eYFP was optimized by reorientation of the N-C terminus of the acceptor, eYFP. pH-Lemon itself may be useful for measuring the trafficking and fusion of enveloped viruses as it can reliably discriminate pH values as high as 6.0-7.0 and low as 4.0-4.5 (Burgstaller 2019, see Chapter 3). Tq2 due to its low pKa could prove a useful FRET donor when used with mCitrine as a FRET acceptor as well. In fact, use of a Tq2-mCitrine FRET pair could maximize brightness and discrimination between low pH values.

<u>The effect of fluorescent labels on pseudovirus infectivity and capsid maturation</u>

Fluorescent labelling of MLV Gag protein is known to inhibit viral infectivity (Sherer et al., 2003). Further, while previous work using the FRET-based pH

sensor mTFP1-eYFP-ICAM1 in a viral membrane noted that a titer had been conducted to assay infectivity of particles bearing the sensor, the associated data was not shown or described (Padilla-Parra et al., 2012). To determine the combined and individual effects of a fluorescent content marker on the interior of the viral particle (mKate2) and a pH sensor (mTFP1-mCitrine-ICAM1) in the membrane, MLV pseudoviruses with varied combinations of labels were prepared in parallel. One viral preparation had neither content marker nor pH sensors. Two viral preparations had either content marker or pH sensor and one viral preparation had both content marker and FRET-based pH sensor. All viral preparations were equipped with VSV-G as a viral entry and fusion protein. Although the preparations were conducted in parallel and every effort was made to ensure all steps were conducted uniformly, one caveat is that slight variations in the aspiration of the supernatant over the viral pellet (see Materials and Methods) can result in slightly variable absolute concentrations of pseudovirus even when preparations are done in parallel.

The viral preparations (prepared in parallel) were diluted 1:100 and assayed for infectivity in parallel on A549 cells (Figure A.2 A). Increasing values of luminescence indicate a greater degree of infection. As expected based on previously reported results (Sherer et al., 2003), the addition of a content maker alone decreased viral infectivity by ~50% compared to unlabeled pseudovirus. The use of the pH sensor alone decreased viral infectivity by ~70% compared to unlabeled pseudovirus. The content marker and pH sensor did not appear to

have an additive effect as combined they decreased infectivity by ~70% compared to unlabeled pseudovirus. All viral preparations (with and without labels) still had substantial infectivity though and individual particles bearing fluorescent labels were observed to infect A549 cells (Chapter 2).

Further optimization of the ratio of labelled MLV Gag plasmid (Gag-mKate2) to unlabeled Gag-pol plasmid in the preparation may be required to maximize viral infectivity. One challenge was that mKate2 was not particularly bright when the amount of plasmid was reduced (data not shown). Using a brighter fluorescent protein such as the recently developed FR-MQV (Mukherjee et al., 2020) might enable using a reduced amount of plasmid encoding labelled Gag and thus improve viral titers.

The viral content marker Gag-mKate2 is encoded as a single protein and undergoes cleavage during virion maturation yielding free mKate2 (Markosyan et al., 2005). To determine whether either label affected viral capsid maturation and whether un-cleaved Gag-mKate2 could be observed, a blot was performed for MLV Gag (Figure A.2B). Equal volumes of each parallel preparation of MLV pseudovirus (as described for Figure A.2 A) were loaded on a gel. The gel was then transferred to a nitrocellulose membrane and immunoblotted for MLV Gag. Bands were observed corresponding to mature MLV capsid (~30 kDa) and immature MLV capsid (~60 kDa) as expected. No band was observed corresponding to the expected mass of mKate2 with mature capsid (~86 kDa), nor does any band corresponds to the mass of ~46 kDa expected for mKate2

covalently bound to mature Gag. Thus, the evidence suggests that mKate2 is cleaved from Gag during maturation as previously described (Markosyan et al., 2005).

The relative amount of mature capsid in pseudoviruses prepared with all four labelling schemes was measured by quantitating band intensity in the blot in Figure A1.2 B corresponding to a mass of ~30 kDa (Figure A.2 C). The band intensities were then normalized to the brightest mature capsid band, which was generated by the pH-sensor alone viral preparation. The absolute band intensity corresponding to mature capsid was also compared to the absolute band intensity representing immature capsid and all preparations had at least ~1.5x as much mature capsid as immature capsid (Figure A.2 D).

Somewhat surprisingly, the band with the lowest intensity corresponding to mature capsid (Figure A.2 C) came from the preparation that was also the most infective, the one without any fluorescent label. The relatively low apparent amount of mature capsid in the most infective preparation may indicate that the no-label viral preparation was particularly dilute. If the preparations were to be normalized by the concentration of particles in the infection assay, it is possible the preparation without any fluorescent labels would be even more infective than we perceived in our assay. To know for certain if the inherent slight variability of particle concentration (see above) affects infectivity, we would need to develop an enzyme linked immunoassay to detect MLV Gag.

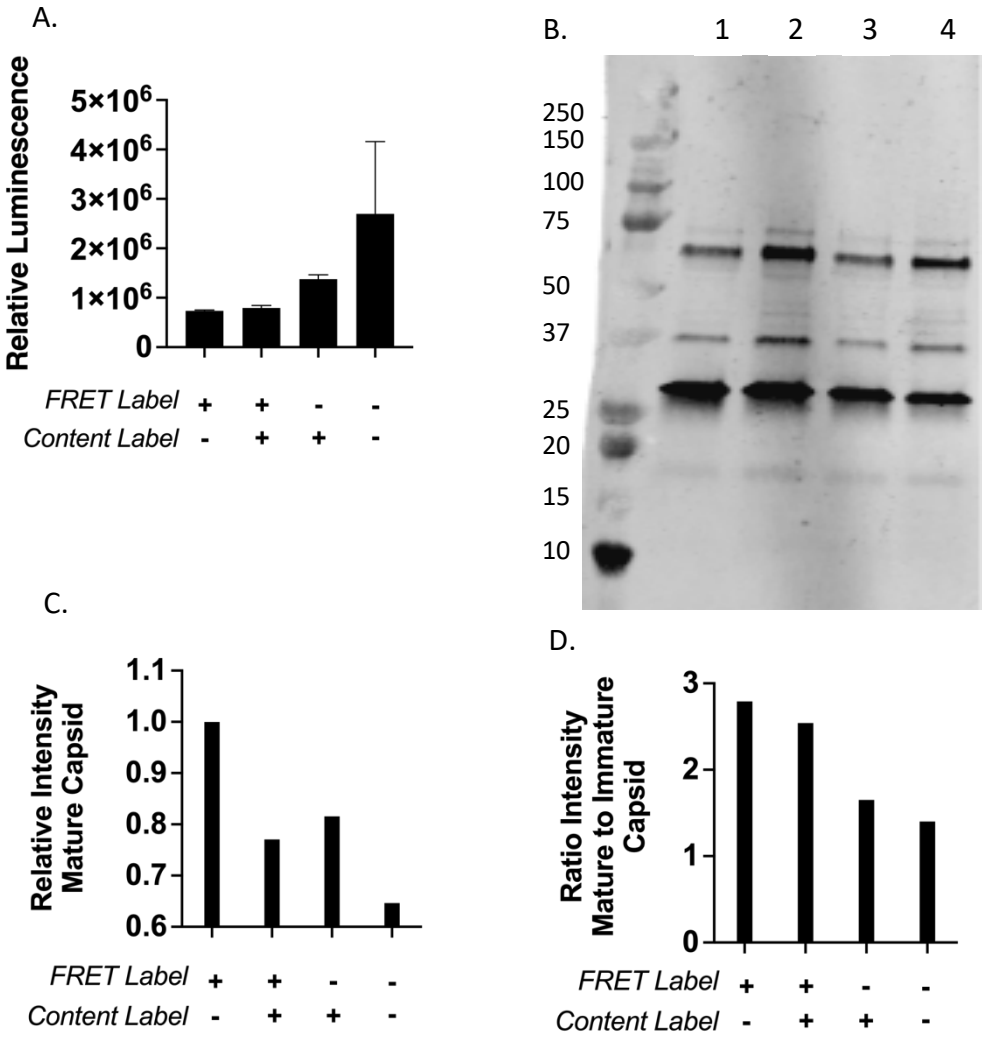

Figure A.2. The effects of the FRET sensor and viral content marker on infectivity and viral proteins. *A)* The infectivity of generated MLV pseudoviruses bearing VSV-G was evaluated by luciferase assay. The pseudoviruses had been prepared identically and parallel except for the combination of labels used. The fluorescent labelling scheme, some combination of mTFP1-mCitrine-ICAM1 (FRET label), gag-mKate2 (content label) or neither, is indicated by the legend directly under the plot. The pseudoviruses were diluted 1:100 and applied to A549 cells. Increasing relative luminescence indicates an increasing degree of infectivity. The assay was conducted once. Error bars represent the standard deviation of three technical replicates. *B)* The same viral preparations as in panel A were immunoblotted for MLV gag protein. The band at ~65 kDa represents uncleaved, immature capsid (structural) protein and the band at ~30 kDa represents cleaved, mature capsid. No band corresponds to the anticipated mass of Gag-mKate2, indicating that the fluorescent content marker is likely cleaved and freely diffusing. *C)* The mature capsid band (~30kDa) was quantitated from the immunoblot in Panel B to

determine if the concentration of mature capsid was unusually low in the viruses carrying a content label. There was no obvious association between one or other of the virus labels and the amount of mature capsid. *D)* The ratio of mature to immature capsid from the blot in Panel B was calculated to determine if a content label was associated with loss of capsid maturation. There is no obvious association with content labels and the ratio indicating the relative amount of mature capsid.

The effect of viral content marker on pH sensing

To ensure that the content marker did not interfere with FRET in the pH sensor, the change in the fluorescence intensity ratio (as described above) in response to buffers of known pH was compared in viral particles that were equipped with Lassa virus glycoprotein, mTFP1-mCitrine-ICAM1 and either had a content marker or had no content marker. The viral particles with and without content marker were prepared in parallel. Two different content markers were tested, Gag-mKO (Figure A.3 A) and Gag-mKate2 (Figure A.3 B). The excitation peak of mKO has substantial overlap with the emissions peak of mCitrine, but Gag-mKO was initially tested because it was bright and readily available. A high degree of FRET efficiency between a fluorescent protein in the viral core and a pH sensor in the viral membrane seemed to be unlikely based on spatial separation. Counter to expectations though, the pH response of the FRET sensor was seriously dampened by the presence of Gag-mKO (Figure A.3 A). In retrospect, this phenomenon has precedent in the literature as transmembrane FRET has previously been reported (Haga et al., 2012). In contrast, mKate2, which absorbs and emits light further to the red than mKO and has little overlap in its excitation peak with the emissions peak of mCitrine, shows little or no effect

on the fluorescence emissions ratio as readout for pH (Figure A.3 B). We urge caution in the use of content markers in combination with any kind of label residing in the membrane when there is spectral overlap between the two. Until there is evidence to the contrary, it should be assumed that fluorescent viral content markers can resonantly transfer energy to fluorophores in or near the viral membrane.

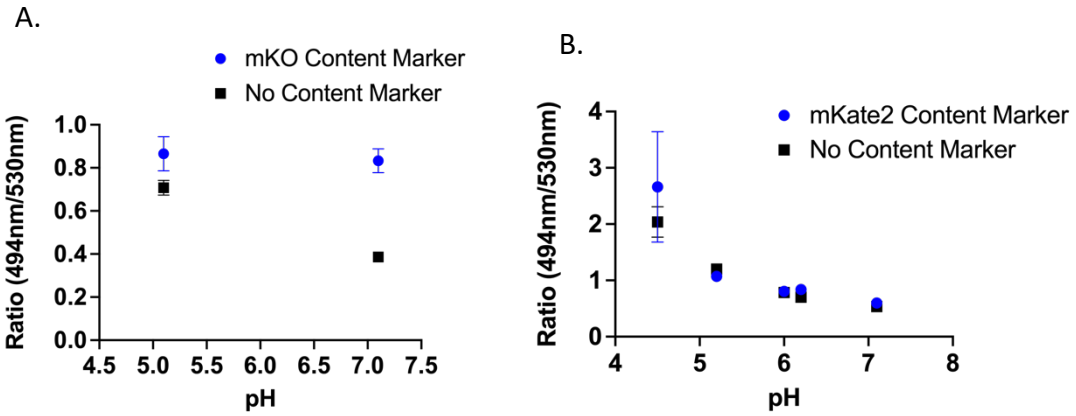

Figure A1.3. The effect of viral particle content markers on pH response of mTFP1-mCitrine. *A)* MLV particles bearing mTFP1-mCitrine-ICAM1 (FRET probe) and Lassa virus glycoprotein were adhered to a coverslip and observed in two buffers of known pH. Two viral preparations were made in parallel, one with the content marker Gag-mKO and one without. For particles with Gag-mKO content marker, n=13 and 27 for pH 7.1 and 5.1, respectively. For particles without Gag-mKO, n=40 and 80 for pH 7.1 and 5.1, respectively. *B)* MLV particles bearing mTFP1-mCitrine-ICAM1 (FRET probe) and VSV-G were adhered to a coverslip and observed in five buffers of known pH. Two viral preparations were made in parallel, one with the content marker Gag-mKate2 and one without. The number of particles per condition at each pH ranged from 23-59. (A-B) The fluorescence intensity of particles was analyzed and ratios were calculated as in Figure A1.1B-C. Error bars represent the standard errors of the mean.

A.3. Materials and Methods

Cell Lines

All cell lines and tissue culture procedures were conducted as described in Chapter 2, Materials and Methods.

Plasmids and cloning

Plasmids were obtained as described in Chapter 2, Materials and Methods. Lassa GP plasmid (Josiah strain, tagless) was a gift of Gregory Melikian, Emory University). mTFP1-eYFP1-ICAM1 was constructed (Figure 2.1) and cloned as described for mTFP1-mCitrine-ICAM1, except that the sequence of mCitrine1 was replaced with the sequence for eYFP.

Preparation of pseudovirus

MLV pseudovirus was prepared and infectivity assayed as described in Chapter 2, Materials and Methods. When indicated, Lassa GP plasmid was used instead of VSV-G, mTFP1-eYFP-ICAM1 was used instead of mTFP1-mCitrine-ICAM1, or Gag-mKO instead of Gag-mKate2. When swapped into cDNA mixtures for viral preparations, these plasmids were used in the same ratios as indicated for the plasmids they replaced. When pseudovirus was prepared without a tagged Gag the amount of plasmid DNA was not replaced with additional Gag-pol plasmid.

Calibration and evaluation of FRET-based pH sensor, particle selection

Calibration of the FRET-based pH sensor and particle selection for calibration experiment was performed as described in Chapter 2, Materials and Methods.

Immunoblot of MLV Gag

Equal volumes of pseudovirus preparation from parallel viral preparations with varying labelling schemes (content marker and/or FRET-based pH sensor present or absent) were boiled in sample buffer containing reducing agent and loaded onto a 4-20% tris-glycine gel (MiniProtean TGX, Bio-Rad). The gel was run to completion (180V, 1 hour) and transferred to nitrocellulose (60V, 1.5 hours). The membrane was blocked at room temperature overnight in Odyssey Intercept buffer (Licor). The membrane was incubated in 1:1500 anti-MLV Gag p30 antibody (Abcam, #130757), washed, incubated in 1:10,000 donkey anti-mouse IR800 secondary antibody (Licor), washed and imaged. The blot image was quantified in ImageJ. Each band was quantified three times and the results averaged.

Plots and Statistics

Plots were prepared using R Studio or Prism (GraphPad). Fitting of calibration curves was conducted in Prism.

Appendix B: Preliminary Investigation Into Inhibitors of Late Endosomal Cation Channels and Ebola Virus Infection

B.1 Introduction

To infect cells, Ebola virus (EBOV) undergoes attachment to the cell, is internalized via a macropinocytosis-like mechanism (Nanbo et al., 2010; Saeed et al., 2010) into the endocytic system and is trafficked to an acidic intracellular compartment, the late endosome containing NPC1, the intracellular receptor for EBOV (Simmons *et al.*, 2016; further details in Chapter 3). While the role of NPC1 and a low pH trigger in EBOV fusion with the host membrane has been well established (Côté et al., 2011; Miller et al., 2012; Mittler et al., 2021; Spence et al., 2019), a late endosomal cation channel, the two-pore channel (TPC1/2), has also been found to be essential for efficient entry of EBOV (Sakurai et al., 2015).

While the activation and selectivity of the two-pore channel has been debated, it can pass calcium ions and its proposed role in EBOV entry is connected to the promotion of EBOV fusion by calcium ions (Das et al., 2020; Fan et al., 2017; Nathan et al., 2019). TPC1 and 3 are distributed throughout the endocytic system and TPC2 localizes particularly to late endosomes and lysosomes (Calcraft et al., 2009). The intracellular location of two pore channels

have made them challenging to study directly. Thus, there has been substantial debate about the selectivity of the channels for cations and the regulation/activation of these channels. The channels have been studied in a variety of reconstituted systems. While initial work supported NAADP as the activator of calcium current through TPCs (Brailoiu et al., 2010; Calcraft et al., 2009; Churchill et al., 2002; Pitt et al., 2010), a more complex picture has emerged whereby $PI(3,5)P_2$, a late endosomal lipid, activates a sodium current through TPC1/2. Further, a binding site for $PI(3,5)P_2$ was found in structures of mouse TPC1 (She et al., 2018) and human TPC2 (She et al., 2019). One challenge in studying TPCs previously was the lack of agonists with high specificity, though very recently two specific agonists that stimulate either Na^+ or Ca^{2+} release have been reported (Gerndt et al., 2020) and these specific agonists helped enable discovery of a specific inhibitor (Müller et al., 2021).

Channels with similar localization that are also activated by $PI(3,5)P_2$ and can localize to late endosomes are TRPML1-3 (Venkatachalam et al., 2015). TRPML1 is particularly well studied. Like TPC2, TRPML1 is stimulated by $PI(3,5)P_2$ and primarily has a calcium conductance (Dong et al., 2010). Initial studies of TPCs in EBOV entry used inhibitors may affect TRPML1 as well (Sakurai et al., 2015). In addition, inhibitors of phosphoinositide kinase (PIKFYVE), the enzyme that converts PI(3)P to $PI(3,5)P_2$, block EBOV infection (Nelson et al., 2017; Qiu et al., 2018). Whether inhibitors act through TRPML1, TPC2, or a third unknown mechanism is unknown. PIKFYVE inhibitors have also

been shown to change the character of late endosomal compartments and/or block trafficking of EBOV to the NPC1+ entry compartment (Kang et al., 2020; Nelson et al., 2017; Qiu et al., 2018), suggesting that TRPML1 or TPC2 may have a role in virus trafficking or regulating late endosomal compartment character in a way that facilitates viral entry. To discriminate between potential roles of TPC2 and TRPML1-3 in EBOV entry, we used TRPML channel specific agonists and antagonists to probe whether stimulating or blocking TRPML1-3 channels affects EBOV entry.

B.2 Results, Methods and Discussion

As a non-pathogenic model for EBOV, we used virus-like particles (VLPs, as described in Chapter 3). Several TRPML agonists and inhibitors shown in Table B2.1 were gifted to us by Haoxing Xu (University of Michigan). In addition, bepridil, a calcium channel inhibitor known to block EBOV infection, and bafilomycin, a V-ATPase inhibitor (see Chapter 3), were used as negative controls for infection of cells by VLPs bearing EBOV GP.

Compound	Action	Specificity
ML-SA1	Agonist	TRPML1, 2, 3 (Shen 2012)
ML-SI3	Inhibitor	TRPML (Samie 2013, Wang 2015)
ML-SI4	Inhibitor	Data not available (Zhang 2016)
Bepridil	Inhibitor	Not channel specific

Table B2.1. Selected compounds perturbing the activity of calcium channels in endolysosomes and their specificity. A TRPML-specific agonist and several inhibitors were provided by the lab of Haoxing Xu. Bepridil (Sigma-Aldrich), a non-specific calcium channel inhibitor was used as a negative control for EBOV entry.

U2OS cells were seeded in a 96-well plate and twenty-four hours later pretreated with inhibitors or agonists against TRPML at 37° C for 1 hour. As described in Chapter 3, VLPs were applied to the cells by spinning at 250 x *g* for one hour at 4° C. The same concentration of inhibitor or agonist as indicated in figures was maintained on cells throughout the experiment. For a mock treatment, 0.05% (v/v) of the inhibitor/agonist solvent DMSO was used. After the VLPs were applied to cells, the plates were shifted to 37° C and the entry assay was completed as described in Chapter 3. The assay readout is the proportion of cells in which cleavage of a cytoplasmic fluorescent substrate has occurred. An enzyme contained in VLPs, β-lactamase, cleaves and converts the fluorescence emission color of the fluorescent substrate once the VLP has entered the cell.

For TRPML inhibitor ML-SI4, entry assays were performed on three separate days using two concentrations of inhibitor, 10 μM and 30 μM. The average percentage of cells entered in the mock condition over all three days was 22%. For each separate experiment, the percent entry at each treatment condition was plotted as a percent entry relative to mock, where 100% indicates that the same amount of entry occurs as in the mock condition (Figure B2.1 A). Treatment with 10 μM ML-SI4 reduced entry to 82% of mock and treatment with 30 μM ML-SI4 reduced entry to 66% of mock.

One potentially confounding factor is the effect of ML-SI4 on cell viability. If ML-SI4 decreases the number of viable cells in each well, the percent entry relative to mock would be expected to decrease regardless of whether or not ML-

SI4 blocks infection. One of the three replicates that comprise the data in Figure B2.1A was conducted in conjunction with an assay that uses cellular ATP levels (CellTiter-Glo, Promega) to assess viability. To assess cellular viability in conjunction with viral entry, two plates were seeded with cells in parallel, one to be used for the viral entry assay as described above and one to be used to assess viability. The plates were treated identically with inhibitors and with changes of cell growth medium until the point where the “stop entry” buffer is added to the viral entry assay plate (see Chapter 3). At that point the viral entry plate was treated as described in Chapter 3 and the cell viability assay was executed as described in the manufacturer’s instructions. The cell viability assay (Figure A2.1 C) showed a decrease in viability in response to treatment with ML-SI4. This decrease in viability was less than the magnitude of inhibition of entry by the compound, but still substantial (Figure A.2 B). It was not possible to conclusively determine therefore whether the reduction in entry was due primarily to loss of cell viability (and thus loss of cells that could be entered) or due to an actual block on virus entering cells.

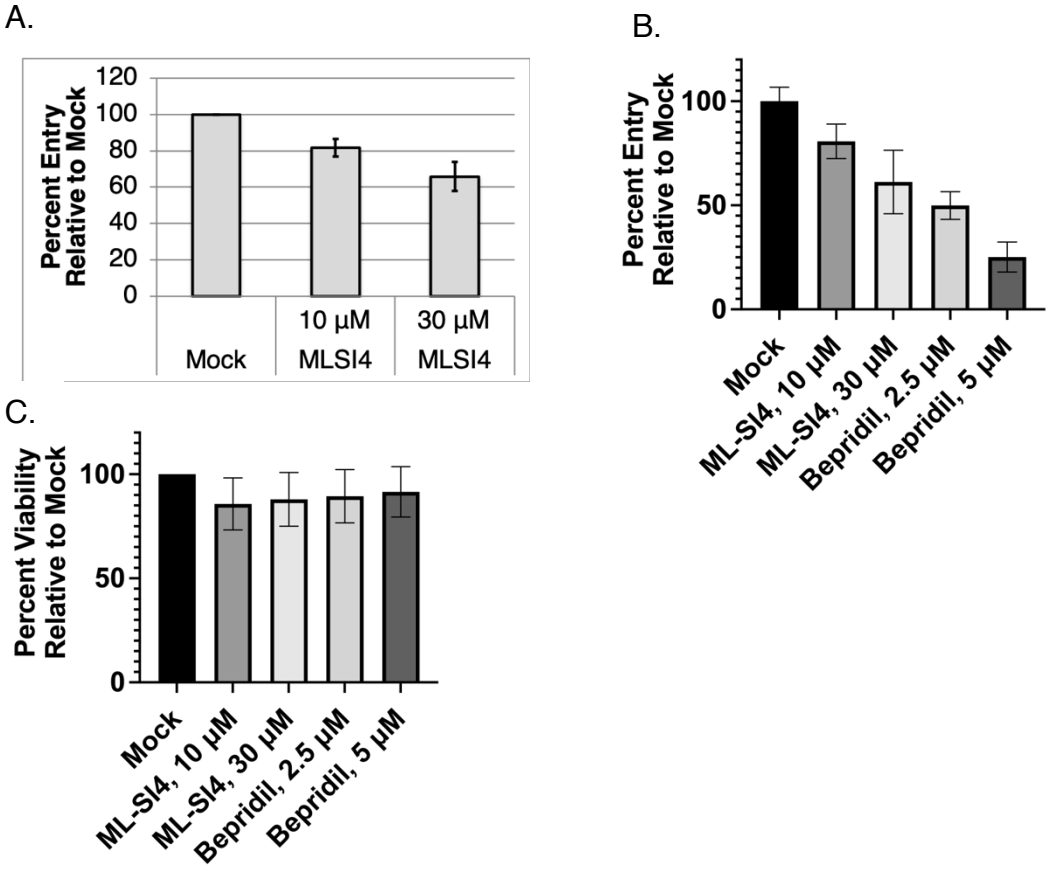

Figure B2.1. Treatment of U2OS cells with the TRPML inhibitor ML-SI4 reduces EBOV viral entry but also reduces cell viability. A) U2OS cells were pre-treated with ML-SI4 and VLPs were applied to the cells. The entry of VLPs into cells was measured by cleavage of a fluorescent substrate. Within each individual assay the percent entry was normalized to the percent entry observed in the mock treatment condition (DMSO). Three entry assays were conducted on separate days and the error bars represent 1SD of entry from all three assays. B) Results from one of the assays included in A) was plotted individually and the inhibition of viral entry by bepridil (negative control for entry) was included. The error bars represent the standard deviation of three technical replicates. C) A parallel assay was conducted on the same day under the same conditions as the assay in (B) to assess cell viability when treated with TRPML inhibitors and bepridil. As for the entry assays, the viability was normalized to mock treatment. Error bars represent the standard deviation of three technical replicates.

The effect of additional TRPML inhibitors and agonists (Table A2.1) on viral entry were examined by entry assay. Entry assays were conducted as described for Figure A2.1. The entry assays were conducted twice with all

compounds (two separate days) and the results for individual assays were plotted separately. No inhibitor or agonist (with the exception of ML-SI4) as described above showed a clear pattern of inhibition that intensified with increasing concentrations of inhibitor or agonist (Figure A2.2 A,B). Unexpectedly, the agonist ML-SA1 and the inhibitor ML-SI3 enhance infection at moderate concentrations while at high concentrations they show some level of inhibiting viral entry. In the case of the inhibitor ML-SI3, high concentrations could have non-specific activity on other channels or cause some perturbation in cellular physiology indirectly that inhibits EBOV trafficking and entry. Cell viability could not be measured due to a limited available amount of the compounds, but it is possible that as for ML-SI4 the other compounds reduce viability, introducing a confounding factor in the interpretation of entry data.

A.

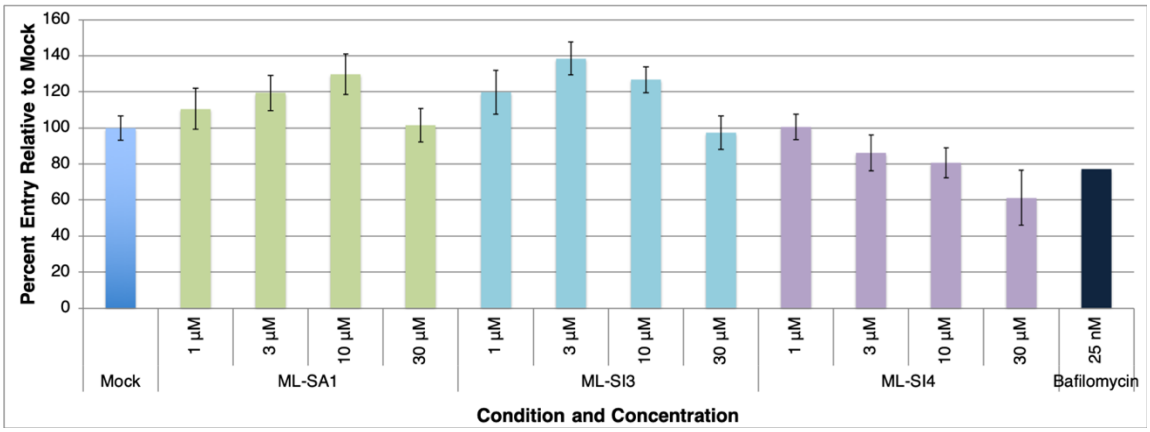

B.

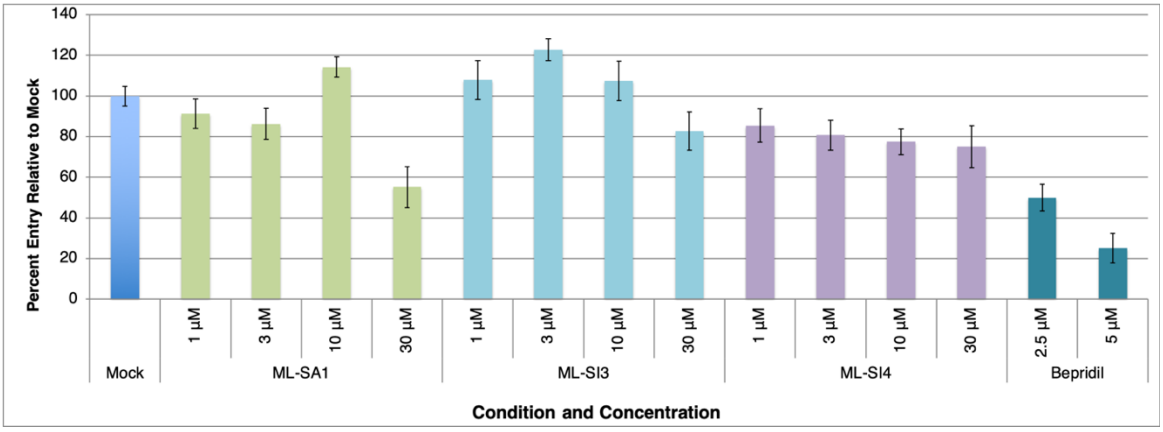

Figure B2.2. The effect of several TRPML inhibitors and agonists on EBOV entry. A-B) The entry assay described in Figure A1.1 was conducted for the TRPML1 agonist MA-SA1 and the inhibitors ML-SI3 and ML-SI4. Error bars represent 1SD of three technical replicates. A) Bafilomycin is used as a negative control for viral entry. B) The results for ML-SI4 and bepridil in this assay are the same as those shown in Figure A1.1 (C). Bepridil is used as a negative control for viral entry.

While the initial data showing a possible effect of TRPML inhibitors and agonists on EBOV entry is intriguing, further study is necessary to determine whether this effect is verifiable and independent of any effect of the compounds on cell viability. First, testing the effect of all compounds on viability would be

necessary to draw firm conclusions. Second, while ML-SI3 (Samie et al., 2013; W. Wang et al., 2015) and ML-SA1 (Shen et al., 2012) have been well described as specific to TRPML channels, ML-SI4 (X. Zhang et al., 2016) has limited data to demonstrate specificity and thus cells where TRPML1-3 are knocked down or knocked out would be required to interpret the results. We attempted to knockout TRPML1 in U2OS cells without success (data not shown), but it is possible a knockdown approach might be more successful.

With respect to viruses other than EBOV, there have been several reports published recently as to the role of TRPML in the trafficking and fusion of enveloped viruses, with conflicting conclusions about the importance of TRPML. TRPML has been investigated in the trafficking and entry of Middle Eastern Respiratory Syndrome Coronavirus (MERS) using a knock down model (Gunaratne et al., 2018). Though the knockdown was not very efficient and there was some reduction in infection, this reduction was not statistically significant. It is also important to note that only TRPML1 was knocked down and that simultaneous knockdown of TPC and TRPML1 or multiple TRPML isoforms was not attempted. Therefore, it is possible that remaining TRPML isoforms acted redundantly to promote normal viral trafficking. The same study did find TPC1/2 to be required for efficient infection and determined that the mechanism was related to a loss of viral trafficking and endosome motility in the absence of functioning TPC (Gunaratne et al., 2018).

More recent reports found a role for TRPML1-3 in flavivirus infection. Zika virus (ZIKV) and Dengue virus (DENV) infection was inhibited through treatment of cells with ML-SA1, a TRPML agonist (Z. Xia et al., 2020). The infection of cells by Japanese encephalitis virus (JEV) was inhibited by TRPML knock-down and berbamine, a compound found to inhibit calcium currents stimulated by the TRPML agonist ML-SA1. The authors hypothesize, as well as provide some evidence to support the idea that inhibiting TRPML perturbs the homeostasis of plasma membrane receptors for JEV by altering trafficking in the endosomal system (L. Huang et al., 2021). Thus, in one case activating TRPML seems to inhibit viral entry and in the other inhibiting TRPML inhibits viral entry, making the role of TRPML in flavivirus entry quite conflicted.

Finally using the tools of overexpression, dominant negative channels and genetic knock-outs, TRPML2 was shown to enhance infection for a wide variety of enveloped viruses including yellow fever virus, influenza virus and equine arteritis virus. The mechanism was determined using microscopy and biochemical assays. While influenza was internalized at normal levels in cells overexpressing TRPML2 it had increased colocalization with late endosomal markers, suggesting that TRPML2 enhances trafficking of influenza to late endosomes, where it can be triggered to fuse by low pH (Rinkenberger & Schoggins, 2018).

In summary, while the recent work seems to report a role for TRPML in the trafficking of at least some enveloped viruses, the mechanism of TRPML in

viral trafficking is quite conflicted. Addressing the role of each TRP channel individually using highly specific tools such as knockouts and knockdowns in parallel with the use of inhibitors may yield more definitive results with multiple approaches hopefully yielding similar outcomes. Definitely, much more work remains to be done to understand the range of enveloped viruses requiring TRPML for entry and infection and the full spectrum of mechanisms by which TRPML may affect viral entry.

References

Adam, B., Lins, L., Stroobant, V., Thomas, A., & Brasseur, R. (2004). Distribution of hydrophobic residues is crucial for the fusogenic properties of the Ebola virus GP2 fusion peptide. *Journal of Virology*, *78*(4), 2131–2136. https://doi.org/10.1128/jvi.78.4.2131-2136.2004

Albertini, A. A. V., Baquero, E., Ferlin, A., & Gaudin, Y. (2012). Molecular and cellular aspects of rhabdovirus entry. *Viruses*, *4*(1), 117–139. https://doi.org/10.3390/v4010117

Alberts, B., Johnson, A., Lewis, J., Raff, M., Roberts, K., & Walter, P. (2002). *Molecular Biology of the Cell* (4th ed.). Garland Science.

Allison, R., Lumb, J. H., Fassier, C., Connell, J. W., Ten Martin, D., Seaman, M. N. J., Hazan, J., & Reid, E. (2013). An ESCRT–spastin interaction promotes fission of recycling tubules from the endosome. *Journal of Cell Biology*, *202*(3), 527–543. https://doi.org/10.1083/jcb.201211045

Amini-Bavil-Olyaee, S., Choi, Y. J., Lee, J. H., Shi, M., Huang, I.-C., Farzan, M., & Jung, J. U. (2013). The Antiviral Effector IFITM3 Disrupts Intracellular Cholesterol Homeostasis to Block Viral Entry. *Cell Host & Microbe*, *13*(4), 452–464. https://doi.org/10.1016/j.chom.2013.03.006

Aoyama, M., Yoshioka, Y., Arai, Y., Hirai, H., Ishimoto, R., Nagano, K., Higashisaka, K., Nagai, T., & Tsutsumi, Y. (2017). Intracellular trafficking of particles inside endosomal vesicles is regulated by particle size. *Journal of Controlled Release*, *260*, 183–193. https://doi.org/10.1016/j.jconrel.2017.06.007

Balderhaar, H. J. kleine, Lachmann, J., Yavavli, E., Bröcker, C., Lürick, A., & Ungermann, C. (2013). The CORVET complex promotes tethering and fusion of Rab5/Vps21-positive membranes. *Proceedings of the National Academy of Sciences*, *110*(10), 3823–3828. https://doi.org/10.1073/pnas.1221785110

Bär, S., Takada, A., Kawaoka, Y., & Alizon, M. (2006). Detection of Cell-Cell Fusion Mediated by Ebola Virus Glycoproteins Detection of Cell-Cell Fusion Mediated by Ebola Virus Glycoproteins Se. *Journal of Virology*, *80*(6), 2815–2822. https://doi.org/10.1128/JVI.80.6.2815

Barnard, R. J. O., Elleder, D., & Young, J. A. T. (2006). Avian sarcoma and leukosis virus-receptor interactions: From classical genetics to novel insights into virus–cell membrane fusion. *Virology*, *344*(1), 25–29. https://doi.org/10.1016/j.virol.2005.09.021

Bayer, N., Schober, D., Prchla, E., Murphy, R. F., Blaas, D., & Fuchs, R. (1998). Effect of Bafilomycin A1 and Nocodazole on Endocytic Transport in HeLa Cells: Implications for Viral Uncoating and Infection. *Journal of Virology*. https://doi.org/10.1128/JVI.72.12.9645-9655.1998

Beilstein, F., Abou Hamdan, A., Raux, H., Belot, L., Ouldali, M., Albertini, A. A., & Gaudin, Y. (2020). Identification of a pH-Sensitive Switch in VSV-G and a Crystal Structure of the G Pre-fusion State Highlight the VSV-G Structural Transition Pathway. *Cell Reports*, *32*(7), 108042. https://doi.org/10.1016/j.celrep.2020.108042

Benčina, M. (2013). Illumination of the Spatial Order of Intracellular pH by Genetically Encoded pH-Sensitive Sensors. *Sensors*, *13*(12), 16736–16758. https://doi.org/10.3390/s131216736

Bissig, C., & Gruenberg, J. (2013). Lipid Sorting and Multivesicular Endosome Biogenesis. *Cold Spring Harbor Perspectives in Biology*, *5*(10), a016816. https://doi.org/10.1101/cshperspect.a016816

Bolte, S., & Cordelieres, F. P. (2006). A guided tour into subcellular colocalisation analysis in light microscopy. *Journal of Microscopy*, *224*(3), 13–232. https://doi.org/10.1111/j.1365-2818.2006.01706.x

Bonam, S. R., Wang, F., & Muller, S. (2019). Lysosomes as a therapeutic target. *Nature Reviews. Drug Discovery*, *18*(12), 923–948. https://doi.org/10.1038/s41573-019-0036-1

Borchers, A.-C., Langemeyer, L., & Ungermann, C. (2021). Who's in control? Principles of Rab GTPase activation in endolysosomal membrane trafficking and beyond. *Journal of Cell Biology*, *220*(9). https://doi.org/10.1083/jcb.202105120

Bortz, R. H., Wong, A. C., Grodus, M. G., Recht, H. S., Pulanco, M. C., Lasso, G., Anthony, S. J., Mittler, E., Jangra, R. K., & Chandran, K. (2020). A Virion-Based Assay for Glycoprotein Thermostability Reveals Key Determinants of Filovirus Entry and Its Inhibition. *Journal of Virology*, *94*(18), e00336-20. https://doi.org/10.1128/JVI.00336-20

Bowman, E. J., Siebers, A., & Altendorf, K. (1988). Bafilomycins: A class of inhibitors of membrane ATPases from microorganisms, animal cells, and plant cells. *Proceedings of the National Academy of Sciences*, *85*(21), 7972–7976. https://doi.org/10.1073/pnas.85.21.7972

Brailoiu, E., Rahman, T., Churamani, D., Prole, D. L., Brailoiu, G. C., Hooper, R., Taylor, C. W., & Patel, S. (2010). An NAADP-gated two-pore channel targeted to the plasma membrane uncouples triggering from amplifying Ca2+ signals. *Journal of Biological Chemistry*, *285*(49), 38511–38516. https://doi.org/10.1074/jbc.M110.162073

Brass, A. L., Huang, I.-C., Benita, Y., John, S. P., Krishnan, M. N., Feeley, E. M., Ryan, B. J., Weyer, J. L., Weyden, L. van der, Fikrig, E., Adams, D. J., Xavier, R. J., Farzan, M., & Elledge, S. J. (2009). The IFITM Proteins Mediate Cellular Resistance to Influenza A H1N1 Virus, West Nile Virus, and Dengue Virus. *Cell*, *139*(7), 1243–1254. https://doi.org/10.1016/j.cell.2009.12.017

Brini, M., & Carafoli, E. (2011). The Plasma Membrane Ca2+ ATPase and the Plasma Membrane Sodium Calcium Exchanger Cooperate in the Regulation of Cell Calcium. *Cold Spring Harbor Perspectives in Biology*, *3*(2), a004168. https://doi.org/10.1101/cshperspect.a004168

Brown, M. S., & Goldstein, J. L. (1979). Receptor-mediated endocytosis: Insights from the lipoprotein receptor system. *Proceedings of the National Academy of Sciences of the United States of America*, *76*(7), 3330–3337. https://doi.org/10.1073/pnas.76.7.3330

Burgstaller, S., Bischof, H., Gensch, T., Stryeck, S., Gottschalk, B., Ramadani-Muja, J., Eroglu, E., Rost, R., Balfanz, S., Baumann, A., Waldeck-Weiermair, M., Hay, J. C., Madl, T., Graier, W. F., & Malli, R. (2019). PH-Lemon, a Fluorescent Protein-Based pH Reporter for Acidic Compartments. *ACS Sensors*, *4*(4), 883–891. https://doi.org/10.1021/acssensors.8b01599

Calcraft, P. J., Ruas, M., Pan, Z., Cheng, X., Arredouani, A., Hao, X., Tang, J., Rietdorf, K., Teboul, L., Chuang, K.-T., Lin, P., Xiao, R., Wang, C., Zhu, Y., Lin, Y., Wyatt, C. N., Parrington, J., Ma, J., Evans, A. M., … Zhu, M. X. (2009). NAADP mobilizes calcium from acidic organelles through two-pore channels. *Nature*, *459*(7246), 596–600. https://doi.org/10.1038/nature08030

Canton, J., & Grinstein, S. (2015). Measuring lysosomal pH by fluorescence microscopy. In *Methods in Cell Biology* (Vol. 126). Elsevier Ltd. https://doi.org/10.1016/bs.mcb.2014.10.021

Cao, T. T., Mays, R. W., & Zastrow, M. von. (1998). Regulated Endocytosis of G-protein-coupled Receptors by a Biochemically and Functionally Distinct Subpopulation of Clathrin-coated Pits *. *Journal of Biological Chemistry*, *273*(38), 24592–24602. https://doi.org/10.1074/jbc.273.38.24592

Carneiro, F. A., Ferradosa, A. S., & Da Poian, A. T. (2001). Low pH-induced conformational changes in vesicular stomatitis virus glycoprotein involve dramatic structure reorganization. *The Journal of Biological Chemistry*, *276*(1), 62–67. https://doi.org/10.1074/jbc.M008753200

Chadwick, S. R., Grinstein, S., & Freeman, S. A. (2021). From the inside out: Ion fluxes at the centre of endocytic traffic. *Current Opinion in Cell Biology*, *71*, 77–86. https://doi.org/10.1016/j.ceb.2021.02.006

Chandran, K., Sullivan, N. J., Felbor, U., Whelan, S. P., & Cunningham, J. (2005). Endosomal Proteolysis of the Ebola Virus Glycoprotein Is Necessary for Infection. *Science*, *308*(5728), 1643–1645. https://doi.org/10.1126/science.1110656

Chen, B.-C., Legant, W. R., Wang, K., Shao, L., Milkie, D. E., Davidson, M. W., Janetopoulos, C., Wu, X. S., Hammer, J. A., Liu, Z., English, B. P., Mimori-Kiyosue, Y., Romero, D. P., Ritter, A. T., Lippincott-Schwartz, J., Fritz-Laylin, L., Mullins, R. D., Mitchell, D. M., Bembenek, J. N., … Betzig, E. (2014). Lattice light-sheet microscopy: Imaging molecules to embryos at high spatiotemporal resolution. *Science*, *346*(6208), 1257998. https://doi.org/10.1126/science.1257998

Chen, C. S., Martin, O. C., & Pagano, R. E. (1997). Changes in the spectral properties of a plasma membrane lipid analog during the first seconds of endocytosis in living cells. *Biophysical Journal*, *72*(1), 37–50. https://doi.org/10.1016/S0006-3495(97)78645-4

Chen, H.-W., Huang, C.-Y., Lin, S.-Y., Fang, Z.-S., Hsu, C.-H., Lin, J.-C., Chen, Y.-I., Yao, B.-Y., & Hu, C.-M. J. (2016). Synthetic virus-like particles prepared via protein corona formation enable effective vaccination in an avian model of coronavirus infection. *Biomaterials*, *106*, 111–118. https://doi.org/10.1016/j.biomaterials.2016.08.018

Chen, Q., She, J., Zeng, W., Guo, J., Xu, H., Bai, X.-C., & Jiang, Y. (2017). Structure of mammalian endolysosomal TRPML1 channel in nanodiscs. *Nature Publishing Group*. https://doi.org/10.1038/nature24035

Chen, Z., & Schmid, S. L. (2020). Evolving models for assembling and shaping clathrin-coated pits. *The Journal of Cell Biology*, *219*(9), e202005126. https://doi.org/10.1083/jcb.202005126

Chernomordik, L. V., Frolov, V. A., Leikina, E., Bronk, P., & Zimmerberg, J. (1998). The Pathway of Membrane Fusion Catalyzed by Influenza Hemagglutinin: Restriction of Lipids, Hemifusion, and Lipidic Fusion Pore Formation. *The Journal of Cell Biology*, *140*(6), 1369–1382.

Chevallier, J., Chamoun, Z., Jiang, G., Prestwich, G., Sakai, N., Matile, S., Parton, R. G., & Gruenberg, J. (2008). Lysobisphosphatidic Acid Controls Endosomal Cholesterol Levels. *Journal of Biological Chemistry*, *283*(41), 27871–27880. https://doi.org/10.1074/jbc.M801463200

Chlanda, P., Mekhedov, E., Waters, H., Schwartz, C. L., Fischer, E. R., Ryham, R. J., Cohen, F. S., Blank, P. S., & Zimmerberg, J. (2016). The hemifusion structure induced by influenza virus haemagglutinin is determined by physical properties of the target membranes. *Nature Microbiology*, *April*, 16050. https://doi.org/10.1038/nmicrobiol.2016.50

Chou, Y.-Y., Upadhyayula, S., Houser, J., He, K., Skillern, W., Scanavachi, G., Dang, S., Sanyal, A., Ohashi, K. G., Di Caprio, G., Kreutzberger, A. J. B., Vadakkan, T. J., & Kirchhausen, T. (2021). Inherited nuclear pore substructures template post-mitotic pore assembly. *Developmental Cell*, *56*(12), 1786-1803.e9. https://doi.org/10.1016/j.devcel.2021.05.015

Christoforidis, S., McBride, H. M., Burgoyne, R. D., & Zerial, M. (1999). The Rab5 effector EEA1 is a core component of endosome docking. *Nature*, *397*(6720), 621–625. https://doi.org/10.1038/17618

Chu, J., Haynes, R. D., Corbel, S. Y., Li, P., González-González, E., Burg, J. S., Ataie, N. J., Lam, A. J., Cranfill, P. J., Baird, M. A., Davidson, M. W., Ng, H.-L., Garcia, K. C., Contag, C. H., Shen, K., Blau, H. M., & Lin, M. Z. (2014). Non-invasive intravital imaging of cellular differentiation with a bright red-excitable fluorescent protein. *Nature Methods*, *11*(5), 572–578. https://doi.org/10.1038/nmeth.2888

Churchill, G. C., Okada, Y., Thomas, J. M., Genazzani, A. A., Patel, S., & Galione, A. (2002). NAADP Mobilizes Ca2+ from Reserve Granules, Lysosome-Related Organelles, in Sea Urchin Eggs. *Cell*, *111*(5), 703–708. https://doi.org/10.1016/S0092-8674(02)01082-6

Clague, M. J., Urbé, S., Aniento, F., & Gruenberg, J. (1994). Vacuolar ATPase activity is required for endosomal carrier vesicle formation. *The Journal of Biological Chemistry*, *269*(1), 21–24.

Cocucci, E., Gaudin, R., & Kirchhausen, T. (2014). Dynamin recruitment and membrane scission at the neck of a clathrin-coated pit. *Molecular Biology of the Cell*, *25*(22), 3595–3609. https://doi.org/10.1091/mbc.E14-07-1240

Comeau, J. W. D., Costantino, S., & Wiseman, P. W. (2006). A Guide to Accurate Fluorescence Microscopy Colocalization Measurements. *Biophysical Journal*, *91*(12), 4611–4622. https://doi.org/10.1529/biophysj.106.089441

Côté, M., Misasi, J., Ren, T., Bruchez, A., Lee, K., Filone, C. M., Hensley, L., Li, Q., Ory, D., Chandran, K., & Cunningham, J. (2011). Small molecule inhibitors reveal Niemann-Pick C1 is essential for Ebola virus infection. *Nature*, *477*(7364), 344–348. https://doi.org/10.1038/nature10380

Cullen, P. J., & Steinberg, F. (2018). To degrade or not to degrade: Mechanisms and significance of endocytic recycling. *Nature Reviews. Molecular Cell Biology*, *19*(11), 679–696. https://doi.org/10.1038/s41580-018-0053-7

Cureton, D. K., Massol, R. H., Saffarian, S., Kirchhausen, T. L., & Whelan, S. P. J. (2009). Vesicular Stomatitis Virus Enters Cells through Vesicles Incompletely Coated with Clathrin That Depend upon Actin for Internalization. *PLOS Pathogens*, *5*(4), e1000394. https://doi.org/10.1371/journal.ppat.1000394

Cureton, D. K., Massol, R. H., Whelan, S. P. J., & Kirchhausen, T. (2010). The Length of Vesicular Stomatitis Virus Particles Dictates a Need for Actin Assembly during Clathrin-Dependent Endocytosis. *PLOS Pathogens*, *6*(9), e1001127. https://doi.org/10.1371/journal.ppat.1001127

Cussler, E. L., Evans, D. F., & Matesich, M. A. (1971). Theoretical and Experimental Basis for a Specific Countertransport System in Membranes. *Science*, *172*(3981), 377–379.

Danieli, T., Pelletier, S., Henis, Y., & White, J. (1996). Membrane fusion mediate by the influenza virus hemagglutinin requires the concerted action of at least three hemagglutinin trimers. *J. Cell Biology*, *133*(3), 559–569. https://doi.org/10.1083/jcb.133.3.559

Das, D. K., Bulow, U., Diehl, W. E., Durham, N. D., Senjobe, F., Chandran, K., Luban, J., & Munro, J. B. (2020). Conformational changes in the Ebola virus membrane fusion machine induced by pH, Ca2+, and receptor binding. *PLOS Biology*, *18*(2), e3000626. https://doi.org/10.1371/journal.pbio.3000626

de Bruyn, P. P., Cho, Y., & Michelson, S. (1983). In vivo endocytosis by bristle coated pits of protein tracers and their intracellular transport in the endothelial cells lining the sinuses of the liver. I. The endosomal disposition. *Journal of Ultrastructure Research*, *85*(3), 272–289. https://doi.org/10.1016/s0022-5320(83)90039-4

De Duve, C., De Barsy, T., Poole, B., Trouet, A., Tulkens, P., & Van Hoof, F. (1974). Lysosomotropic agents. *Biochemical Pharmacology*, *23*(18), 2495–2531. https://doi.org/10.1016/0006-2952(74)90174-9

De Luca, M., & Bucci, C. (2014). A new V-ATPase regulatory mechanism mediated by the rab interacting lysosomal protein (RILP). *Communicative and Integrative Biology*, *7*(5), 1–5. https://doi.org/10.4161/cib.29616

De Luca, M., Cogli, L., Progida, C., Nisi, V., Pascolutti, R., Sigismund, S., Di Fiore, P. P., & Bucci, C. (2014). RILP regulates vacuolar ATPase through interaction with the V1G1 subunit. *Journal of Cell Science*, *127*(12), 2697–2708. https://doi.org/10.1242/jcs.142604

Delos, S. E., La, B., Gilmartin, A., & White, J. M. (2010). Studies of the “chain reversal regions” of the avian sarcoma/leukosis virus (ASLV) and ebolavirus fusion proteins: Analogous residues are important, and a His residue unique to EnvA affects the pH dependence of ASLV entry. *Journal of Virology*, *84*(11), 5687–5694. https://doi.org/10.1128/JVI.02583-09

Derivery, E., Sousa, C., Gautier, J. J., Lombard, B., Loew, D., & Gautreau, A. (2009). The Arp2/3 activator WASH controls the fission of endosomes through a large multiprotein complex. *Developmental Cell*, *17*(5), 712–723. https://doi.org/10.1016/j.devcel.2009.09.010

Desai, T. M., Marin, M., Mason, C., & Melikyan, G. B. (2017). PH regulation in early endosomes and interferon-inducible transmembrane proteins control avian retrovirus fusion. *Journal of Biological Chemistry*, *292*(19), 7817–7827. https://doi.org/10.1074/jbc.M117.783878

Dias, C., & Nylandsted, J. (2021). Plasma membrane integrity in health and disease: Significance and therapeutic potential. *Cell Discovery*, *7*(1), 1–18. https://doi.org/10.1038/s41421-020-00233-2

Diaz, R., Mayorga, L., & Stahl, P. (1988). In vitro fusion of endosomes following receptor-mediated endocytosis. *Journal of Biological Chemistry*, *263*(13), 6093–6100. https://doi.org/10.1016/S0021-9258(18)68754-X

Diaz-Rohrer, B. B., Levental, K. R., Simons, K., & Levental, I. (2014). Membrane raft association is a determinant of plasma membrane localization. *Proceedings of the National Academy of Sciences*, *111*(23), 8500–8505. https://doi.org/10.1073/pnas.1404582111

Dickson, R. B., Beguinot, L., Hanover, J. A., Richert, N. D., Willingham, M. C., & Pastan, I. (1983). Isolation and characterization of a highly enriched preparation of receptosomes (endosomes) from a human cell line. *Proceedings of the National Academy of Sciences of the United States of America*, *80*(17), 5335–5339. https://doi.org/10.1073/pnas.80.17.5335

Dimitrov, D. S. (2004). Virus entry: Molecular mechanisms and biomedical applications. *Nature Reviews Microbiology*, *2*(2), 109–122. https://doi.org/10.1038/nrmicro817

Dong, X., Shen, D., Wang, X., Dawson, T., Li, X., Zhang, Q., Cheng, X., Zhang, Y., Weisman, L. S., Delling, M., & Xu, H. (2010). PI(3,5)P(2) controls membrane trafficking by direct activation of mucolipin Ca(2+) release channels in the endolysosome. *Nature Communications*, *1*(4), 38. https://doi.org/10.1038/ncomms1037

Eidelman, O., Schlegel, R., Tralka, T. S., & Blumenthal, R. (1984). PH-dependent fusion induced by vesicular stomatitis virus glycoprotein reconstituted into phospholipid vesicles. *The Journal of Biological Chemistry*, *259*(7), 4622–4628.

Esposito, A., Gralle, M., Dani, M. A. C., Lange, D., & Wouters, F. S. (2008). pHlameleons: A Family of FRET-Based Protein Sensors for Quantitative pH Imaging. *Biochemistry*, *47*(49), 13115–13126. https://doi.org/10.1021/bi8009482

Fan, H., Du, X., Zhang, J., Zheng, H., Lu, X., Wu, Q., Li, H., Wang, H., Shi, Y., Gao, G., Zhou, Z., Tan, D.-X., & Li, X. (2017). Selective inhibition of Ebola entry with selective estrogen receptor modulators by disrupting the endolysosomal calcium. *Scientific Reports*, *7*(January), 41226. https://doi.org/10.1038/srep41226

Fedeli, C., Moreno, H., & Kunz, S. (2020). The Role of Receptor Tyrosine Kinases in Lassa Virus Cell Entry. *Viruses*, *12*(8), E857. https://doi.org/10.3390/v12080857

Feeley, E. M., Sims, J. S., John, S. P., Chin, C. R., Pertel, T., Chen, L.-M., Gaiha, G. D., Ryan, B. J., Donis, R. O., Elledge, S. J., & Brass, A. L. (2011). IFITM3 inhibits influenza A virus infection by preventing cytosolic entry. *PLoS Pathogens*, *7*(10), e1002337. https://doi.org/10.1371/journal.ppat.1002337

Feldmann, D. F. and H. (2015). Delineating Ebola entry. *Science*, *347*(6225), 947–948. https://doi.org/10.1126/science.aaa8121

Feldmann, H., Sanchez, A., & Geisbert, T. W. (2013). Filoviridae: Marburg and Ebola Viruses. In *Fields Virology*.

Fénéant, L., Wijs, K. M. S., Nelson, E. A., & White, J. M. (2019). An exploration of conditions proposed to trigger the Ebola virus glycoprotein for fusion. *PLOS ONE*, *14*(7), e0219312. https://doi.org/10.1371/journal.pone.0219312

Finkelshtein, D., Werman, A., Novick, D., Barak, S., & Rubinstein, M. (2013). LDL receptor and its family members serve as the cellular receptors for vesicular stomatitis virus. *Proceedings of the National Academy of Sciences*, *110*(18), 7306–7311. https://doi.org/10.1073/pnas.1214441110

Fischer, D. G., Tal, N., Novick, D., Barak, S., & Rubinstein, M. (1993). An antiviral soluble form of the LDL receptor induced by interferon. *Science (New York, N.Y.)*, *262*(5131), 250–253. https://doi.org/10.1126/science.8211145

Floyd, D. L., Ragains, J. R., Skehel, J. J., Harrison, S. C., & van Oijen, A. M. (2008). Single-particle kinetics of influenza virus membrane fusion. *Proceedings of the National Academy of Sciences*, *105*(40), 15382–15387. https://doi.org/10.1073/pnas.0807771105

Franke, C., Repnik, U., Segeletz, S., Brouilly, N., Kalaidzidis, Y., Verbavatz, J., & Zerial, M. (2019). Correlative single-molecule localization microscopy and electron tomography reveals endosome nanoscale domains. *Traffic (Copenhagen, Denmark)*, *20*(8), 601–617. https://doi.org/10.1111/tra.12671

Fredericksen, B. L., & Whitt, M. A. (1995). Vesicular stomatitis virus glycoprotein mutations that affect membrane fusion activity and abolish virus infectivity. *Journal of Virology*, *69*(3), 1435–1443.

Freeman, S. A., Uderhardt, S., Saric, A., Collins, R. F., Buckley, C. M., Mylvaganam, S., Boroumand, P., Plumb, J., Germain, R. N., Ren, D., & Grinstein, S. (2020). Lipid-gated monovalent ion fluxes regulate endocytic traffic and support immune surveillance. *Science*, *367*(6475), 301–305. https://doi.org/10.1126/science.aaw9544

Freitas, M. S., Follmer, C., Costa, L. T., Vilani, C., Lucia Bianconi, M., Achete, C. A., & Silva, J. L. (2011). Measuring the strength of interaction between the Ebola fusion peptide and lipid rafts: Implications for membrane fusion and virus infection. *PLoS ONE*, *6*(1). https://doi.org/10.1371/journal.pone.0015756

Fuchs, R., Schmid, S., & Mellman, I. (1989). A possible role for Na+,K+-ATPase in regulating ATP-dependent endosome acidification. *Proceedings of the National Academy of Sciences of the United States of America*, *86*(2), 539–543. https://doi.org/10.1073/pnas.86.2.539

Gagescu, R., Demaurex, N., Parton, R. G., Hunziker, W., Huber, L. A., & Gruenberg, J. (2000). The Recycling Endosome of Madin-Darby Canine Kidney Cells Is a Mildly Acidic Compartment Rich in Raft Components. *Molecular Biology of the Cell*, *11*(8), 2775–2791. https://doi.org/10.1091/mbc.11.8.2775

Gautreau, A., Oguievetskaia, K., & Ungermann, C. (2014). Function and Regulation of the Endosomal Fusion and Fission Machineries. *Cold Spring Harbor Perspectives in Biology*, *6*(3), a016832. https://doi.org/10.1101/cshperspect.a016832

Geoghegan, N. D., Evelyn, C., Whitehead, L. W., Pasternak, M., McDonald, P., Triglia, T., Marapana, D. S., Kempe, D., Thompson, J. K., Mlodzianoski, M. J., Healer, J., Biro, M., Cowman, A. F., & Rogers, K. L. (2021). 4D analysis of malaria parasite invasion offers insights into erythrocyte membrane remodeling and parasitophorous vacuole formation. *Nature Communications*, *12*(1), 3620. https://doi.org/10.1038/s41467-021-23626-7

Gerlach, T., Hensen, L., Matrosovich, T., Bergmann, J., Winkler, M., Peteranderl, C., Klenk, H.-D., Weber, F., Herold, S., Pöhlmann, S., & Matrosovich, M. (2017). PH Optimum of Hemagglutinin-Mediated Membrane Fusion Determines Sensitivity of Influenza A Viruses to the Interferon-Induced Antiviral State and IFITMs. *Journal of Virology*, *91*(11), e00246-17. https://doi.org/10.1128/JVI.00246-17

Gerndt, S., Chen, C.-C., Chao, Y.-K., Yuan, Y., Burgstaller, S., Scotto Rosato, A., Krogsaeter, E., Urban, N., Jacob, K., Nguyen, O. N. P., Miller, M. T., Keller, M., Vollmar, A. M., Gudermann, T., Zierler, S., Schredelseker, J., Schaefer, M., Biel, M., Malli, R., … Grimm, C. (2020). Agonist-mediated switching of ion selectivity in TPC2 differentially promotes lysosomal function. *ELife*, *9*, e54712. https://doi.org/10.7554/eLife.54712

Gething, M. J., Doms, R. W., York, D., & White, J. (1986). Studies on the mechanism of membrane fusion: Site-specific mutagenesis of the hemagglutinin of influenza virus. *The Journal of Cell Biology*, *102*(1), 11–23. https://doi.org/10.1083/jcb.102.1.11

Geuze, H. J., Slot, J. W., & Schwartz, A. L. (1987). Membranes of sorting organelles display lateral heterogeneity in receptor distribution. *The Journal of Cell Biology*, *104*(6), 1715–1723. https://doi.org/10.1083/jcb.104.6.1715

Geuze, H. J., Slot, J. W., Strous, G. J., & Schwartz, A. L. (1983). The pathway of the asialoglycoprotein-ligand during receptor-mediated endocytosis: A morphological study

with colloidal gold/ligand in the human hepatoma cell line, Hep G2. *European Journal of Cell Biology*, *32*(1), 38–44.

Ghaffarian, R., & Muro, S. (2014). Distinct Subcellular Trafficking Resulting from Monomeric vs Multimeric Targeting to Endothelial ICAM-1: Implications for Drug Delivery. *Molecular Pharmaceutics*, *11*(12), 4350–4362. https://doi.org/10.1021/mp500409y

Ghosh, J. K., Peisajovich, S. G., & Shai, Y. (2000). Sendai virus internal fusion peptide: Structural and functional characterization and a plausible mode of viral entry inhibition. *Biochemistry*, *39*(38), 11581–11592. https://doi.org/10.1021/bi0005963

Gillooly, D. J., Morrow, I. C., Lindsay, M., Gould, R., Bryant, N. J., Gaullier, J. M., Parton, R. G., & Stenmark, H. (2000). Localization of phosphatidylinositol 3-phosphate in yeast and mammalian cells. *The EMBO Journal*, *19*(17), 4577–4588. https://doi.org/10.1093/emboj/19.17.4577

Goldstein, J. L., Anderson, R. G., & Brown, M. S. (1982). Receptor-mediated endocytosis and the cellular uptake of low density lipoprotein. *Ciba Foundation Symposium*, *92*, 77–95. https://doi.org/10.1002/9780470720745.ch5

Goldstein, T., Anthony, S. J., Gbakima, A., Bird, B. H., Bangura, J., Tremeau-Bravard, A., Belaganahalli, M. N., Wells, H. L., Dhanota, J. K., Liang, E., Grodus, M., Jangra, R. K., DeJesus, V. A., Lasso, G., Smith, B. R., Jambai, A., Kamara, B. O., Kamara, S., Bangura, W., … Mazet, J. A. K. (2018). The discovery of Bombali virus adds further support for bats as hosts of ebolaviruses. *Nature Microbiology*, *3*(10), 1084–1089. https://doi.org/10.1038/s41564-018-0227-2

Grabe, M., & Oster, G. (2001). Regulation of Organelle Acidity. *The Journal of General Physiology*, *117*(4), 329–344. https://doi.org/doi: 10.1085/jgp.117.4.329

Graven, S. N., Estrada-O, S., & Lardy, H. A. (1966). Alkali metal cation release and respiratory inhibition induced by nigericin in rat liver mitochondria. *Proceedings of the National Academy of Sciences of the United States of America*, *56*(2), 654–658.

Gray, E. R., Illingworth, C. J. R., Coffin, J. M., & Stoye, J. P. (2011). Binding of more than one Tva800 molecule is required for ASLV-A entry. *Retrovirology*, *8*, 96. https://doi.org/10.1186/1742-4690-8-96

Gregory, S. M., Harada, E., Liang, B., Delos, S. E., White, J. M., & Tamm, L. K. (2011). Structure and function of the complete internal fusion loop from Ebolavirus glycoprotein 2. *Proceedings of the National Academy of Sciences of the United States of America*, *108*(27), 11211–11216. https://doi.org/10.1073/pnas.1104760108

Griesbeck, O., Baird, G. S., Campbell, R. E., Zacharias, D. A., & Tsien, R. Y. (2001). Reducing the Environmental Sensitivity of Yellow Fluorescent Protein: MECHANISM AND APPLICATIONS*. *Journal of Biological Chemistry*, *276*(31), 29188–29194. https://doi.org/10.1074/jbc.M102815200

Gruenberg, J. (2020). Life in the lumen: The multivesicular endosome. *Traffic (Copenhagen, Denmark)*, *21*(1), 76–93. https://doi.org/10.1111/tra.12715

Gunaratne, G. S., Yang, Y., Li, F., Walseth, T. F., & Marchant, J. S. (2018). NAADP-dependent Ca2+ signaling regulates Middle East respiratory syndrome-coronavirus pseudovirus translocation through the endolysosomal system. *Cell Calcium*, *75*, 30–41. https://doi.org/10.1016/j.ceca.2018.08.003

Guo, X., Steinkühler, J., Marin, M., Li, X., Lu, W., Dimova, R., & Melikyan, G. B. (2021). Interferon-Induced Transmembrane Protein 3 Blocks Fusion of Diverse Enveloped Viruses by Altering Mechanical Properties of Cell Membranes. *ACS Nano*, *15*(5), 8155–8170. https://doi.org/10.1021/acsnano.0c10567

Haga, Y., Ishii, K., Hibino, K., Sako, Y., Ito, Y., Taniguchi, N., & Suzuki, T. (2012). Visualizing specific protein glycoforms by transmembrane fluorescence resonance energy transfer. *Nature Communications*, *3*(1), 907. https://doi.org/10.1038/ncomms1906

Hallam, S. J., Koma, T., Maruyama, J., & Paessler, S. (2018). Review of Mammarenavirus Biology and Replication. *Frontiers in Microbiology*, *9*. https://www.frontiersin.org/article/10.3389/fmicb.2018.01751

Han, X., Bushweller, J. H., Cafiso, D. S., & Tamm, L. K. (2001). Membrane structure and fusion-triggering conformational change of the fusion domain from influenza hemagglutinin. *Nature Structural Biology*, *8*(8), 715–720. https://doi.org/10.1038/90434

Hansen, S. H., Sandvig, K., & van Deurs, B. (1991). The preendosomal compartment comprises distinct coated and noncoated endocytic vesicle populations. *The Journal of Cell Biology*, *113*(4), 731–741. https://doi.org/10.1083/jcb.113.4.731

Harding, C., Heuser, J., & Stahl, P. (1983). Receptor-mediated endocytosis of transferrin and recycling of the transferrin receptor in rat reticulocytes. *The Journal of Cell Biology*, *97*(2), 329–339. https://doi.org/10.1083/jcb.97.2.329

Harikumar, P., & Reeves, J. P. (1983). The lysosomal proton pump is electrogenic. *Journal of Biological Chemistry*, *258*(17), 10403–10410. https://doi.org/10.1016/S0021-9258(17)44471-1

Harter, C., James, P., Bächi, T., Semenza, G., & Brunner, J. (1989). Hydrophobic binding of the ectodomain of influenza hemagglutinin to membranes occurs through the "fusion peptide." *The Journal of Biological Chemistry*, *264*(11), 6459–6464.

Hastie, K. M., & Saphire, E. O. (2018). Lassa virus glycoprotein: Stopping a moving target. *Current Opinion in Virology*, *31*, 52–58. https://doi.org/10.1016/j.coviro.2018.05.002

Henne, W. M., Stenmark, H., & Emr, S. D. (2013). Molecular Mechanisms of the Membrane Sculpting ESCRT Pathway. *Cold Spring Harbor Perspectives in Biology*, *5*(9), a016766. https://doi.org/10.1101/cshperspect.a016766

Herman, B., & Albertini, D. F. (1983). Ligand-induced rapid redistribution of lysosomes is temporally distinct from endosome translocation. *Nature*, *304*(5928), 738–740. https://doi.org/10.1038/304738a0

Hernandez-Gonzalez, M., Larocque, G., & Way, M. (2021). Viral use and subversion of membrane organization and trafficking. *Journal of Cell Science*, *134*(5), jcs252676. https://doi.org/10.1242/jcs.252676

Hilger, D., Masureel, M., & Kobilka, B. K. (2018). Structure and dynamics of GPCR signaling complexes. *Nature Structural & Molecular Biology*, *25*(1), 4–12. https://doi.org/10.1038/s41594-017-0011-7

Hink, M. A., Griep, R. A., Borst, J. W., van Hoek, A., Eppink, M. H., Schots, A., & Visser, A. J. (2000). Structural dynamics of green fluorescent protein alone and fused with a single chain Fv protein. *The Journal of Biological Chemistry*, *275*(23), 17556–17560. https://doi.org/10.1074/jbc.M001348200

Hirschi, M., Herzik Jr, M. A., Wie, J., Suo, Y., Borschel, W. F., Ren, D., Lander, G. C., & Lee, S.-Y. (2017). Cryo-electron microscopy structure of the lysosomal calcium-permeable channel TRPML3. *Nature*, *550*(7676), 411–414. https://doi.org/10.1038/nature24055

Hoffmann, M., González Hernández, M., Berger, E., Marzi, A., & Pöhlmann, S. (2016). The Glycoproteins of All Filovirus Species Use the Same Host Factors for Entry into Bat and Human Cells but Entry Efficiency Is Species Dependent. *PloS One*, *11*(2), e0149651. https://doi.org/10.1371/journal.pone.0149651

Hoffmann, M., Kleine-Weber, H., Schroeder, S., Krüger, N., Herrler, T., Erichsen, S., Schiergens, T. S., Herrler, G., Wu, N.-H., Nitsche, A., Müller, M. A., Drosten, C., & Pöhlmann, S. (2020). SARS-CoV-2 Cell Entry Depends on ACE2 and TMPRSS2 and Is Blocked by a Clinically Proven Protease Inhibitor. *Cell*, *181*(2), 271-280.e8. https://doi.org/10.1016/j.cell.2020.02.052

Hoyer, M. J., Chitwood, P. J., Ebmeier, C. C., Striepen, J. F., Qi, R. Z., Old, W. M., & Voeltz, G. K. (2018). A Novel Class of ER Membrane Proteins Regulates ER-Associated Endosome Fission. *Cell*, *175*(1), 254-265.e14. https://doi.org/10.1016/j.cell.2018.08.030

Huang, F., Khvorova, A., Marshall, W., & Sorkin, A. (2004). Analysis of clathrin-mediated endocytosis of epidermal growth factor receptor by RNA interference. *The Journal of Biological Chemistry*, *279*(16), 16657–16661. https://doi.org/10.1074/jbc.C400046200

Huang, L., Li, H., Ye, Z., Xu, Q., Fu, Q., Sun, W., Qi, W., & Yue, J. (2021). Berbamine inhibits Japanese encephalitis virus (JEV) infection by compromising TPRMLs-mediated

endolysosomal trafficking of low-density lipoprotein receptor (LDLR). *Emerging Microbes & Infections*, *10*(1), 1257–1271. https://doi.org/10.1080/22221751.2021.1941276

Hulseberg, C. E., Fénéant, L., Szymańska, K. M., & White, J. M. (2018). Lamp1 Increases the Efficiency of Lassa Virus Infection by Promoting Fusion in Less Acidic Endosomal Compartments. *MBio*, *9*(1), e01818-17. https://doi.org/10.1128/mBio.01818-17

Hulseberg, C. E., Fénéant, L., Szymańska-de Wijs, K. M., Kessler, N. P., Nelson, E. A., Shoemaker, C. J., Schmaljohn, C. S., Polyak, S. J., & White, J. M. (2019). Arbidol and Other Low-Molecular-Weight Drugs That Inhibit Lassa and Ebola Viruses. *Journal of Virology*, *93*(8), e02185-18. https://doi.org/10.1128/JVI.02185-18

Huotari, J., & Helenius, A. (2011). Endosome maturation. *The EMBO Journal*, *30*(17), 3481–3500. https://doi.org/10.1038/emboj.2011.286

Jacob, S. T., Crozier, I., Fischer, W. A., Hewlett, A., Kraft, C. S., Vega, M.-A. de L., Soka, M. J., Wahl, V., Griffiths, A., Bollinger, L., & Kuhn, J. H. (2020). Ebola virus disease. *Nature Reviews Disease Primers*, *6*(1), 1–31. https://doi.org/10.1038/s41572-020-0147-3

Jae, L. T., Raaben, M., Herbert, A. S., Kuehne, A. I., Wirchnianski, A. S., Soh, T. K., Stubbs, S. H., Janssen, H., Damme, M., Saftig, P., Whelan, S. P., Dye, J. M., & Brummelkamp, T. R. (2014). Lassa virus entry requires a trigger-induced receptor switch. *Science (New York, N.Y.)*, *344*(6191), 1506–1510. https://doi.org/10.1126/science.1252480

Jahn, R., & Scheller, R. H. (2006). SNAREs—Engines for membrane fusion. *Nature Reviews Molecular Cell Biology*, *7*(9), 631–643. https://doi.org/10.1038/nrm2002

Jean-Alphonse, F., & Hanyaloglu, A. C. (2011). Regulation of GPCR signal networks via membrane trafficking. *Molecular and Cellular Endocrinology*, *331*(2), 205–214. https://doi.org/10.1016/j.mce.2010.07.010

Jeon, H., & Blacklow, S. C. (2005). Structure and physiologic function of the low-density lipoprotein receptor. *Annual Review of Biochemistry*, *74*, 535–562. https://doi.org/10.1146/annurev.biochem.74.082803.133354

Johannes, L., Parton, R. G., Bassereau, P., & Mayor, S. (2015). Building endocytic pits without clathrin. *Nature Reviews Molecular Cell Biology*, *16*(5), 311–321. https://doi.org/10.1038/nrm3968

Johannsdottir, H. K., Mancini, R., Kartenbeck, J., Amato, L., & Helenius, A. (2009). Host Cell Factors and Functions Involved in Vesicular Stomatitis Virus Entry. *Journal of Virology*, *83*(1), 440–453. https://doi.org/10.1128/JVI.01864-08

Johnson, D. E., Ai, H. W., Wong, P., Young, J. D., Campbell, R. E., & Casey, J. R. (2009). Red fluorescent protein pH biosensor to detect concentrative nucleoside transport. *Journal of Biological Chemistry*, *284*(31), 20499–20511. https://doi.org/10.1074/jbc.M109.019042

Johnson, D. E., Ostrowski, P., Jaumouillé, V., & Grinstein, S. (2016). The position of lysosomes within the cell determines their luminal pH. *The Journal of Cell Biology*, *212*(6), 677–692. https://doi.org/10.1083/jcb.201507112

Johnson, L. S., Dunn, K. W., Pytowski, B., & McGraw, T. E. (1993). Endosome acidification and receptor trafficking: Bafilomycin A1 slows receptor externalization by a mechanism involving the receptor's internalization motif. *Molecular Biology of the Cell*, *4*(12), 1251–1266. https://doi.org/10.1091/mbc.4.12.1251

Kaksonen, M., & Roux, A. (2018). Mechanisms of clathrin-mediated endocytosis. *Nature Reviews Molecular Cell Biology*, *19*(5), 313–326. https://doi.org/10.1038/nrm.2017.132

Kalaidzidis, I., Miaczynska, M., Brewińska-Olchowik, M., Hupalowska, A., Ferguson, C., Parton, R. G., Kalaidzidis, Y., & Zerial, M. (2015). APPL endosomes are not obligatory endocytic intermediates but act as stable cargo-sorting compartments. *The Journal of Cell Biology*, *211*(1), 123–144. https://doi.org/10.1083/jcb.201311117

Kamentseva, R., Kosheverova, V., Kharchenko, M., Zlobina, M., Salova, A., Belyaeva, T., Nikolsky, N., & Kornilova, E. (2020). Functional cycle of EEA1-positive early endosome: Direct evidence for pre-existing compartment of degradative pathway. *PloS One*, *15*(5), e0232532. https://doi.org/10.1371/journal.pone.0232532

Kang, Y.-L., Chou, Y.-Y., Rothlauf, P. W., Liu, Z., Soh, T. K., Cureton, D., Case, J. B., Chen, R. E., Diamond, M. S., Whelan, S. P. J., & Kirchhausen, T. (2020). Inhibition of PIKfyve kinase prevents infection by Zaire ebolavirus and SARS-CoV-2. *Proceedings of the National Academy of Sciences of the United States of America*, *117*(34), 20803–20813. https://doi.org/10.1073/pnas.2007837117

Kartenbeck, J., Schmid, E., Müller, H., & Franke, W. W. (1981). Immunological identification and localization of clathrin and coated vesicles in cultured cells and in tissues. *Experimental Cell Research*, *133*(1), 191–211. https://doi.org/10.1016/0014-4827(81)90369-4

Kielian, M. C., Marsh, M., & Helenius, A. (1986). Kinetics of endosome acidification detected by mutant and wild-type Semliki Forest virus. *The EMBO Journal*, *5*(12), 3103–3109.

Kim, H., Ju, J., Lee, H. N., Chun, H., & Seong, J. (2021). Genetically Encoded Biosensors Based on Fluorescent Proteins. *Sensors (Basel, Switzerland)*, *21*(3), 795. https://doi.org/10.3390/s21030795

Kim, I. S., Jenni, S., Stanifer, M. L., Roth, E., Whelan, S. P. J., van Oijen, A. M., & Harrison, S. C. (2016). Mechanism of membrane fusion induced by vesicular stomatitis virus G protein. *Proceedings of the National Academy of Sciences*, *114*(1), E28–E36. https://doi.org/10.1073/pnas.1618883114

Klöpper, T. H., Kienle, N., Fasshauer, D., & Munro, S. (2012). Untangling the evolution of Rab G proteins: Implications of a comprehensive genomic analysis. *BMC Biology*, *10*, 71. https://doi.org/10.1186/1741-7007-10-71

Kobayashi, T., Stang, E., Fang, K. S., de Moerloose, P., Parton, R. G., & Gruenberg, J. (1998). A lipid associated with the antiphospholipid syndrome regulates endosome structure and function. *Nature*, *392*(6672), 193–197. https://doi.org/10.1038/32440

Kolter, T., & Sandhoff, K. (2010). Lysosomal degradation of membrane lipids. *FEBS Letters*, *584*(9), 1700–1712. https://doi.org/10.1016/j.febslet.2009.10.021

Kozlovsky, Y., Chernomordik, L. V., & Kozlov, M. M. (2002). Lipid Intermediates in Membrane Fusion: Formation, Structure, and Decay of Hemifusion Diaphragm. *Biophysical Journal*, *83*(5), 2634–2651. https://doi.org/10.1016/S0006-3495(02)75274-0

Kuhn, J. H. (2021). Virus Taxonomy. *Encyclopedia of Virology*, 28–37. https://doi.org/10.1016/B978-0-12-809633-8.21231-4

Kunz, S., Edelmann, K. H., de la Torre, J.-C., Gorney, R., & Oldstone, M. B. A. (2003). Mechanisms for lymphocytic choriomeningitis virus glycoprotein cleavage, transport, and incorporation into virions. *Virology*, *314*(1), 168–178. https://doi.org/10.1016/S0042-6822(03)00421-5

Lafourcade, C., Sobo, K., Kieffer-Jaquinod, S., Garin, J., & van der Goot, F. G. (2008). Regulation of the V-ATPase along the Endocytic Pathway Occurs through Reversible Subunit Association and Membrane Localization. *PLoS ONE*, *3*(7), e2758. https://doi.org/10.1371/journal.pone.0002758

Lakadamyali, M., Rust, M. J., Babcock, H. P., & Zhuang, X. (2003). Visualizing infection of individual influenza viruses. *Proceedings of the National Academy of Sciences*, *100*(16), 9280–9285. https://doi.org/10.1073/pnas.0832269100

Lakadamyali, M., Rust, M. J., & Zhuang, X. (2006). Ligands for clathrin-mediated endocytosis are differentially sorted into distinct populations of early endosomes. *Cell*, *124*(5), 997–1009. https://doi.org/10.1016/j.cell.2005.12.038

Le Blanc, I., Luyet, P.-P., Pons, V., Ferguson, C., Emans, N., Petiot, A., Mayran, N., Demaurex, N., Fauré, J., Sadoul, R., Parton, R. G., & Gruenberg, J. (2005). Endosome-to-cytosol transport of viral nucleocapsids. *Nature Cell Biology*, *7*(7), 653–664. https://doi.org/10.1038/ncb1269

Lee, J., Nyenhuis, D. A., Nelson, E. A., Cafiso, D. S., White, J. M., & Tamm, L. K. (2017). Structure of the Ebola virus envelope protein MPER/TM domain and its interaction with the fusion loop explains their fusion activity. *Proceedings of the National Academy of Sciences*, 201708052. https://doi.org/10.1073/pnas.1708052114

Lee, R. J., Wang, S., & Low, P. S. (1996). Measurement of endosome pH following folate receptor-mediated endocytosis. *Biochimica Et Biophysica Acta*, *1312*(3), 237–242. https://doi.org/10.1016/0167-4889(96)00041-9

Lees, J. A., Li, P., Kumar, N., Weisman, L. S., & Reinisch, K. M. (2020). Insights into Lysosomal PI(3,5)P2 Homeostasis from a Structural-Biochemical Analysis of the PIKfyve Lipid Kinase Complex. *Molecular Cell*, *80*(4), 736-743.e4. https://doi.org/10.1016/j.molcel.2020.10.003

Li, X., Saha, P., Li, J., Blobel, G., & Pfeffer, S. R. (2016). Clues to the mechanism of cholesterol transfer from the structure of NPC1 middle lumenal domain bound to NPC2. *Proceedings of the National Academy of Sciences*, *18*, 201611956. https://doi.org/10.1073/pnas.1611956113

Li, Y., & Tamm, L. K. (2007). Structure and plasticity of the human immunodeficiency virus gp41 fusion domain in lipid micelles and bilayers. *Biophysical Journal*, *93*(3), 876–885. https://doi.org/10.1529/biophysj.106.102335

Liese, S., Wenzel, E. M., Kjos, I., Molina, R. R., Schultz, S. W., Brech, A., Stenmark, H., Raiborg, C., & Carlson, A. (2020). Protein crowding mediates membrane remodeling in upstream ESCRT-induced formation of intraluminal vesicles. *Proceedings of the National Academy of Sciences*, *117*(46), 28614–28624. https://doi.org/10.1073/pnas.2014228117

Linders, P. T. A., Ioannidis, M., Ter Beest, M., & van den Bogaart, G. (2022). Fluorescence Lifetime Imaging of pH along the Secretory Pathway. *ACS Chemical Biology*, *17*(1), 240–251. https://doi.org/10.1021/acschembio.1c00907

Liu, G., Cao, W., Salawudeen, A., Zhu, W., Emeterio, K., Safronetz, D., & Banadyga, L. (2021). Vesicular Stomatitis Virus: From Agricultural Pathogen to Vaccine Vector. *Pathogens*, *10*(9), 1092. https://doi.org/10.3390/pathogens10091092

Lorent, J. H., Diaz-Rohrer, B., Lin, X., Spring, K., Gorfe, A. A., Levental, K. R., & Levental, I. (2017). Structural determinants and functional consequences of protein affinity for membrane rafts. *Nature Communications*, *8*, 1219. https://doi.org/10.1038/s41467-017-01328-3

Lorieau, J. L., Louis, J. M., Schwieters, C. D., & Bax, A. (2012). PH-triggered, activated-state conformations of the influenza hemagglutinin fusion peptide revealed by NMR. *Proceedings of the National Academy of Sciences*, *109*(49), 19994–19999. https://doi.org/10.1073/pnas.1213801109

Louten, J. (2016). Virus Structure and Classification. *Essential Human Virology*, 19–29. https://doi.org/10.1016/B978-0-12-800947-5.00002-8

Lozach, P.-Y., Huotari, J., & Helenius, A. (2011). Late-penetrating viruses. *Current Opinion in Virology*, *1*(1), 35–43. https://doi.org/10.1016/j.coviro.2011.05.004

Lucas, M., Gershlick, D. C., Vidaurrazaga, A., Rojas, A. L., Bonifacino, J. S., & Hierro, A. (2016). Structural Mechanism for Cargo Recognition by the Retromer Complex. *Cell*, *167*(6), 1623-1635.e14. https://doi.org/10.1016/j.cell.2016.10.056

Lürick, A., Gao, J., Kuhlee, A., Yavavli, E., Langemeyer, L., Perz, A., Raunser, S., & Ungermann, C. (2017). Multivalent Rab interactions determine tether-mediated membrane fusion. *Molecular Biology of the Cell*, *28*(2), 322–332. https://doi.org/10.1091/mbc.E16-11-0764

Luzio, J. P., Hackmann, Y., Dieckmann, N. M. G., & Griffiths, G. M. (2014). The Biogenesis of Lysosomes and Lysosome-Related Organelles. *Cold Spring Harbor Perspectives in Biology*, *6*(9), a016840. https://doi.org/10.1101/cshperspect.a016840

Ma, L., Ouyang, Q., Werthmann, G. C., Thompson, H. M., & Morrow, E. M. (2017). Live-cell Microscopy and Fluorescence-based Measurement of Luminal pH in Intracellular Organelles. *Frontiers in Cell and Developmental Biology*, *5*, 71. https://doi.org/10.3389/fcell.2017.00071

Macías-Vidal, J., Girós, M., Guerrero, M., Gascón, P., Serratosa, J., Bachs, O., & Coll, M. J. (2014). The proteasome inhibitor bortezomib reduced cholesterol accumulation in fibroblasts from Niemann-Pick type C patients carrying missense mutations. *The FEBS Journal*, *281*(19), 4450–4466. https://doi.org/10.1111/febs.12954

Maeda, T., & Ohnishi, S. (1980). Activation of influenza virus by acidic media causes hemolysis and fusion of erythrocytes. *FEBS Letters*, *122*(2), 283–287. https://doi.org/10.1016/0014-5793(80)80457-1

Mahon, M. J. (2011). pHluorin2: An enhanced, ratiometric, pH-sensitive green florescent protein. *Advances in Bioscience and Biotechnology (Print)*, *2*(3), 132–137. https://doi.org/10.4236/abb.2011.23021

Mao, X., Kikani, C. K., Riojas, R. A., Langlais, P., Wang, L., Ramos, F. J., Fang, Q., Christ-Roberts, C. Y., Hong, J. Y., Kim, R.-Y., Liu, F., & Dong, L. Q. (2006). APPL1 binds to adiponectin receptors and mediates adiponectin signalling and function. *Nature Cell Biology*, *8*(5), 516–523. https://doi.org/10.1038/ncb1404

Markosyan, R. M., Cohen, F. S., & Melikyan, G. B. (2005). Time-resolved Imaging of HIV-1 Env-mediated Lipid and Content Mixing between a Single Virion and Cell Membrane. *Molecular Biology of the Cell*, *16*(12), 5502–5513. https://doi.org/10.1091/mbc.E05-06-0496

Martynov, V. I., Pakhomov, A. A., Deyev, I. E., & Petrenko, A. G. (2018). Genetically encoded fluorescent indicators for live cell pH imaging. *Biochimica et Biophysica Acta (BBA) - General Subjects*, *1862*(12), 2924–2939. https://doi.org/10.1016/j.bbagen.2018.09.013

Matlashov, M. E., Shcherbakova, D. M., Alvelid, J., Baloban, M., Pennacchietti, F., Shemetov, A. A., Testa, I., & Verkhusha, V. V. (2020). A set of monomeric near-infrared fluorescent proteins for multicolor imaging across scales. *Nature Communications*, *11*(1), 239. https://doi.org/10.1038/s41467-019-13897-6

Matos, P. M., Marin, M., Ahn, B., Lam, W., Santos, N. C., & Melikyan, G. B. (2013). Anionic lipids are required for vesicular stomatitis virus G protein-mediated single particle fusion with supported lipid bilayers. *The Journal of Biological Chemistry*, *288*(18), 12416–12425. https://doi.org/10.1074/jbc.M113.462028

Matsumoto, N., & Nakanishi-Matsui, M. (2019). Proton pumping V-ATPase inhibitor bafilomycin A1 affects Rab7 lysosomal localization and abolishes anterograde trafficking of osteoclast secretory lysosomes. *Biochemical and Biophysical Research Communications*, *510*(3), 421–426. https://doi.org/10.1016/j.bbrc.2019.01.118

Mayor, S., Presley, J., & Maxfield, F. R. (1993). Sorting of membrane components from endosomes and subsequent recycling to the cell surface occurs by a bulk flow process. *The Journal of Cell Biology*, *121*(6), 1257–1269.

McNally, K. E., Faulkner, R., Steinberg, F., Gallon, M., Ghai, R., Pim, D., Langton, P., Pearson, N., Danson, C. M., Nägele, H., Morris, L. L., Singla, A., Overlee, B. L., Heesom, K. J., Sessions, R., Banks, L., Collins, B. M., Berger, I., Billadeau, D. D., … Cullen, P. J. (2017). Retriever is a multiprotein complex for retromer-independent endosomal cargo recycling. *Nature Cell Biology*, *19*(10), 1214–1225. https://doi.org/10.1038/ncb3610

Melikyan, G. B., Barnard, R. J. O., Abrahamyan, L. G., Mothes, W., & Young, J. A. T. (2005). Imaging individual retroviral fusion events: From hemifusion to pore formation and growth. *Proceedings of the National Academy of Sciences of the United States of America*, *102*(24), 8728–8733. https://doi.org/10.1073/pnas.0501864102

Mellman, I. (1996). Endocytosis and molecular sorting. *Annual Review of Cell and Developmental Biology*, *12*, 575–625. https://doi.org/10.1146/annurev.cellbio.12.1.575

Melo, M. N., Sousa, F. J. R., Carneiro, F. A., Castanho, M. A. R. B., Valente, A. P., Almeida, F. C. L., Da Poian, A. T., & Mohana-Borges, R. (2009). Interaction of the Dengue virus fusion peptide with membranes assessed by NMR: The essential role of the envelope protein Trp101 for membrane fusion. *Journal of Molecular Biology*, *392*(3), 736–746. https://doi.org/10.1016/j.jmb.2009.07.035

Mendes, Y. S., Alves, N. S., Souza, T. L. F., Sousa, I. P., Bianconi, M. L., Bernardi, R. C., Pascutti, P. G., Silva, J. L., Gomes, A. M. O., & Oliveira, A. C. (2012). The structural dynamics of the flavivirus fusion peptide-membrane interaction. *PloS One*, *7*(10), e47596. https://doi.org/10.1371/journal.pone.0047596

Mercer, J., & Helenius, A. (2009). Virus entry by macropinocytosis. *Nature Cell Biology*, *11*(5), 510–520. https://doi.org/10.1038/ncb0509-510

Miaczynska, M., Christoforidis, S., Giner, A., Shevchenko, A., Uttenweiler-Joseph, S., Habermann, B., Wilm, M., Parton, R. G., & Zerial, M. (2004). APPL proteins link Rab5 to nuclear signal transduction via an endosomal compartment. *Cell*, *116*(3), 445–456. https://doi.org/10.1016/s0092-8674(04)00117-5

Miesenböck, G., De Angelis, D. A., & Rothman, J. E. (1998). Visualizing secretion and synaptic transmission with pH-sensitive green fluorescent proteins. *Nature*, *394*(6689), 192–195. https://doi.org/10.1038/28190

Miller, E. H., Obernosterer, G., Raaben, M., Herbert, A. S., Deffieu, M. S., Krishnan, A., Ndungo, E., Sandesara, R. G., Carette, J. E., Kuehne, A. I., Ruthel, G., Pfeffer, S. R., Dye, J. M., Whelan, S. P., Brummelkamp, T. R., & Chandran, K. (2012). Ebola virus entry requires the host-programmed recognition of an intracellular receptor. *The EMBO Journal*, *31*(8), 1947–1960. https://doi.org/10.1038/emboj.2012.53

Mima, J., Hickey, C. M., Xu, H., Jun, Y., & Wickner, W. (2008). Reconstituted membrane fusion requires regulatory lipids, SNAREs and synergistic SNARE chaperones. *The EMBO Journal*, *27*(15), 2031–2042. https://doi.org/10.1038/emboj.2008.139

Mingo, R. M., Simmons, J. a, Shoemaker, C. J., Nelson, E. a, Schornberg, K. L., D'Souza, R. S., Casanova, J. E., & White, J. M. (2015). Ebola virus and severe acute respiratory syndrome coronavirus display late cell entry kinetics: Evidence that transport to NPC1+ endolysosomes is a rate-defining step. *Journal of Virology*, *89*(5), 2931–2943. https://doi.org/10.1128/JVI.03398-14

Mittler, E., Alkutkar, T., Jangra, R. K., & Chandran, K. (2021). Direct Intracellular Visualization of Ebola Virus-Receptor Interaction by In Situ Proximity Ligation. *MBio*, *12*(1), e03100-20. https://doi.org/10.1128/mBio.03100-20

Miyauchi, K., Marin, M., & Melikyan, G. B. (2011). Visualization of retrovirus uptake and delivery into acidic endosomes. *The Biochemical Journal*, *434*(3), 559–569. https://doi.org/10.1042/BJ20101588

Mukherjee, S., Hung, S.-T., Douglas, N., Manna, P., Thomas, C., Ekrem, A., Palmer, A. E., & Jimenez, R. (2020). Engineering of a Brighter Variant of the FusionRed Fluorescent Protein Using Lifetime Flow Cytometry and Structure-Guided Mutations. *Biochemistry*, *59*(39), 3669–3682. https://doi.org/10.1021/acs.biochem.0c00484

Mukherjee, S., Soe, T. T., & Maxfield, F. R. (1999). Endocytic sorting of lipid analogues differing solely in the chemistry of their hydrophobic tails. *The Journal of Cell Biology*, *144*(6), 1271–1284. https://doi.org/10.1083/jcb.144.6.1271

Müller, M., Gerndt, S., Chao, Y.-K., Zisis, T., Nguyen, O. N. P., Gerwien, A., Urban, N., Müller, C., Gegenfurtner, F. A., Geisslinger, F., Ortler, C., Chen, C.-C., Zahler, S., Biel, M., Schaefer, M., Grimm, C., Bracher, F., Vollmar, A. M., & Bartel, K. (2021). Gene editing and synthetically accessible inhibitors reveal role for TPC2 in HCC cell proliferation and tumor growth. *Cell Chemical Biology*, *28*(8), 1119-1131.e27. https://doi.org/10.1016/j.chembiol.2021.01.023

Mundy, D. I., Li, W. P., Luby-Phelps, K., & Anderson, R. G. W. (2012). Caveolin targeting to late endosome/lysosomal membranes is induced by perturbations of lysosomal pH and cholesterol content. *Molecular Biology of the Cell*, *23*(5), 864–880. https://doi.org/10.1091/mbc.E11-07-0598

Nanbo, A., Imai, M., Watanabe, S., Noda, T., Takahashi, K., Neumann, G., Halfmann, P., & Kawaoka, Y. (2010). Ebolavirus Is Internalized into Host Cells via Macropinocytosis in a Viral Glycoprotein-Dependent Manner. *PLOS Pathogens*, *6*(9), e1001121. https://doi.org/10.1371/journal.ppat.1001121

Narayan, S., Barnard, R. J. O., & Young, J. A. T. (2003). Two Retroviral Entry Pathways Distinguished by Lipid Raft Association of the Viral Receptor and Differences in Viral Infectivity. *Journal of Virology*, *77*(3), 1977–1983. https://doi.org/10.1128/JVI.77.3.1977-1983.2003

Nathan, L., Lai, A., Millet, J., Straus, M., Whittaker, G. R., Freed, J. H., & Daniel, S. (2019). Calcium ions directly interact with the Ebola virus fusion peptide to promote structure-function changes that enhance infection. *ACS Infectious Diseases*. https://doi.org/10.1021/acsinfecdis.9b00296

Nelson, E. A., Dyall, J., Hoenen, T., Barnes, A. B., Zhou, H., Liang, J. Y., Michelotti, J., Dewey, W. H., Dewald, E., Bennett, R. S., Morris, P. J., Guha, R., Klumpp-, C., Mcknight, C., Chen, Y., Xu, X., Wang, A., Hughes, E., Martin, S., … White, J. M. (2017). *The phosphatidylinositol-3-phosphate 5-kinase inhibitor apilimod blocks filoviral entry and infection*. 1–22. https://doi.org/10.1371/journal.pntd.0005540

Nilsson, C., Kågedal, K., Johansson, U., & Öllinger, K. (2004). Analysis of cytosolic and lysosomal pH in apoptotic cells by flow cytometry. *Methods in Cell Science*, *25*(3), 185–194. https://doi.org/10.1007/s11022-004-8228-3

Nour, A. M., Li, Y., Wolenski, J., & Modis, Y. (2013). Viral membrane fusion and nucleocapsid delivery into the cytoplasm are distinct events in some flaviviruses. *PLoS Pathogens*, *9*(9), e1003585. https://doi.org/10.1371/journal.ppat.1003585

Novikoff, A. B., Beaufay, H., & de Duve, C. (1956). Electron Microscopy of Lysosome-Rich Fractions From Rat Liver. *The Journal of Biophysical and Biochemical Cytology*, *2*(4), 179–184.

Ohkuma, S., & Poole, B. (1978). Fluorescence probe measurement of the intralysosomal pH in living cells and the perturbation of pH by various agents. *Proceedings of the National Academy of Sciences of the United States of America*, *75*(7), 3327–3331. https://doi.org/10.1073/pnas.75.7.3327

Oppliger, J., Torriani, G., Herrador, A., & Kunz, S. (2016). Lassa Virus Cell Entry via Dystroglycan Involves an Unusual Pathway of Macropinocytosis. *Journal of Virology*, *90*(14), 6412–6429. https://doi.org/10.1128/JVI.00257-16

Otterstrom, J. J., Brandenburg, B., Koldijk, M. H., Juraszek, J., Tang, C., Mashaghi, S., Kwaks, T., Goudsmit, J., Vogels, R., Friesen, R. H. E., & van Oijen, A. M. (2014). Relating influenza virus membrane fusion kinetics to stoichiometry of neutralizing antibodies at the single-particle level. *Proceedings of the National Academy of Sciences of the United States of America*, *111*(29), E5143-8. https://doi.org/10.1073/pnas.1411755111

Owczarek, K., Chykunova, Y., Jassoy, C., Maksym, B., Rajfur, Z., & Pyrc, K. (2019). Zika virus: Mapping and reprogramming the entry. *Cell Communication and Signaling*, *17*(1), 41. https://doi.org/10.1186/s12964-019-0349-z

Padilla-Parra, S., Matos, P. M., Kondo, N., Marin, M., Santos, N. C., & Melikyan, G. B. (2012). Quantitative imaging of endosome acidification and single retrovirus fusion with distinct pools of early endosomes. *Proceedings of the National Academy of Sciences*, *109*(43), 17627–17632. https://doi.org/10.1073/pnas.1211714109

Parton, R. G., & Simons, K. (2007). The multiple faces of caveolae. *Nature Reviews Molecular Cell Biology*, *8*(3), 185–194. https://doi.org/10.1038/nrm2122

Pasqual, G., Rojek, J. M., Masin, M., Chatton, J.-Y., & Kunz, S. (2011). Old World Arenaviruses Enter the Host Cell via the Multivesicular Body and Depend on the Endosomal Sorting Complex Required for Transport. *PLOS Pathogens*, *7*(9), e1002232. https://doi.org/10.1371/journal.ppat.1002232

Perini, E. D., Schaefer, R., Stöter, M., Kalaidzidis, Y., & Zerial, M. (2014). Mammalian CORVET Is Required for Fusion and Conversion of Distinct Early Endosome Subpopulations. *Traffic*, *15*(12), 1366–1389. https://doi.org/10.1111/tra.12232

Perreira, J. M., Chin, C. R., Feeley, E. M., & Brass, A. L. (2013). IFITMs Restrict the Replication of Multiple Pathogenic Viruses. *Journal of Molecular Biology*, *425*(24), 4937–4955. https://doi.org/10.1016/j.jmb.2013.09.024

Perrin, P., Janssen, L., Janssen, H., Broek, B. van den, Voortman, L. M., Elsland, D. van, Berlin, I., & Neefjes, J. (2021). Retrofusion of intralumenal MVB membranes parallels viral infection and coexists with exosome release. *Current Biology*, *31*(17), 3884-3893.e4. https://doi.org/10.1016/j.cub.2021.06.022

Petershans, A., Wedlich, D., & Fruk, L. (2011). Bioconjugation of CdSe/ZnS nanoparticles with SNAP tagged proteins. *Chemical Communications (Cambridge, England)*, *47*(38), 10671–10673. https://doi.org/10.1039/c1cc12874d

Pitt, S. J., Funnell, T. M., Sitsapesan, M., Venturi, E., Rietdorf, K., Ruas, M., Ganesan, A., Gosain, R., Churchill, G. C., Zhu, M. X., Parrington, J., Galione, A., & Sitsapesan, R. (2010). TPC2 is a novel NAADP-sensitive Ca2+ release channel, operating as a dual sensor of luminal pH and Ca2+. *Journal of Biological Chemistry*, *285*(45), 35039–35046. https://doi.org/10.1074/jbc.M110.156927

Poston, D., Weisblum, Y., Hobbs, A., & Bieniasz, P. D. (2021). VPS29 exerts opposing effects on endocytic viral entry. *BioRxiv*, 2021.08.06.455441. https://doi.org/10.1101/2021.08.06.455441

Qian, H., Sheetz, M. P., & Elson, E. L. (1991). Single particle tracking. Analysis of diffusion and flow in two-dimensional systems. *Biophysical Journal*, *60*(4), 910–921.

Qiu, S., Leung, A., Bo, Y., Kozak, R. A., Anand, S. P., Warkentin, C., Salambanga, F. D. R., Cui, J., Kobinger, G., Kobasa, D., & Côté, M. (2018). Ebola virus requires phosphatidylinositol (3,5) bisphosphate production for efficient viral entry. *Virology*, *513*, 17–28. https://doi.org/10.1016/j.virol.2017.09.028

Quinn, S. E., Huang, L., Kerkvliet, J. G., Swanson, J. A., Smith, S., Hoppe, A. D., Anderson, R. B., Thiex, N. W., & Scott, B. L. (2021). The structural dynamics of macropinosome formation and PI3-kinase-mediated sealing revealed by lattice light sheet microscopy. *Nature Communications*, *12*(1), 4838. https://doi.org/10.1038/s41467-021-25187-1

Quirin, K., Eschli, B., Scheu, I., Poort, L., Kartenbeck, J., & Helenius, A. (2008). Lymphocytic choriomeningitis virus uses a novel endocytic pathway for infectious entry via late endosomes. *Virology*, *378*(1), 21–33. https://doi.org/10.1016/j.virol.2008.04.046

Remec Pavlin, M., & Hurley, J. H. (2020). The ESCRTs – converging on mechanism. *Journal of Cell Science*, *133*(18). https://doi.org/10.1242/jcs.240333

Rheinemann, L., & Sundquist, W. I. (2021). Virus Budding. *Encyclopedia of Virology*, 519–528. https://doi.org/10.1016/B978-0-12-814515-9.00023-0

Richard, A. S., Zhang, A., Park, S.-J., Farzan, M., Zong, M., & Choe, H. (2015). Virion-associated phosphatidylethanolamine promotes TIM1-mediated infection by Ebola, dengue, and West Nile viruses. *Proceedings of the National Academy of Sciences of the United States of America*, *112*(47), 14682–14687. https://doi.org/10.1073/pnas.1508095112

Rink, J., Ghigo, E., Kalaidzidis, Y., & Zerial, M. (2005). Rab Conversion as a Mechanism of Progression from Early to Late Endosomes. *Cell*, *122*(5), 735–749. https://doi.org/10.1016/j.cell.2005.06.043

Rinkenberger, N., & Schoggins, J. W. (2018). Mucolipin-2 Cation Channel Increases Trafficking Efficiency of Endocytosed Viruses. *MBio*. https://doi.org/10.1128/mBio.02314-17

Rivera-Molina, F. E., & Novick, P. J. (2009). A Rab GAP cascade defines the boundary between two Rab GTPases on the secretory pathway. *Proceedings of the National Academy of Sciences*, *106*(34), 14408–14413. https://doi.org/10.1073/pnas.0906536106

Roby, J. A., Setoh, Y. X., Hall, R. A., & Khromykh, A. A. (2015). Post-translational regulation and modifications of flavivirus structural proteins. *The Journal of General Virology*, *96*(Pt 7), 1551–1569. https://doi.org/10.1099/vir.0.000097

Roche, S., Bressanelli, S., Rey, F. A., & Gaudin, Y. (2006). Crystal Structure of the Low-pH Form of the Vesicular Stomatitis Virus Glycoprotein G. *Science*, *313*(5784), 187–191. https://doi.org/10.1126/science.1127683

Roche, S., Rey, F. A., Gaudin, Y., & Bressanelli, S. (2007). Structure of the Prefusion Form of the Vesicular Stomatitis Virus Glycoprotein G. *Science*, *315*(5813), 843–848. https://doi.org/10.1126/science.1135710

Rohrer, J., Schweizer, A., Russell, D., & Kornfeld, S. (1996). The targeting of lamp1 to lysosomes is dependent on the spacing of its cytoplasmic tail tyrosine sorting motif relative to the membrane. *Journal of Cell Biology*, *132*(4), 565–576. https://doi.org/10.1083/jcb.132.4.565

Rojek, J. M., Perez, M., & Kunz, S. (2008a). Cellular Entry of Lymphocytic Choriomeningitis Virus. *Journal of Virology*, *82*(3), 1505–1517. https://doi.org/10.1128/JVI.01331-07

Rojek, J. M., Perez, M., & Kunz, S. (2008b). Cellular Entry of Lymphocytic Choriomeningitis Virus. *Journal of Virology*, *82*(3), 1505–1517. https://doi.org/10.1128/JVI.01331-07

Roth, S. L., & Whittaker, G. R. (2011). Promotion of vesicular stomatitis virus fusion by the endosome-specific phospholipid bis(monoacylglycero)phosphate (BMP). *FEBS Letters*, *585*(6), 865–869. https://doi.org/10.1016/j.febslet.2011.02.015

Ruas, M., Chuang, K.-T., Davis, L. C., Al-Douri, A., Tynan, P. W., Tunn, R., Teboul, L., Galione, A., & Parrington, J. (2014). TPC1 has two variant isoforms, and their removal has different effects on endo-lysosomal functions compared to loss of TPC2. *Molecular and Cellular Biology*, *34*(21), 3981–3992. https://doi.org/10.1128/MCB.00113-14

Rupprecht, C. E., & Bleck, T. P. (1997). Rhabdoviruses. In *Clinical virology* (pp. 879–897). Churchill Livingstone.

Saeed, M. F., Kolokoltsov, A. A., Albrecht, T., & Davey, R. A. (2010). Cellular Entry of Ebola Virus Involves Uptake by a Macropinocytosis-Like Mechanism and Subsequent Trafficking through Early and Late Endosomes. *PLOS Pathogens*, *6*(9), e1001110. https://doi.org/10.1371/journal.ppat.1001110

Saeed, M. F., Kolokoltsov, A. A., & Davey, R. A. (2006). Novel, rapid assay for measuring entry of diverse enveloped viruses, including HIV and rabies. *Journal of Virological Methods*, *135*(2), 143–150. https://doi.org/10.1016/j.jviromet.2006.02.011

Sakurai, Y., Kolokoltsov, A. A., Chen, C., Tidwell, M. W., Bauta, W. E., Klugbauer, N., Grimm, C., Wahl-schott, C., Biel, M., & Davey, R. A. (2015). Two-Pore Channels Control Ebola Virus Host Cell Entry and Are Drug Targets for Disease Treatment. *Science*, *347*(6225), 995–998.

Samie, M., Wang, X., Zhang, X., Goschka, A., Li, X., Cheng, X., Gregg, E., Azar, M., Zhuo, Y., Garrity, A. G., Gao, Q., Slaugenhaupt, S., Pickel, J., Zolov, S. N., Weisman, L. S., Lenk, G. M., Titus, S., Bryant-Genevier, M., Southall, N., … Xu, H. (2013). A TRP channel in the lysosome regulates large particle phagocytosis via focal exocytosis. *Developmental Cell*, *26*(5), 511–524. https://doi.org/10.1016/j.devcel.2013.08.003

Sankaranarayanan, S., De Angelis, D., Rothman, J. E., & Ryan, T. A. (2000). The Use of pHluorins for Optical Measurements of Presynaptic Activity. *Biophysical Journal*, *79*(4), 2199–2208. https://doi.org/10.1016/S0006-3495(00)76468-X

Sapoznik, E., Chang, B.-J., Huh, J., Ju, R. J., Azarova, E. V., Pohlkamp, T., Welf, E. S., Broadbent, D., Carisey, A. F., Stehbens, S. J., Lee, K.-M., Marín, A., Hanker, A. B., Schmidt, J. C., Arteaga, C. L., Yang, B., Kobayashi, Y., Tata, P. R., Kruithoff, R., … Fiolka, R. P. (2020). A versatile oblique plane microscope for large-scale and high-resolution imaging of subcellular dynamics. *ELife*, *9*, e57681. https://doi.org/10.7554/eLife.57681

Saxton, M. J., & Jacobson, K. (1997). SINGLE-PARTICLE TRACKING: Applications to Membrane Dynamics. *Annual Review of Biophysics & Biomolecular Structure*, *26*(1), 373. https://doi.org/10.1146/annurev.biophys.26.1.373

Sbrissa, D., Ikonomov, O. C., Fu, Z., Ijuin, T., Gruenberg, J., Takenawa, T., & Shisheva, A. (2007). Core protein machinery for mammalian phosphatidylinositol 3,5-bisphosphate synthesis and turnover that regulates the progression of endosomal transport. Novel Sac phosphatase joins the ArPIKfyve-PIKfyve complex. *The Journal of Biological Chemistry*, *282*(33), 23878–23891. https://doi.org/10.1074/jbc.M611678200

Schmid, S. L., Fuchs, R., Keilian, M., Helenius, A., & Mellman, I. (1989). Acidification of endosome subpopulations in wild-type Chinese hamster ovary cells and temperature-sensitive acidification-defective mutants. *The Journal of Cell Biology*, *108*(4), 1291–1300.

Schmid, S. L., Sorkin, A., & Zerial, M. (2014). Endocytosis: Past, Present, and Future. *Cold Spring Harbor Perspectives in Biology*, *6*(12), a022509. https://doi.org/10.1101/cshperspect.a022509

Schmiege, P., Fine, M., Blobel, G., & Li, X. (2017). Human TRPML1 channel structures in open and closed conformations. *Nature*. https://doi.org/10.1038/nature24036

Schneider, C., & Williams, J. G. (1985). Molecular Dissection of the Human Transferrin Receptor. *Journal of Cell Science*, *1985*(Supplement_3), 139–149. https://doi.org/10.1242/jcs.1985.Supplement_3.14

Schornberg, K., Matsuyama, S., Kabsch, K., Delos, S., Bouton, A., & White, J. (2006). Role of Endosomal Cathepsins in Entry Mediated by the Ebola Virus Glycoprotein Role of Endosomal Cathepsins in Entry Mediated by the Ebola Virus Glycoprotein. *Journal of Virology*, *80*(8), 4174–4178. https://doi.org/10.1128/JVI.80.8.4174

Scott, B. L., & Hoppe, A. D. (2015). Optimizing fluorescent protein trios for 3-Way FRET imaging of protein interactions in living cells. *Scientific Reports*, *5*, 1–13. https://doi.org/10.1038/srep10270

Sezgin, E., Levental, I., Mayor, S., & Eggeling, C. (2017). The mystery of membrane organization: Composition, regulation and physiological relevance of lipid rafts. *Nature Reviews. Molecular Cell Biology*, *18*(6), 361–374. https://doi.org/10.1038/nrm.2017.16

She, J., Guo, J., Chen, Q., Zeng, W., Jiang, Y., & Bai, X. (2018). Structural insights into the voltage and phospholipid activation of the mammalian TPC1 channel. *Nature*, *556*(7699), 130–134. https://doi.org/10.1038/nature26139

She, J., Zeng, W., Guo, J., Chen, Q., Bai, X.-C., & Jiang, Y. (2019). Structural mechanisms of phospholipid activation of the human TPC2 channel. *ELife*, *8*, e45222. https://doi.org/10.7554/eLife.45222

Shen, D., Wang, X., Li, X., Zhang, X., Yao, Z., Dibble, S., Dong, X., Yu, T., Lieberman, A. P., Showalter, H. D., & Xu, H. (2012). Lipid storage disorders block lysosomal trafficking by inhibiting a TRP channel and lysosomal calcium release. *Nature Communications*, *3*, 731. https://doi.org/10.1038/ncomms1735

Sherer, N. M., Lehmann, M. J., Jimenez-Soto, L. F., Ingmundson, A., Horner, S. M., Cicchetti, G., Allen, P. G., Pypaert, M., Cunningham, J. M., & Mothes, W. (2003). Visualization of Retroviral Replication in Living Cells Reveals Budding into Multivesicular Bodies: Retroviral Budding. *Traffic*, *4*(11), 785–801. https://doi.org/10.1034/j.1600-0854.2003.00135.x

Shewan, A., Eastburn, D. J., & Mostov, K. (2011). Phosphoinositides in Cell Architecture. *Cold Spring Harbor Perspectives in Biology*, *3*(8), a004796. https://doi.org/10.1101/cshperspect.a004796

Shoemaker, C. J., Schornberg, K. L., Delos, S. E., Scully, C., Pajouhesh, H., Olinger, G. G., Johansen, L. M., & White, J. M. (2013). Multiple Cationic Amphiphiles Induce a Niemann-Pick C Phenotype and Inhibit Ebola Virus Entry and Infection. *PLoS ONE*, *8*(2). https://doi.org/10.1371/journal.pone.0056265

Simmons, J. A., D'Souza, R. S., Ruas, M., Galione, A., Casanova, J. E., & White, J. M. (2016). Ebolavirus Glycoprotein Directs Fusion through NPC1 + Endolysosomes. *Journal of Virology*, *90*(1), 605–610. https://doi.org/10.1128/JVI.01828-15

Smith, E. C., Gregory, S. M., Tamm, L. K., Creamer, T. P., & Dutch, R. E. (2012). Role of sequence and structure of the Hendra fusion protein fusion peptide in membrane fusion. *The Journal of Biological Chemistry*, *287*(35), 30035–30048. https://doi.org/10.1074/jbc.M112.367862

Sood, C., Francis, A. C., Desai, T. M., & Melikyan, G. B. (2017). An improved labeling strategy enables automated detection of single-virus fusion and assessment of HIV-1 protease activity in single virions. *Journal of Biological Chemistry*, *292*, jbc.M117.818088. https://doi.org/10.1074/jbc.M117.818088

Soppina, V., Rai, A. K., Ramaiya, A. J., Barak, P., & Mallik, R. (2009). Tug-of-war between dissimilar teams of microtubule motors regulates transport and fission of endosomes. *Proceedings of the National Academy of Sciences of the United States of America*, *106*(46), 19381–19386. https://doi.org/10.1073/pnas.0906524106

Spence, J. S., He, R., Hoffmann, H.-H., Das, T., Thinon, E., Rice, C. M., Peng, T., Chandran, K., & Hang, H. C. (2019). IFITM3 directly engages and shuttles incoming virus particles to lysosomes. *Nature Chemical Biology*, 1. https://doi.org/10.1038/s41589-018-0213-2

Spence, J. S., Krause, T. B., Mittler, E., Jangra, R. K., & Chandran, K. (2016). *Direct Visualization of Ebola Virus Fusion Triggering in the Endocytic Pathway*. *7*(1), 1–12. https://doi.org/10.1128/mBio.01857-15.Invited

Srikantiah, P., Vora, P., & Klugman, K. P. (2021). Assessing the Full Burden of Respiratory Syncytial Virus in Young Infants in Low- and Middle-Income Countries: The Importance of Community Mortality Studies. *Clinical Infectious Diseases*, *73*(Supplement_3), S177–S179. https://doi.org/10.1093/cid/ciab486

Steinberg, B. E., Huynh, K. K., Brodovitch, A., Jabs, S., Stauber, T., Jentsch, T. J., & Grinstein, S. (2010). A cation counterflux supports lysosomal acidification. *Journal of Cell Biology*, *189*(7), 1171–1186. https://doi.org/10.1083/jcb.200911083

Stenbeck, G., & Horton, M. A. (2004). Endocytic trafficking in actively resorbing osteoclasts. *Journal of Cell Science*, *117*(Pt 6), 827–836. https://doi.org/10.1242/jcs.00935

Stroupe, C., Collins, K. M., Fratti, R. A., & Wickner, W. (2006). Purification of active HOPS complex reveals its affinities for phosphoinositides and the SNARE Vam7p. *The EMBO Journal*, *25*(8), 1579–1589. https://doi.org/10.1038/sj.emboj.7601051

Stroupe, C., Hickey, C. M., Mima, J., Burfeind, A. S., & Wickner, W. (2009). Minimal membrane docking requirements revealed by reconstitution of Rab GTPase-dependent membrane fusion from purified components. *Proceedings of the National Academy of Sciences of the United States of America*, *106*(42), 17626–17633. https://doi.org/10.1073/pnas.0903801106

Suddala, K. C., Lee, C. C., Meraner, P., Marin, M., Markosyan, R. M., Desai, T. M., Cohen, F. S., Brass, A. L., & Melikyan, G. B. (2019). Interferon-induced transmembrane protein 3 blocks fusion of sensitive but not resistant viruses by partitioning into virus-carrying endosomes. *PLOS Pathogens*, *15*(1), e1007532. https://doi.org/10.1371/journal.ppat.1007532

Sun, E., He, J., & Zhuang, X. (2013). Live cell imaging of viral entry. *Current Opinion in Virology*, *3*(1), 34–43. https://doi.org/10.1016/j.coviro.2013.01.005

Sun, F., Xia, Z., Han, Y., Gao, M., Wang, L., Wu, Y., Sabatier, J.-M., Miao, L., & Cao, Z. (2020). Topology, Antiviral Functional Residues and Mechanism of IFITM1. *Viruses*, *12*(3). https://doi.org/10.3390/v12030295

Sun, X., Yau, V. K., Briggs, B. J., & Whittaker, G. R. (2005). Role of clathrin-mediated endocytosis during vesicular stomatitis virus entry into host cells. *Virology*, *338*(1), 53–60. https://doi.org/10.1016/j.virol.2005.05.006

Sun, X., Zeng, H., Kumar, A., Belser, J. A., Maines, T. R., & Tumpey, T. M. (2016). Constitutively Expressed IFITM3 Protein in Human Endothelial Cells Poses an Early Infection Block to Human Influenza Viruses. *Journal of Virology*, *90*(24), 11157–11167. https://doi.org/10.1128/JVI.01254-16

Superti, F., Seganti, L., Ruggeri, F. M., Tinari, A., Donelli, G., & Orsi, N. Y. 1987. (1987). Entry Pathway of Vesicular Stomatitis Virus into Different Host Cells. *Journal of General Virology*, *68*(2), 387–399. https://doi.org/10.1099/0022-1317-68-2-387

Suresh, B., Saminathan, A., Chakraborty, K., Zajac, M., Cui, C., Becker, L., & Krishnan, Y. (2021). Tubular lysosomes harbor active ion gradients and poise macrophages for phagocytosis. *Proceedings of the National Academy of Sciences of the United States of America*, *118*(41), e2113174118. https://doi.org/10.1073/pnas.2113174118

Tanida, I., Ueno, T., & Uchiyama, Y. (2014). A Super-Ecliptic, pHluorin-mKate2, Tandem Fluorescent Protein-Tagged Human LC3 for the Monitoring of Mammalian Autophagy. *PLOS ONE*, *9*(10), e110600. https://doi.org/10.1371/journal.pone.0110600

Tatulian, S. A., Hinterdorfer, P., Baber, G., & Tamm, L. K. (1995). Influenza hemagglutinin assumes a tilted conformation during membrane fusion as determined by attenuated total reflection FTIR spectroscopy. *The EMBO Journal*, *14*(22), 5514–5523.

Tinevez, J.-Y., Perry, N., Schindelin, J., Hoopes, G. M., Reynolds, G. D., Laplantine, E., Bednarek, S. Y., Shorte, S. L., & Eliceiri, K. W. (2017). TrackMate: An open and extensible platform for single-particle tracking. *Methods*, *115*, 80–90. https://doi.org/10.1016/j.ymeth.2016.09.016

Traub, L. M., & Bonifacino, J. S. (2013). Cargo Recognition in Clathrin-Mediated Endocytosis. *Cold Spring Harbor Perspectives in Biology*, *5*(11), a016790. https://doi.org/10.1101/cshperspect.a016790

Tycko, B., Keith, C. H., & Maxfield, F. R. (1983). Rapid acidification of endocytic vesicles containing asialoglycoprotein in cells of a human hepatoma line. *The Journal of Cell Biology*, *97*(6), 1762–1776.

Ukkonen, P., Lewis, V., Marsh, M., Helenius, A., & Mellman, I. (1986). Transport of macrophage Fc receptors and Fc receptor-bound ligands to lysosomes. *The Journal of Experimental Medicine*, *163*(4), 952–971.

Vasile, E., Simionescu, M., & Simionescu, N. (1983). Visualization of the binding, endocytosis, and transcytosis of low-density lipoprotein in the arterial endothelium in situ. *The Journal of Cell Biology*, *96*(6), 1677–1689. https://doi.org/10.1083/jcb.96.6.1677

Vela, E. M., Zhang, L., Colpitts, T. M., Davey, R. A., & Aronson, J. F. (2007). Arenavirus Entry Occurs Through a Cholesterol-Dependent, Non-Caveolar, Clathrin-Mediated Endocytic Mechanism. *Virology*, *369*(1), 1–11. https://doi.org/10.1016/j.virol.2007.07.014

Venkatachalam, K., Wong, C. O., & Zhu, M. X. (2015). The role of TRPMLs in endolysosomal trafficking and function. *Cell Calcium*, *58*(1), 48–56. https://doi.org/10.1016/j.ceca.2014.10.008

Volchkov, V. E., Feldmann, H., Volchkova, V. A., & Klenk, H. D. (1998). Processing of the Ebola virus glycoprotein by the proprotein convertase furin. *Proceedings of the National Academy of Sciences of the United States of America*, *95*(10), 5762–5767. https://doi.org/10.1073/pnas.95.10.5762

Vorselen, D., Barger, S. R., Wang, Y., Cai, W., Theriot, J. A., Gauthier, N. C., & Krendel, M. (2021). Phagocytic 'teeth' and myosin-II 'jaw' power target constriction during phagocytosis. *ELife*, *10*, e68627. https://doi.org/10.7554/eLife.68627

Wandinger-Ness, A., & Zerial, M. (2014). Rab Proteins and the Compatmentalization of the Endosomal System. *Cold Spring Harbor Perspectives in Biology*, *6*(11), a022616. https://doi.org/10.1101/cshperspect.a022616

Wang, C., Niederstrasser, H., Douglas, P. M., Lin, R., Jaramillo, J., Li, Y., Oswald, N. W., Zhou, A., McMillan, E. A., Mendiratta, S., Wang, Z., Zhao, T., Lin, Z., Luo, M., Huang, G., Brekken, R. A., Posner, B. A., MacMillan, J. B., Gao, J., & White, M. A. (2017). Small-molecule TFEB pathway agonists that ameliorate metabolic syndrome in mice and extend C. elegans lifespan. *Nature Communications*, *8*, 2270. https://doi.org/10.1038/s41467-017-02332-3

Wang, C., Wang, Y., Li, Y., Bodemann, B., Zhao, T., Ma, X., Huang, G., Hu, Z., Deberardinis, R. J., White, M. A., & Gao, J. (2015). A nanobuffer reporter library for fine-scale imaging and perturbation of endocytic organelles. *Nature Communications*, *6*, 1–11. https://doi.org/10.1038/ncomms9524

Wang, W., Gao, Q., Yang, M., Zhang, X., Yu, L., Lawas, M., Li, X., Bryant-Genevier, M., Southall, N. T., Marugan, J., Ferrer, M., & Xu, H. (2015). Up-regulation of lysosomal TRPML1 channels is essential for lysosomal adaptation to nutrient starvation. *Proceedings of the National Academy of Sciences*, 201419669. https://doi.org/10.1073/pnas.1419669112

Wang, X., Zhang, X., Dong, X.-P., Samie, M., Li, X., Cheng, X., Goschka, A., Shen, D., Zhou, Y., Harlow, J., Zhu, M. X., Clapham, D. E., Ren, D., & Xu, H. (2012). TPC proteins are phosphoinositide- activated sodium-selective ion channels in endosomes and lysosomes. *Cell*, *151*(2), 372–383. PubMed. https://doi.org/10.1016/j.cell.2012.08.036

Wang, Z.-G., Zhao, L., Chen, L.-L., Liu, H.-Y., Wang, L., Hu, Y., Shi, X.-H., Zhao, D., Liu, S.-L., & Pang, D.-W. (n.d.). Spatiotemporal Quantification of Endosomal Acidification on the Viral Journey. *Small*, 2104200. https://doi.org/10.1002/smll.202104200

Wang, Z.-G., Zhao, L., Chen, L.-L., Liu, H.-Y., Wang, L., Hu, Y., Shi, X.-H., Zhao, D., Liu, S.-L., & Pang, D.-W. (2022). Spatiotemporal Quantification of Endosomal Acidification on the Viral Journey. *Small*, *18*(2), 2104200. https://doi.org/10.1002/smll.202104200

Wassmer, T., Attar, N., Harterink, M., van Weering, J. R. T., Traer, C. J., Oakley, J., Goud, B., Stephens, D. J., Verkade, P., Korswagen, H. C., & Cullen, P. J. (2009). The Retromer Coat Complex Coordinates Endosomal Sorting and Dynein-Mediated Transport, with Carrier Recognition by the trans-Golgi Network. *Developmental Cell*, *17*(1), 110–122. https://doi.org/10.1016/j.devcel.2009.04.016

Watt, A., Moukambi, F., Banadyga, L., Groseth, A., Callison, J., Herwig, A., Ebihara, H., Feldmann, H., & Hoenen, T. (2014). A Novel Life Cycle Modeling System for Ebola Virus Shows a Genome Length-Dependent Role of VP24 in Virus Infectivity. *Journal of Virology*, *88*(18), 10511–10524. https://doi.org/10.1128/JVI.01272-14

Webb, B. A., Aloisio, F. M., Charafeddine, R. A., Cook, J., Wittmann, T., & Barber, D. L. (2021). pHLARE: A new biosensor reveals decreased lysosome pH in cancer cells. *Molecular Biology of the Cell*, *32*(2), 131–142. https://doi.org/10.1091/mbc.E20-06-0383

White, J., & Helenius, A. (1980). PH-dependent fusion between the Semliki Forest virus membrane and liposomes. *Proceedings of the National Academy of Sciences of the United States of America*, *77*(6), 3273–3277.

White, J., Kartenbeck, J., & Helenius, A. (1980). Fusion of Semliki forest virus with the plasma membrane can be induced by low pH. *The Journal of Cell Biology*, *87*(1), 264–272. https://doi.org/10.1083/jcb.87.1.264

White, J. M., Whittaker, G. R., Author, C., & White, J. M. (2016). *Fusion of Enveloped Viruses in Endosomes*. *19*, 593–614. https://doi.org/10.1111/tra.12389

White, J., Matlin, K., & Helenius, A. (1981). Cell fusion by Semliki Forest, influenza, and vesicular stomatitis viruses. *The Journal of Cell Biology*, *89*(3), 674–679. https://doi.org/10.1083/jcb.89.3.674

Wichner, S. M., Mann, V. R., Powers, A. S., Segal, M. A., Mir, M., Bandaria, J. N., DeWitt, M. A., Darzacq, X., Yildiz, A., & Cohen, B. E. (2017). Covalent Protein Labeling and Improved Single-Molecule Optical Properties of Aqueous CdSe/CdS Quantum Dots. *ACS Nano*, *11*(7), 6773–6781. https://doi.org/10.1021/acsnano.7b01470

Wollert, T., & Hurley, J. H. (2010). Molecular Mechanism of Multivesicular Body Biogenesis by ESCRT Complexes. *Nature*, *464*(7290), 864–869. https://doi.org/10.1038/nature08849

Wollert, T., Wunder, C., Lippincott-Schwartz, J., & Hurley, J. H. (2009). Membrane scission by the ESCRT-III complex. *Nature*, *458*(7235), 172–177. https://doi.org/10.1038/nature07836

Xia, L., Zhang, L.-J., Tang, H.-W., & Pang, D.-W. (2021). Revealing Microtubule-Dependent Slow-Directed Motility by Single-Particle Tracking. *Analytical Chemistry*, *93*(12), 5211–5217. https://doi.org/10.1021/acs.analchem.0c05377

Xia, Z., Wang, L., Li, S., Tang, W., Sun, F., Wu, Y., Miao, L., & Cao, Z. (2020). ML-SA1, a selective TRPML agonist, inhibits DENV2 and ZIKV by promoting lysosomal acidification and protease activity. *Antiviral Research*, *182*, 104922. https://doi.org/10.1016/j.antiviral.2020.104922

Xie, X., Brown, M. S., Shelton, J. M., Richardson, J. A., Goldstein, J. L., & Liang, G. (2011). Amino acid substitution in NPC1 that abolishes cholesterol binding reproduces phenotype of complete NPC1 deficiency in mice. *Proceedings of the National Academy of Sciences*, *108*(37), 15330–15335. https://doi.org/10.1073/pnas.1112751108

Yadati, T., Houben, T., Bitorina, A., & Shiri-Sverdlov, R. (2020). The Ins and Outs of Cathepsins: Physiological Function and Role in Disease Management. *Cells*, *9*(7), E1679. https://doi.org/10.3390/cells9071679

Yamada, E. (1955). The Fine Structure of the Gall Bladder Epithelium of the Mouse. *The Journal of Biophysical and Biochemical Cytology*, *1*(5), 445–458.

Yeager, M., Wilson-Kubalek, E. M., Weiner, S. G., Brown, P. O., & Rein, A. (1998). Supramolecular organization of immature and mature murine leukemia virus revealed by electron cryo-microscopy: Implications for retroviral assembly mechanisms. *Proceedings*

of the National Academy of Sciences of the United States of America, *95*(13), 7299–7304. https://doi.org/10.1073/pnas.95.13.7299.

Yoshimori, T., Yamamoto, A., Moriyama, Y., Futai, M., & Tashiro, Y. (1991). Bafilomycin A1, a specific inhibitor of vacuolar-type H(+)-ATPase, inhibits acidification and protein degradation in lysosomes of cultured cells. *The Journal of Biological Chemistry*, *266*(26), 17707–17712.

Zhang, L.-J., Wang, S., Xia, L., Lv, C., Tang, H.-W., Liang, Z., Xiao, G., & Pang, D.-W. (2020). Lipid-Specific Labeling of Enveloped Viruses with Quantum Dots for Single-Virus Tracking. *MBio*, *11*(3), e00135-20. https://doi.org/10.1128/mBio.00135-20

Zhang, X., Cheng, X., Yu, L., Yang, J., Calvo, R., Patnaik, S., Hu, X., Gao, Q., Yang, M., Lawas, M., Delling, M., Marugan, J., Ferrer, M., & Xu, H. (2016). MCOLN1 is a ROS sensor in lysosomes that regulates autophagy. *Nature Communications*, *7*, 12109. https://doi.org/10.1038/ncomms12109